Functional analysis of the *Arabidopsis thaliana* meiotic proteins AtPCH2 and AtCHR24

by

KOMSUN NUNTASOONTORN

A thesis submitted to
The University of Birmingham
for the degree of
DOCTOR OF PHILOSOPHY

School of Biosciences
University of Birmingham
September 2013

UNIVERSITY OF BIRMINGHAM

University of Birmingham Research Archive

e-theses repository

Abstract

In the past decade *Arabidopsis thaliana* has become an important system for studying meiosis in flowering plants. The identification of meiotic mutants has provided an important approach to studying plant meiosis. The availability of the *Arabidopsis* genome sequence together with developments in proteomics and bioinformatics provides an additional route for the identification of meiotic proteins and analysis of their functional interrelationships. This study has used a proteomics approach to identify a member of the SWI2/SNF2 chromatin remodelling gene family (*Atchr24*). Although a variety defects was observed in *Atchr24* male meiocytes cytogenetic, at least two T-DNA insertion lines on this gene appear normal. Secondly, this research has also used a bioinformatics approach to identify a potential orthologue of Pch2/TRIP13 in *Arabidopsis*. PCH2 (Pachytene checkpoint 2) is a member of the AAA+ ATPase family of proteins. This study reveals that AtPCH2 plays an essential role in the controlled formation of meiotic crossovers (COs). Cytogenetic analysis of two *Atpch2* T-DNA insertion lines revealed a high frequency of univalents at MI. The number of chiasmata (COs) is reduced to ~ 70% of wild-type (WT). Genetic analysis revealed that *Atpch2* has significantly weaker CO interference than WT leading to a redistribution of COs along the chromosomes. The recombination defect is accompanied by incomplete chromosome synapsis. Immunolocalisation of the chromosome axis protein AtASY3 and cohesin, AtSYN1 appears normal. However in contrast to WT, AtASY1 co-localises with the synaptonemal protein AtZYP1 in

Atpch2 rather than becoming depleted in regions of synapsis and the meiotic progression of *Atpch2* is delayed during pachytene by ~5 hours. These observations suggest a defect in remodeling of the chromosome axes and highlight how this process is essential for normal CO control.

Acknowledgements

List of Contents

Chapter 5
Analysis of *Atchr24*, a SWI2/SNF2 chromatin remodeling family member

Chapter 6
Discussion

Reference list

List of Figures

List of tables

List of Abbreviations

AE	**Axial elements**
Ab	**Antibody**
AESP	**Arabidopsis separase homologue**
APD	**Abnormal Pollen Development**
ASY1	**Asynaptic 1**
At	***Arabidopsis thaliana***
ATP	**Adenosine tri-phosphate**
BIO	**Biotin**
BLAP75	**BLM-associated polypeptide**
BPC	**Biotechnology Performance Certified**
BrdU	**Bromo-deoxyuridine**
BSA	**Bovine serum albumin**
CAP	**Chromosome associated protein**
Cdc	**Cell-division-cycle protein**
cDNA	**Copy DNA**
CENP	**Centromere protein**
CO	**Crossover**
Col-0	***Arabidopsis* Columbia ecotype**
CHR24	**Chromatin remodeling 24**
DAPI	**4, 6-diaminido-2-phenlyinidole**
DEPC	**diethyl procarbonate**
dHj	**Double Holliday junction**
DIG	**Digoxygenin**
D-loop	**Displacement loop**
DMC1	**Disruption of meiotic control 1**
DNA	**Deoxyribonucleic acid**
DSB	**Double strand break**
DsRed2	***Discosoma* sp. red fluorescent protein**
eCFP	**Enhanced cyan fluorescent protein**
ECL	**Enhanced chemiluminescence**
EDTA	**Ethylene diamine-tetra-acetic acid**
EdU	**5-ethynyl-2'-deoxyuridine**
EM	**Electron microscope**
EME1	**Essential meiotic endonuclease I**
eYFP	**Enhanced yellow fluorescent protein**
FISH	**Fluorescent *in situ* hybridisation**
FITC	**Fluorescein isothiocyanate**
FTLs	**Fluorescent-tagged lines**

GAPD	Glyceraldehyde-3-phosphate dehydrogenase
GFP	Green fluorescent protein
HIS	Histidine
HOP1	HomologuePairing 1
HORMA	Domain common in: Hop1p, Rev7p and MAD2
HRP	Horseradish peroxidase
H2AX	Histone 2AX
IPTG	Isopropylthio-β-D-galactosidase
KLE2	Kleisin protein 2
LB	Lysogeny Broth
LE	Lateral elements
MI	First meiotic division
MEK1	Meiotic kinase 1
Mer	Meiotic recombination defective
MEI2	Meiosis gene 2
MLH	MutL homologue1
MLH3	MutL homologue3
MMS4	Methyl methanesulfonate sensitive 4
MND1	Meiotic nuclear division 1
MRE11	Meiotic recombination 11
mRNA	Messenger RNA
MS	Murashige and Skoog
MSH	MutS homologue
MUS81	MMS and UV sensitive 81
NASC	National Arabidopsis stock centre
NBS1	Nijmegen breakage syndrome 1
NCO	Non crossover
Ni-NTA	Nickel-nitrilotriacetic acid
NORs	Nucleolar organizing regions
O/N	Overnight
PBS	Phosphate buffered saline
PCH2	Pachytene checkpoint 2
PCR	Polymerase chain reaction
PMC	Pollen mother cell
PRD	Putative recombination defect
qrt1	Quartet mutant 1
RAD	Radiation sensitive protein
RCA	Regulation of chromosome architecture
rDNA	Ribosomal DNA
REC	Abnormal recombination
RED1	Reduction division defective 1

RMI1	**RecQ mediated genome instability 1**
RNA	**Ribonucleic acid**
RNAi	**RNA interference**
RPA	**Replication protein A**
RT	**Room temperature**
RT-PCR	**Reverse-transcription polymerase chain reaction**
SAIL	**Syngenta Arabidopsis Insertion Library**
SEI	**Single-end invasion**
SC	**Synaptonemal complex**
SCC	**Sister chromatid cohesion protein**
SDS-PAGE	**Sodium-dodecyl-sulphate polyacrylamide gel electrophoresis**
SDSA	**Synthesis-dependant strand annealing**
SDW	**Sterile distilled water**
SMC	**Structural maintenance of chromosomes**
SNF	**Sucrose non-fermenting**
SPO11	**Sporulation specific protein 11**
ssDNA	**Single-stranded DNA**
SWI	**Switching**
SYCP	**Synaptonemal complex protein**
SYN1	**Synapsis 1**
T-DNA	**Transfer DNA**
TF	**Transverse filament**
TOP3α	**Topoisomerase 3 alpha**
Topo	**Topoisomerase**
Trip13	**Thyroid hormone receptor interactor 13**
WT	**Wild-type**
YCG1	**Yeast CAP G protein 1**
XRCC	**X-ray repair complementing defective repair in Chinese hamster cells**

Chapter I

Introduction

1.1 An overview of meiosis

Meiosis is a specialized cell-division process that is essential for sexually reproducing organisms. It ensures accurate chromosome segregation and creates genetic variation. Meiosis consists of one round of DNA replication followed by two rounds of nuclear division, meiosis I and II. The products of meiosis are gametes that possess half the genetic material from the parental cells. As a result, the ploidy and level of genetic complexity of the parent can be restored in the next generation by the fusion of two gametes during fertilization (Ma, 2006). Each round of meiosis can be divided into four sub stages that are similar to those of mitosis; prophase, metaphase, anaphase and telophase. At prophase I of meiosis, chromosome behaviour can be divided into five sub-stages; leptotene, zygotene, pachytene, diplotene and diakinesis (Tease and Hultén, 2006, **Figure 1.1**). During prophase I the homologous chromosomes undergo pairing, synapsis and recombination to form genetic crossovers (COs) which are essential for accurate chromosome segregation at the first meiotic division. Prophase I is a highly complex process that involves a large number of proteins to coordinate the progression of meiosis. These include components of recombination machinery and proteins that form meiosis specific structures such as the chromosome axes and synaptonemal complex (SC) (Osman *et al*., 2011).
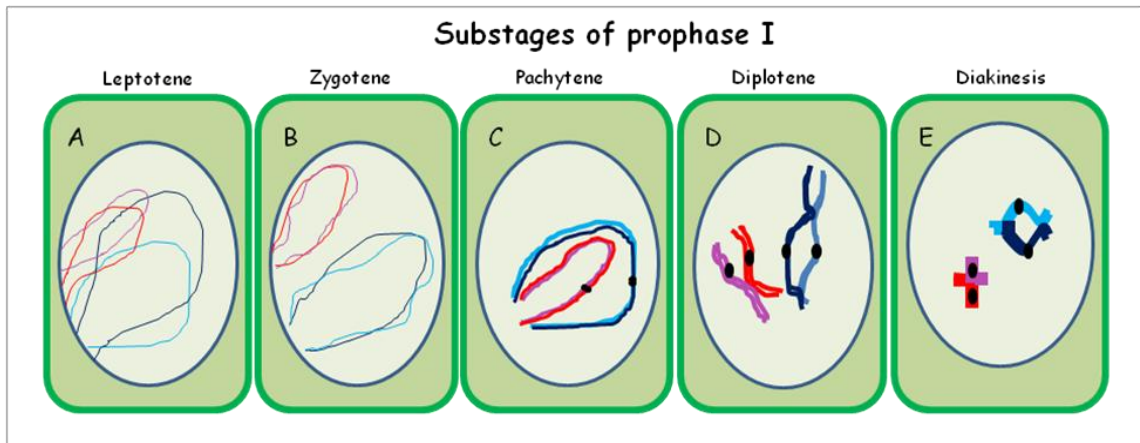
Figure 1. 1: Cytological stages of prophase I
During meiotic prophase I, the chromosomes are seen as thin thread-like structures at leptotene (**A**). At zygotene (**B**) the roughly aligned homologous chromosomes initiate synapsis. At pachytene (**C**), chromosomes are more condensed and homologous chromosome pairs are completely synapsed. All chromosome pairs are gradually condensed through diplotene (**D**) and are seen as bivalents at diakinesis (**E**). The individual bivalents are linked by chiasmata and chromosomes continue to condense until metaphase I, when they are fully condensed (Armstrong and Jones, 2003).

1.2 Prophase I of meiosis

1.2.1 G2/Leptotene

During meiotic S-phase, cohesion is established between sister chromatids due to the activity of a multi-subunit complex called the cohesin complex. The cohesin complex has been widely studied in yeast and animals, and some of their homologues have been identified in plants. The complex has a ring shaped configuration, consisting of SCC1/MDC1 (homologous to RAD21) and SCC3 and two structural maintenance of chromosome proteins, SMC1 and SMC3 (**Figure 1.2**) (Losada *et al.*, 1998; Nasmyth, 1999; Orr-Weaver, 1999). During meiosis, the meiosis-specific protein, REC8 replaces the SCC1/MDC1 (RAD21) protein found in somatic cells (Orr-Weaver, 1999). In

some organisms, SMC1 is also replaced in meiosis by its paralogue, SMC1ß, while

SCC3 is replaced by STAG3 in animals and Rec11 in fission yeast (Prieto *et al*., 2001;

Revenkova *et al*., 2001; Kitajima *et al*., 2003).
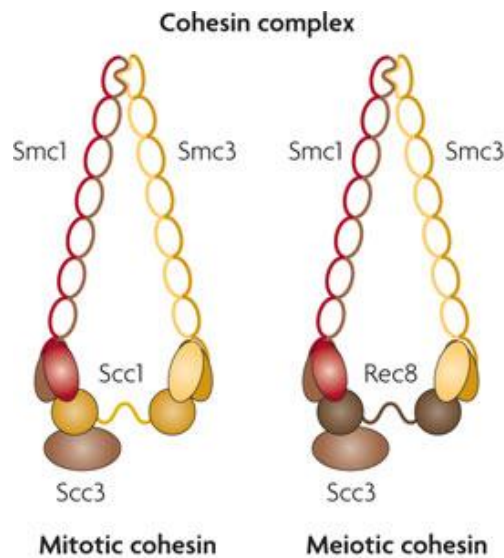
Figure 1. 2: Organization of the cohesin complex (Wood, 2010)

Walker A and Walker B motif are the nucleotide-binding domains (NBDs) that are

lain on the amino and carboxyl termini of SMC proteins, respectively. Each SMC

protein, the two antiparallel coiled coils are formed by folding back on itself becoming

a central region that are linked one end by the hinge domain and another end by a head

domain that comprises the Walker A and Walker B motifs. Dimerization of the two

SMC proteins occurs via interactions between the hinge domain of each SMC protein

and their head domains, which bind and interact with non-SMC subunits. Most of the

non-SMC subunits are the members of the kleisin family that associates with the two

head domains. In this configuration, it is possible for the SMC complexes to function

by surrounding one or more DNA strands (**Figure 1.2**) (Wood *et al.*, 2010). Sister chromatid cohesion (SCC) establishment is linked with replication, with the strong possibility that cohesion initiates at replication forks (Lengronne, *et al.*, 2006). In yeast, the acetyltransferase, Eco1, acetylates at least two lysine residues in the Smc3 head region in order to establish cohesion (Ben-Shahar *et al.*, 2008; Rowland *et al.*, 2009; Unal *et al.*, 2008; Zhang *et al.*, 2008). Also, SCC can be established by activation of DNA damage signalling in G2/M phase (Strom *et al.*, 2007; Unal *et al.*, 2007). However, Eco1-dependent acetylation of a cohesin subunit is required for both at the break site and on undamaged chromosomes during S phase but different subunits are associated (Wood *et al.*, 2010). At anaphase, the kleisin subunit Scc1 of cohesin is cleaved by separase and consequently, sister chromatids are separated (Alexandru *et al.*, 2001). In yeast, phosphorylation by Cdc5 encourages separase-independent release of cohesin from chromosomes during prophase I of meiotic cell division (Yu and Koshland, 2005), and cohesin phosphorylated by polo and aurora B-type kinases are also involved in many eukaryotes (Nasmyth and Haering, 2009).

1.2.1.1 Meiotic cohesin in plants

In plants, replacement of cohesin proteins between meiosis and mitosis is still ambiguous. The *Arabidopsis* genome has only SCC3 sequence and no STAG3 sequence (Chelysheva *et al.*, 2005; Wood *et al.*, 2010). However, several mutants have indicated that regulation of chromosome structure by the meiotic cohesin complex in

plant meiosis is completely required for meiotic progression (Hamant, 2006). Immunolocalization experiments show that SYN1, homolog of Rec A, is localized to chromosomes from interphase to pachytene, and decreases rapidly at diplotene and diakinesis when it is degraded in the nucleoplasm (Cai *et al*., 2003). In *Arabidopsis*, AtSMC1 and AtSMC3 might play important roles in sister chromatid cohesion during both meiosis and mitosis (Lam *et al*., 2005). Similar to SYN1, AtSCC3 in *Arabidopsis,* functions in sister chromatid cohesion at centromeres (Cai *et al*., 2003; Chelysheva *et al*., 2005).

1.2.1.2 Chromosome axis-morphogenesis

At late G2 through to early leptotene, the chromosomes start to appear as thin thread-like structures due to the condensation of the chromatin and formation of the axial elements in leptotene (Zickler and Kleckner, 1999). During this step, axis associated proteins are required in order for meiotic recombination to proceed; these include Hop1 and Red1 in budding yeast (Kim *et al*., 2010); AtASY1 and Hormad1/2 are the Hop1-related proteins in *Arabidopsis* and mouse respectively (Caryl *et al*., 2000; Shin *et al*., 2010; Wojtasz *et al*., 2009), while AtASY3 is the Red1 homologue protein in *Arabidopsis* (Ferdous *et al*., 2012) (discussed later). The proteinaceous axis organizes the sister chromatids into a series of chromatin loops along its length (**Figure 1.3**) (Kleckner, 2006). The size of the loops varies between species, but is quite consistent

within each species. However, the loop density (20 per µm) is highly conserved

between different species (Zickler and Kleckner, 1999; Ma, 2006).

In early leptotene in *Arabidopsis*, the nucleolus which has a volume of around one-

third that of the total nuclear volume is located in the central region of the nucleus. By

late leptotene it moves to the nuclear perimeter and remains there until the end of

prophase I. In *Arabidopsis* the telomeres seem to cluster to the nucleolus instead of on

the nuclear envelope during interphase (Armstrong *et al*., 2001) and it is thought that

this is important for successful pre-synaptic alignment (**Figure 1.3**) and pairing of the

homologous chromosomes which occurs in leptotene (Scherthan, 2001).
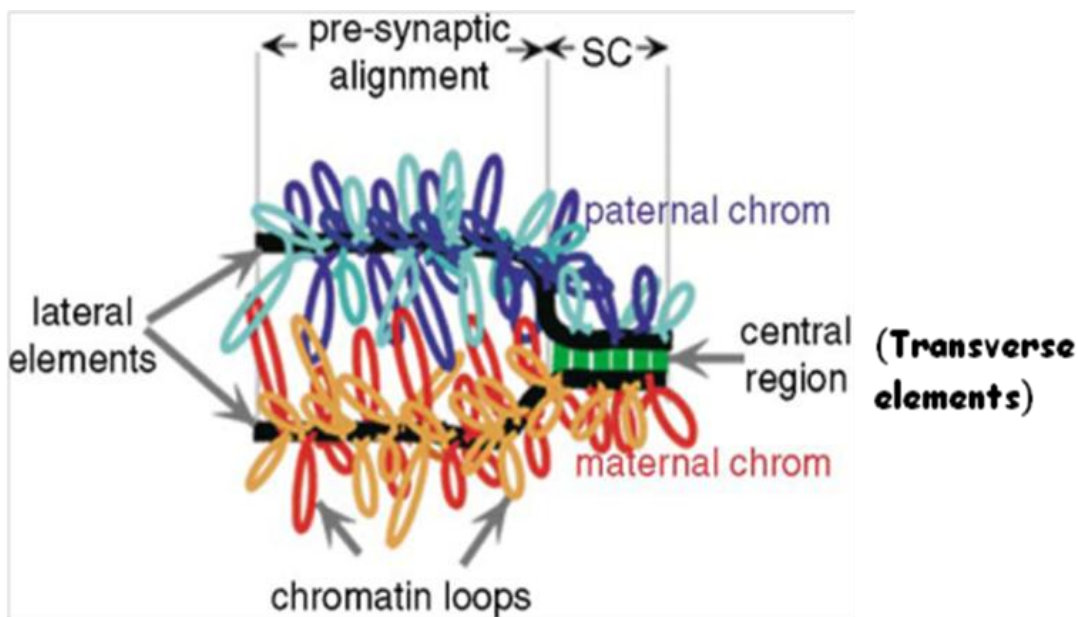
Figure 1. 3 : Schematic of a Zygotene sister chromosome
 (Bishop and Zickler, 2004). Both maternal sister chromatids and paternal sister
chromatids are formed from a set of loops along the axial elements (black). The SC
(green bars) polymerises between aligned axial elements, which are then called lateral
elements.

1.2.2 Zygotene/Pachytene

After juxtaposition and alignment of the homologous chromosomes at late leptotene, the synaptonemal complex (SC) starts to establish between the homologues. The SC is a tripartite proteinaceous structure that is comprised of the two sets of conjoined protein axes linked by transverse filaments (TF) (**Figure 1.3**). Once the axial elements are organized into the completely assembled SC, they are called lateral elements (Page and Hawley, 2004). The central region of the SC, as seen using transmission electron microscopy (Zickler and Kleckner, 1999) consists of the overlapping heads of transverse elements, which are rod-shaped proteins that link the lateral elements of the homologues (Page and Hawley, 2004). Each tail region of these proteins binds a lateral element. As a result, the fully synapsed SC looks like a zipper (**Figure 1.4**).
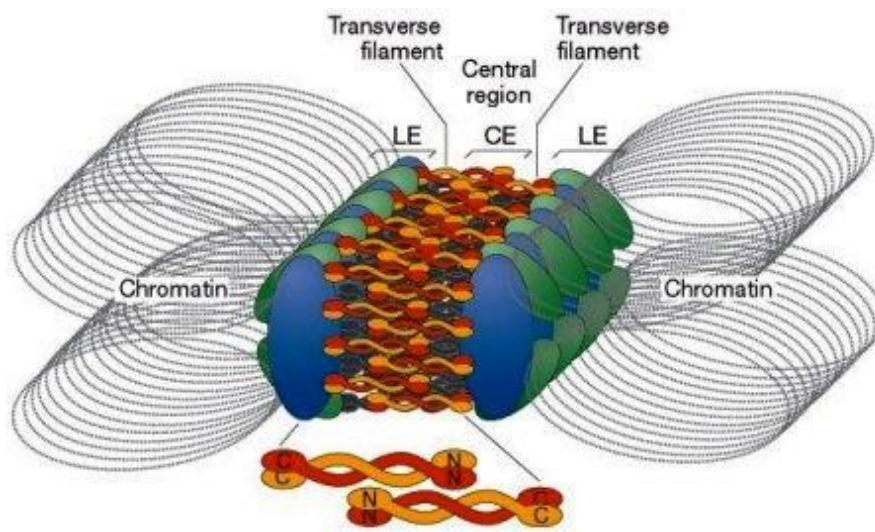
Figure 1. 4: The synaptonemal complex (SC) structure
The overlapping heads (N-termini) of transverse elements, rod-shaped proteins, are located in the central element (CE), whereas their tails (C-termini) are vertical to conjoin at the lateral elements (LE) (Costa *et al*., 2004; Ma, 2006; Bishop and Zickler, 2004).

The Zip1 protein has been identified as the major component of the central element (Sym *et al*., 1993). In budding yeast, several studies demonstrated that Zip1 is the transverse filament component of the synaptonemal complex. Absence of Zip1 in budding yeast mutants results in the failure of synapsis while complete axial elements are still formed (Sym *et al*., 1993; Sym and Roeder, 1995; Tung and Roeder, 1998). Immunolocalisation studies have revealed that Zip1 localises to the regions undergoing synapsis and stretches of complete SC, whereas the protein is absent in unsynapsed regions (Sym *et al*., 1993). The Zip1 protein sequence has been proposed to be formed α-helical coiled coil with globular domains at the N- and C- terminals (Heyting, 1996; Page and Hawley, 2004), and establishes in a rod-shaped homodimer (Sym and Roeder, 1995). Experiments in budding yeast which introduced alterations in the length of the Zip1 coiled-coil region were found to modulate the gap of the SC, suggesting the Zip1 molecules are arranged vertical to the axial elements (Tung and Roeder, 1998). Immuno-gold electron microscopy using domain-specific anti-Zip1 antibody, indicates that the Zip1 N-termini are located in the middle of the central region of the SC, while the Zip1 C-termini are positioned in line with the lateral elements. These results indicate that two Zip1 dimers arranged head-to-head, span between the lateral elements of the SC (Dong and Roeder, 2000) (**Figure 1.4**). The TF proteins and gene encoding them have been identified in a number of species. These include the canonical Zip1 from budding yeast, its homolog SCP1in animals including rat, mice and humans and Syn1 in hamsters (Meuwissen *et al*., 1992; 1997; Dopson *et al*., 1994; Liu *et al*., 1996); SYP1, SYP2, SYP3 and SYP4 from *C. elegans* (Schild-

Prüfert *et al*., 2011); C(3)G from *Drosophila*; ZEP1 in rice (Wang *et al*., 2010) and ZYP1 in barley (Higgins and Franklin, unpublished work) and *Arabidopsis* (Zickler and Kleckner, 1999; Page and Hawley, 2004; Hamer *et al*., 2006; Colaiacovo *et al*., 2003; Higgins *et al*., 2005; Osman *et al*., 2006). An interesting feature of the TF proteins is that despite the structural conservation of the SC, they share little primary amino acid sequence similarity. However, they exhibit conservation at the secondary structure level (Ma, 2006). The exception is *C. elegans* where two Zip1 homologues have been identified SYP1 and SYP2, which thought to form heterodimers in the central element of SC (Schild-Prüfert *et al*., 2011).

1.2.3 Diplotene to Tetrad stage

During diplotene, the SC starts to progressively disassemble. The central region disappears and the chromosomes appear decondensed and diffuse in late diplotene. Progression into diakinesis is characterized by the recondensation of the chromatin to form condensed bivalent structures. Chiasmata, the sites of genetic COs that are present along each bivalent, become visible at this stage (Bishop, 2006). Bivalent chromosomes are fully condensed at metaphase I, and align along the metaphase plate. The associated homologous chromosomes are then separated and move towards the opposite poles during anaphase I. The chromosomes reach the cell poles at telophase I, with the sister chromatids of each chromosome still associated together at centromere region (Armstrong and Jones, 2002). The sister chromatids are then separated at the

second meiotic division, as they would in mitosis, and producing four nuclei at the tetrad stage (Bishop, 2006).

1.3 Meiotic recombination pathways

Crossover (CO) formation is a product of homologous recombination that occurs in meiotic prophase I via the formation of programmed DNA double-strand breaks (DSBs). An overview of our current understanding of meiotic recombination in *Arabidopsis* together with the key enzymes, which are discussed below, is shown in **Figure 1.5** (Osman *et al*., 2011).
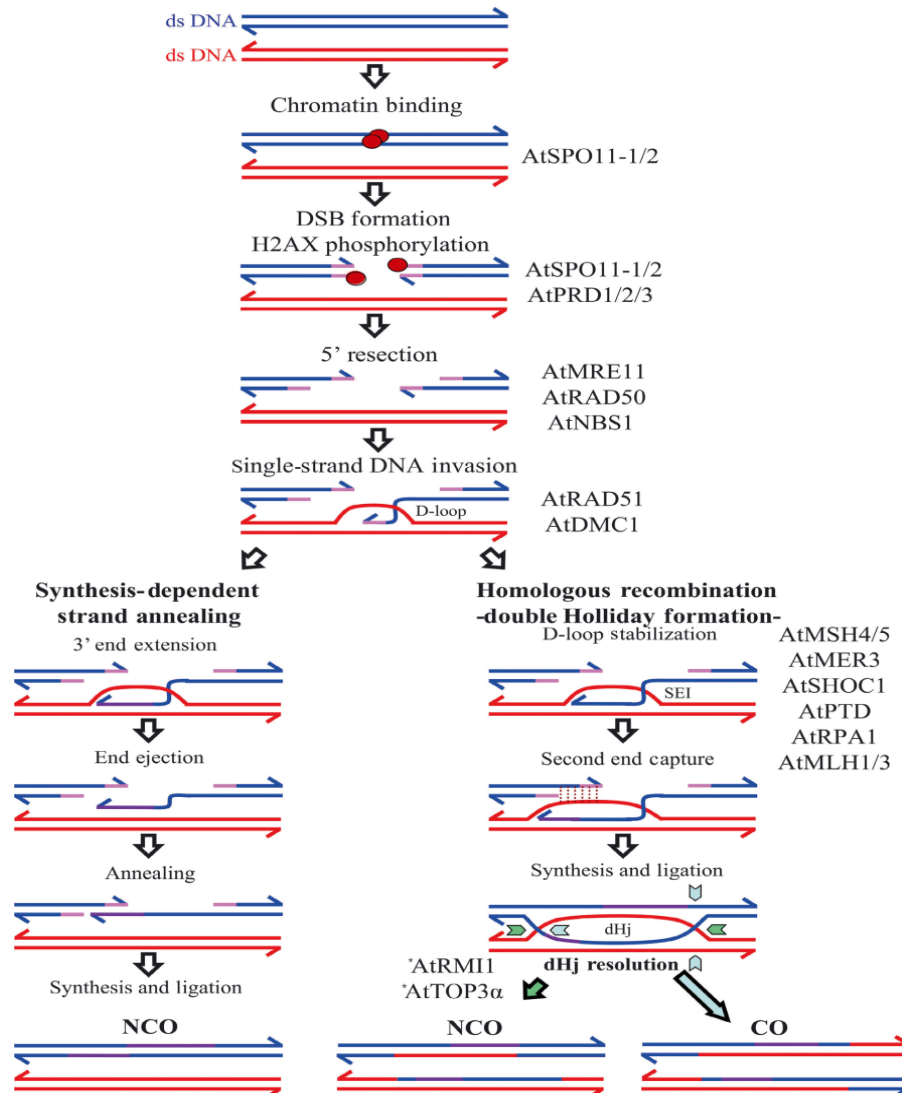
Figure 1. 5: The *Arabidopsis* recombination pathways (Osman *et al*., 2011)

1.3.1 Initiation of recombination

In budding yeast, at least three groups of proteins bind at sites on the shared axis of the conjoined sister chromatids as they condense. These are the pre-DSB recombinosome subunits (Spo11, Mre2, Rec114 and Mei4), the meiotic axis components (Hop1/Red1) and the cohesin complex (**Figure 1.6**). DSB formation in budding yeast requires a large number of proteins including Spo11, Rad50, Mre11, Xrs2, Mer1, Mer2, Mei4,

Mre2, Rec102, Rec104, Rec114 (Paques and Haber, 1999) and Ski8 (reviewed in Cole *et al*., 2010). However, the *Arabidopsis* SKI8 orthologue, AtMRE11 and AtRAD50 are not required for DSB formation in *A. thaliana* (Jolivet *et al*., 2006). Spo11 plays a central role in DSB formation in budding and fission yeasts (called Rec12 in the latter) and mouse (Cervantes *et al*., 2000; Romanienko and Camerini-Otero, 2000; Zenvirth and Simchen, 2000). Spo11 is a topoisomerase II-like protein that cuts the DNA and releases a 3'- OH end while remaining attached to the 5' end of the DNA via a phospho-tyrosyl linkage. The tyrosine residue at the active site of the protein is critical for its function and is conserved in all SPO11 homologues, such as Tyr-35 in budding yeast Spo11p (Bergerat *et al*., 1997; Diaz *et al*., 2002) and Tyr-103 and Tyr-124 in SPO11-1 and SPO11-2 respectively, in *Arabidopsis* (Hartung and Puchta, 2000; Hartung *et al*., 2007). Loss of SPO11 in budding yeast results in a reduction of meiotic recombination and SC formation (Klapholz *et al*., 1985; Wagstaff *et al*., 1985; Giroux *et al*., 1989). In the majority of species studied to date DSB formation is a prerequisite for homologous chromosome pairing. However, a few species possess DSB-independent mechanisms such as *Caenorhabditis elegans* (MacQueen *et al*, 2002; Page and Hawley, 2003; Dernburg *et al*., 1998; Gerton and Hawley, 2005); *Drosophila melanogaster* (McKim *et al*., 1998); *Coprinus cinereus* (Celerin *et al*., 2000). Unusually, *Arabidopsis* has three SPO11 paralogues (Hartung and Puchta, 2000, 2001). Both AtSPO11-1 and AtSPO11-2 are involved in DSB initiation, whereas AtSPO11-3 is implicated in somatic endoreduplication (Hartung *et al*., 2007).

In addition, there are some differences in the accessory proteins that are required for DSB formation in *Arabidopsis*. The proteins AtPRD1, AtPRD2 and AtPRD3 have been shown to be involved in DSB formation in *Arabidopsis* (De Muyt *et al*., 2007). AtPRD1 is proposed to be the functional homologue of the mammalian DSB protein MEI1, and to interact with AtSPO11-1 (Libby *et al*., 2003; De Muyt *et al*., 2007). AtPRD2 appears to be an orthologue of budding yeast and mouse *MEI4* (Kumar *et al*., 2010). While AtPRD3 is an ortholog of PAIR1 in rice (Nonomura *et al*., 2004), possibly promoting DSB formation by linking the DSB complex to the chromosome axis (Osman *et al.*, 2011).

Recent studies have begun to dissect the mechanism of DSB formation and its regulation. Single activated DSB hotspots within the loops become juxtaposed to the axis and are cleaved, forming DNA breaks (**Figure 1.6**, Panizza *et al.*, 2011; Carballo *et al.*, 2013). Immediately, following DSB formation a negative feedback program starts to inhibit cleavage of neighbouring hotspots (Carballo *et al*., 2013; Joyce *et al*., 2011; Lange *et al*., 2011; Zhang *et al*., 2011).
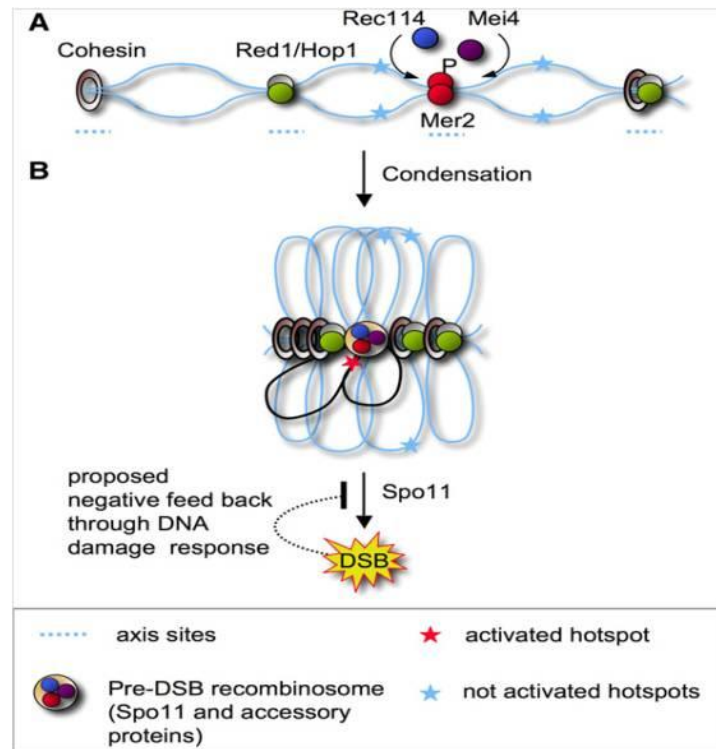
Figure 1. 6: Model of axis tethering of the DSB machinery (Panizza *et al*., 2011).
 (**A**) After premeiotic DNA replication, sister chromatids (blue line) are bound with cohesin (brown ring), axial element components Hop1 and Red1 (gray and green balls) and the pre-DSB recombinosome subunits Mer2, Rec114 and Mei4 (red, blue and violet balls) at axis sites (blue dotted lines). (**B**) Further axis formation leads to the emergence of linear arrays of loops conjoined with the axis. The Spo11-containing pre-DSB recombinosome exists at the axis and can cleave one of the surrounding hotspots. Pre-DSB recombinosomes are a locally limited resource and negative feedback through DNA damage response results in strong competition between neighbouring hotspots, as only a single hotspot can be cleaved at a time.

Maintaining the number of meiotic DSBs require both positive and negative programs of regulating break formation. Recent studies revealed that ATM/ATR family proteins, mammalian ATM-kinase (*tefu+*) and ATM homologs in *Drosophila* and budding yeast (*TEL1*), have roles in down-regulating meiotic DSB formation (Joyce *et al.*, 2011; Lange *et al.*, 2011; Zhang *et al.*, 2011). Furthermore, experiments in budding yeast suggested that Rec114 is a direct target of Tel1/Mec1 (ATM/ATR homologues

in budding yeast) in that Tel1/Mec1 phosphorylation of Rec114 following DSB formation, reduces its interaction with DSB-hotspots and results in reduced DSB formation (Carballo *et al*., 2013). Regulation of DSB formation also requires the activity of Cdk1 which phosphorylates the Mer2/Rec107 accessory proteins (Henderson *et al*., 2006; Manfrini *et al*., 2010).

1.3.2 DSB end resection and single end invasion (SEI)

Following the establishment of SPO11-dependent DSBs in yeast, the single-stranded ends are formed by strand resection. Spo11 is removed and 3'single-stranded DNA (ssDNA) tail, approximately 0.5-1 kb in length, is formed (Bishop, 2006). Genetic analysis has shown that RAD50, MRE11 and XRS2/NBS1 (the MRX/MRN complex) are involved in this step (Hartsuiker *et al*., 2009; Milman *et al*., 2009; Rothenberg *et al*., 2009). These proteins function together with Com1/Sae2/CtIP (MRN and CtIP in mammals and MRX and Com1/Sae2 in budding yeast) and Exo1 (Mimitou and Symington, 2009; Hodgson *et al*., 2010; Keelagher *et al*., 2010; Manfrini *et al*., 2010; Zakharyevich *et al*., 2010). Homologues of MRX complex are also found in *Arabidopsis* (reviewed in Osman *et al*., 2011). Experiments with *Atrad50* and *Atmre11* mutant lines revealed that DSB repair is defective as evidenced by the presence of a large number of chromosome fragments at metaphase I (Bleuyard *et al*., 2004; Puizina *et al*., 2004). An analysis of *Atcom1* mutant revealed a similar phenotype to *Atmre11*

and *Atrad50* (Uanschou *et al.*, 2007) indicating that the function of this protein is also conserved in *Arabidopsis*. Strand invasion is promoted by the Rad51 and Dmc1 recombinases (Smith *et al.*, 1987; Smith and Wang, 1989; Cox, 1999; Bishop *et al.*, 1992). Rad51 and Dmc1 are RecA-related recombinases (Shinohara *et al.*, 1992; Ogawa *et al.*, 1993; Benson *et al.*, 1994; Story *et al.*, 1993). Rad51 and Dmc1 are revealed promoting DNA strand exchange through a similar mechanism to RecA (Li *et al.*, 1997; Hong *et al.*, 2001). Rad51 and Dmc1 promote strand exchange with homologous double-stranded DNA by forming helical nucleoprotein filaments on 3'single-stranded DNA (ssDNA) tails as right-handed filaments. As a result, DNA joint molecules are formed through formation of displacement loops (D-loops). This process is called single end invasion (Sung, 1994; Sehorn *et al.*, 2004; Hunter and Kleckner, 2001; Bugreev *et al.*, 2005; Lee *et al.*, 2005). After formation of D-loops, Rad51 and Dmc1 have been proposed to remain associated with the DNA joint molecules in order to prevent dissociation of the structure (Symington and Heyer, 2006). One important difference between the recombinases is that RAD51 plays a role both in mitosis and in meiosis, while DMC1 functions specifically in meiosis (Krogh and Symington, 2004; Masson and West, 2001). The nucleoprotein filaments search and pair with the sister chromatid or the homologous chromosome template depending on whether the filaments are associated with Rad51 or Dmc1, respectively (Hunter, 2007). Although the activities of Rad51 and Dmc1 seem to be similar, *in vivo* studies indicate that they are controlled by different groups of accessory factors. Rad52 and Rad55-Rad57 may be involved in promotion of Rad51 assembly forming

nucleoproteins at DSBs (Gasior *et al*., 2001), whereas Dmc1 is proposed to depend on Rad51 (Shinohara *et al*., 1997b) and appears to be regulated by the Sae3-Mei5 (Hayase *et al*., 2004; Tsubouchi and Roeder, 2004). Rad51 is activated by the accessory proteins Rad54 and Tid1, while Dmc1 is specifically activated by Tid1 (Nimonkar *et al*., 2012). In addition, Hop2-Mnd1 is propose to be an accessory protein which stimulates Dmc1-dependent recombination (Chen *et al*., 2004; Henry *et al*., 2006). During meiotic single-strand exchange in budding yeast, Hed1 has been reported to influence Rad51 activity through a direct interaction, and in mitotic cells has a specific role in inhibition of Rad51-dependent repair (Tsubouchi and Roeder, 2006). In meiosis, Hed1 suppresses the Rad51 nucleofilament formation by blocking access of Rad54 (Busygina *et al*., 2011; Busygina *et al*., 2008) thus promoting Dmc1-dependent inter-homolog recombination. To date Hed1 has not been identified in multi-cellular organisms.

In *Arabidopsis*, RAD51 paralogues not only consist of AtRAD51 and AtDMC1, but also AtRAD51B, AtRAD51C, AtRAD51D, AtXRCC2, and AtXRCC3. (Doutriaux *et al*., 1998; Couteau *et al*., 1999; Osakabe *et al*., 2002; 2005; Bleuyard and White, 2004; Li *et al*., 2004; Bleuyard *et al*., 2005; Li *et al*., 2005; Li and Ma, 2006; Osman *et al*., 2011; Roth *et al.,* 2012; Bleuyard *et al*., 2006). In *Arabidopsis*, loss of RAD51 or DMC1 leads to sterility but somatic growth appears normal (Couteau *et al*., 1999; Pradillo *et al*., 2011; Sanchez-Moran *et al*., 2007; Li *et al*., 2004). The *Atrad51* mutant is defective in pairing, synapsis and DSB repair, leading to the presence of

chromosome fragments at metaphase I (Li *et al*., 2004). The *Atdmc1* mutant exhibits univalents at late prophase I, indicating AtDMC1 is vital for chromosome segregation and the formation of bivalents in *Arabidopsis* meiosis but not DSB repair (Couteau *et al*., 1999). RAD51C and XRCC3co-operate with RAD51 where they are proposed to facilitate loading of RAD51 onto DNA (Badie *et al*., 2009; Bishop *et al*., 1998; Masson *et al*., 2001; Tarsounas *et al*., 2004; van Veelen *et al*., 2005a; 2005b). AtRAD51B, AtRAD51C, AtXRCC2 and AtXRCC3 are also implicated in DNA repair, in both somatic cells and in meiotic recombination (Bleuyard *et al*., 2004; 2005; Abe *et al*., 2005; Li *et al*., 2005; Vignard *et al*., 2007; Da Ines *et al*., 2012; 2013; Roth *et al*., 2012; Bleuyard and White, 2004). The other paralogues AtRAD51D and AtXRCC2 are involved in developmental processes (Durrant *et al*., 2007; Inagaki *et al*., 2009). The phenotype of *xrcc3* and *rad51c* mutants in *Arabidopsis* is similar to that of *rad51* mutants in that chromosome fragmentation is observed at late prophase I/metaphase I, leading to sterility (Abe *et al*., 2005; Bleuyard *et al*., 2004; 2005; Bleuyard and White, 2004; Li *et al*., 2005). Recent studies also show that the RAD51 protein and its paralogues, RAD51C and XRCC3, are required for synapsis of chromosome arms, while a DMC1-dependent process is required for stabilizing pairing of homologous centromeric regions (Da Ines *et al*., 2012).

1.3.3 Interhomolog recombination

In yeast, Red1, Hop1 and Mek1 are revealed to promote meiotic inter-homolog recombination by suppressing Dmc1-independent recombination (Schwacha and

Kleckner, 1997; Pecina *et al.*, 2002). Hop1 and Red1 are involved in the homologue bias of meiotic recombination, which favours inter-homologue recombination in preference to inter-sister chromatid recombination. However, recent studies also suggest that inter-sister events may be more prevalent than previously thought (Kim *et al.*, 2010; Goldfarb and Lichten, 2010). Red1/Hop1/Mek1proteins act as a complex to regulate recombination through phosphorylation of Hop1 (Carballo *et al.*, 2008; Niu *et al.*, 2005; Ho and Burgess, 2011). Recent studies in budding yeast have revealed that Hop1 phosphorylation is dependent on two partially redundant pathways. One pathway involves the proteins Tel1, Pch2 and Xrs2 that respond to the presence of unprocessed DSBs. The other pathway involves Mec1 and Rad17 proteins which respond to the presence of resected DSB intermediates, during homologous recombination (Farmer *et al.*, 2012). Studies in an inhibitor-sensitive allele of *MEK1* reveal that Mek1 is not required for normal level of DSB formation,(Xu *et al.*, 1997). Loss of Red1 leads to a dramatic effect on axial structure, while Mek1 does not (Rockmill and Roeder, 1990; 1991). When Dmc1 and Mek1 kinase activity is lost, meiotic DSBs are still repaired efficiently via recombination with the sister chromatid (Wan *et al.*, 2004). Red1 and Hop1 are required to recruit Mek1 to the chromosome axes, where the kinase activity of Mek1 is vital to promote the recombination partner choice of the homologous chromosome (Wan *et al.*, 2004). Furthermore, the efficiency of Hed1 to inhibit Rad51 is dependent on Mek1 kinase activity (Wan *et al.*, 2004). Although Rad51 activity seems to be inhibited by Hed1, observations suggest that it is also required for interhomolog preference. In addition, Dmc1 nucleofilament may be

supported by the Rad51 which requires Mek1 phosphorylation to assist (Tsubouchi and Roeder, 2006). AtASY1 is a chromosome axis protein in *Arabidopsis* which contains a HORMA domain conserved in Hop1 and HIM3 in yeast and *C. elegans*, respectively (Caryl *et al*., 2000). AtASY1 and HORMAD1/2 in mouse are proposed to perform the same function in these species (Caryl *et al*., 2000; Shin *et al*., 2010; Wojtasz *et al*., 2009). Absence of ASY1 results in numerous univalents at metaphase I, however chiasmata are still produced at ~15% of wild-type levels (Ross *et al*., 1997; Sanchez-Moran *et al*., 2001). Furthermore, the initiation of recombination is normal in an *asy1* mutant, as DSBs are efficiently repaired, though without the normal subset progressing to CO formation (Sanchez-Moran *et al*., 2007). AtASY3, which appears to be a functional homolog of Red1, may cooperate with AtASY1 to play a key role in preference to inter-homologue recombination in *Arabidopsis* (Ferdous *et al*., 2012).

1.4 Crossover formation and its control

1.4.1 DSBs repaired through activity of ZMMs

Following single-end invasion stage of the recombination process, joint molecules can then by processed to form CO products by a group of conserved proteins referred to as the ZMMs. The ZMM group consists of at least seven functionally co-organized proteins Zip1, Zip2, Zip3, Zip4, Msh4, Msh5 and Mer3 (Borner *et al*., 2004). ZMM proteins have been proposed to play roles in both formation of crossovers and the SC. An important feature of ZMM-dependent COs is that they are sensitive to CO interference. This is a phenomenon that prevents the occurrence of COs in close

proximity to each other along the chromosomes. These are referred to as class I COs. A small proportion of COs, called class II crossovers, arise via a ZMM-independent route, and do not exhibit interference. Further details of class I and class II COs are discussed later in **section 1.4.3**. In budding yeast, Mer3 is suggested to be epistatic to Zip1/2/3/4 and Msh4/5 (Borner *et al*., 2004). Based on *in vivo* studies, Mer3 is proposed to stabilize Dmc1/Rad51-mediated nascent DNA heteroduplex molecules and heteroduplex DNA extension (Mazina *et al*., 2004; Terasawa *et al*., 2007). This is supported by earlier biochemical studies which demonstrated that Mer3 and the Msh4/Msh5 heterodimer are involved in the potential promotion or stabilization the strand invasion intermediate (Nakagawa *et al*., 2001). In *Arabidopsis*, AtMER3 (also called ROCK-N-ROLLERS [RCK]), was identified and its loss was found to result in a severe reduction in fertility (Chen *et al*., 2005; Mercier *et al*., 2005). Although SC formation was normal in *Atmer3*, chiasma frequency was reduced to almost 70% of the wild-type level (Chen *et al*., 2005; Mercier *et al*., 2005). Zip3 is a protein that may contain ubiquitin or small ubiquitin-like modifier (SUMO) ligase activity (Cheng *et al*., 2006; Agarwal and Roeder, 2000). Following loss of this gene in budding yeast, SC assembly is observed along chromosomes, but without recombination initiation and homologue pairing. This suggests that Zip1 is regulated by Zip3 to ensure that SC formation is contingent on earlier events of chromosomal activities (McQueen and Roeder, 2009). These results are supported by the analysis of the Zip3 orthologue in *C. elegans*, ZHP-3. Loss of ZHP-3 resulted in normal SC formation, but with an absence of chiasmata (Jantsch *et al*., 2004). Human Enhancer of Invasion 10 (HEI10) which is

involved in cell cycle progression (Toby *et al*., 2003), has been recently identified in rice and is proposed to be the homolog of Zip3 and ZHP-3 (Wang *et al*., 2012). HEI10/ZIP3 has also been identified in *Arabidopsis* where it is also required for CO formation (Chelysheva *et al*., 2012). Zip4 in budding yeast, also known as Spo22, co-operates with Zip2 to promote Zip1 assembly. In terms of CO formation, Zip4 is epistatic to all ZMM proteins (Tsubouchi *et al*., 2006). Extensive co-localisation between ZMM proteins is observed in yeast, such as between Zip2-Msh4, Zip2-Zip3 and Zip4-Zip2 associations (Agarwal and Roeder, 2000; Novak *et al*., 2001; Tsubouchi *et al*., 2006). This indicates that most ZMM proteins function at the same sites on chromosomes during meiosis. Analysis of AtZIP4 in *Arabidopsis*, the Zip4 homologue, revealed that *AtZIP4* and *AtMSH4* are in the same epistasis group. Loss of AtZIP4 did not result in a defect in AtZYP1 polymerization (Chelysheva *et al*., 2007). The *Arabidopsis* genes epistatic to the *Arabidopsis* ZMM proteins also include *PARTING DANCERS (PTD)* and *Shortage in Chiasmata (SHOC1)* (Wijeratne *et al*., 2006; Macaisne *et al*., 2008). Loss of either AtPTD or AtSHOC1 resulted in a dramatic reduction of chiasma frequency in *Arabidopsis* indicating both proteins were required for class I pathway of meiotic recombination (Wijeratne *et al*., 2006; Macaisne *et al*., 2008). AtSHOC1 is the ortholog of Zip2 (Macaisne *et al.*, 2008; 2011) and has been suggested to have a similar role to it in production of class I COs, and may also be implicated in single-end invasion promotion/stabilization (Macaisne *et al*., 2008). Ligation of the ends of newly synthesized segments to the resected 5'ends creates a specific joint molecule, known as double-Holliday junction (dHJ) (Hunter

and Kleckner, 2001; Collins and Newlon, 1994; Schwacha and Kleckner, 1994; 1995). AtPTD has also been proposed to be implicated in dHJ resolution due to recombination intermediates pre-determined to be COs, being repaired as NCOs in the absence of AtPTD (Wijeratne *et al.*, 2006). Msh4 and Msh5 function as a heterodimer and are both homologous to the bacterial MutS protein (Ross-Macdonald and Roeder, 1994; Snowden *et al.*, 2004; Hollingsworth *et al.*, 1995; Lynn *et al.*, 2007; Higgins *et al.*, 2004).The Msh4/5 heterodimer, unlike MutS in *E. coli*, does not function in the mismatch repair (MMR) system, as they lack the MutS I domain required for DNA base mismatch recognition (Ross-Macdonald and Roeder, 1994; Lamers *et al.*, 2000). Further studies based on human Msh4/5 dimers (hMSH4/5) reveals that the complex might initially stabilize a single-end invasion intermediate, enabling its development into a stable dHJ and subsequent resolution as either a CO or NCO (Snowden *et al.*, 2004). In *Arabidopsis*, AtMSH4 and AtMSH5 were identified on the basis of sequence homology (Higgins *et al.*, 2004; Osman *et al.*, 2009; Higgins *et al.*, 2008a; b). In *C. elegans*, mouse, *Arabidopsis* and budding yeast, loss of MSH4 or MSH5 results in the presence of univalents at metaphase I, with a few residual COs arising via the class II pathway (Zalevsky *et al.*, 1999; Kelly *et al.*, 2000; Jantsch *et al.*, 2004). In mouse and *Arabidopsis*, the number of Msh4 foci observed is considerably greater than the number of COs, indicating that Msh4 may associate with intermediates that are not destined to be resolved as COs (Moens *et al.*, 2002; de Boer *et al.*, 2006). It is thought that this may be due to the fact that synapsis initiation sites in these species outnumber CO events. In mouse, Msh4 co-localises with Mlh1 at sites that give rise to COs

(Moens *et al*., 2002). Mlh1 and Mlh3, the crossover-specific marker proteins that present on the SC at pachytene, are proposed to determine the crossover resolution sites (Lynn *et al*., 2004). Mlh1 foci are observed by cytological markers which co-localise to chiasmata at premature condensation (Marcon and Moens, 2003). During the DSB repair process, a joint-molecule intermediate (JM) that is formed via DNA strand exchange must be resolved in order to allow accurate chromosome segregation. The resolutions of JMs which are joined by Holliday junctions require endonucleases (West, 1997). Based on *in vitro* JM cleaving activities, three distinct eukaryotic endonucleases have been identified: first, MUS81-EME1/Mms4 (Mus81-Mms4 in budding yeast), this protein is able to cleave a variety of branched structures (Schwartz and Heyer, 2011); SLX1is also one of three eukaryotic endonucleases which contains a characteristic of the URI-YIG family of endonucleases (Dunin-Horkawicz *et al*., 2006). Its activity is dependent on an interaction with SLX4 (also known as BTBD12). SLX1-SLX4 complexes in budding yeast and human are capable of cleaving 5'- end of the DNA and HJs (Fricke and Brill, 2003; Munoz *et al*., 2009; Svendsen *et al*., 2009). Furthermore, meiotic crossing-over in *Drosophila* and *C. elegans* is generated by the SLX4 homologues, MUS312 and HIM18 respectively (Saito *et al*., 2009; Yildiz *et al*., 2002). The third eukaryotic endonucleases is GEN1/Yen1 (Yen1 in budding yeast) is a member of the Rad2/XPG endonucleases family and, based on its biochemical properties, is a HJ-resolving endonucleases (Furukawa *et al*., 2003; Ip *et al*., 2008; Ishikawa *et al*., 2004). Yen1 has been suggested to partially suppress the

recombination and damage-sensitivity phenotypes of *mus81* mutants (Agmon *et al*., 2011; Blanco *et al*., 2010; Ho *et al*., 2010; Tay and Wu, 2010).

In budding yeast, the polo-like kinase, Cdc5, is required for CO resolution (Clyne *et al*., 2003; Matos *et al*., 2011; Sourirajan and Lichten, 2008), whereas NCOs are yielded via Cdc5-independent activity (Allers and Lichten, 2001; Sourirajan and Lichten, 2008). Based on *in vivo* analysis during meiosis in budding yeast, the co-operation of Mus81-Mms4, Slx1–Slx4, Yen1, Sgs1 and Exo1-MutLγ are all involved in meiotic JM resolution. It has also been indicated that Sgs1 acts as a central regulator and mediator of meiotic JM resolution with unanticipated roles in both NCO and CO formation (Zakharyevich *et al*., 2012).

1.4.2 Mechanisms of interference

In most organisms, each chromosome arm usually gets one crossover/chiasma per meiotic division. Chiasmata are essential for alignment of bivalents at metaphase I and accurate segregation of homologous chromosomes at anaphase I. The existence of a crossover in one chromosome region reduces the probability of another forming in a nearby region; this phenomenon is known as crossover interference (Jones and Franklin, 2006).

Several models to explain the mechanism of interference have been proposed. First is the counting model (Foss and Stahl, 1995) which hypothesizes that a limited number

of NCOs may define the length of space between any two adjacent COs. The counting model satisfactorily accounts for CO data from budding yeast (Stahl *et al*., 2004), *Arabidopsis* (Lam *et al*., 2005; Copenhaver *et al*., 2002) and humans (Housworth and Stahl, 2003), provided the existence of a few non-interfering COs is accounted for (de los Santos *et al*., 2003; Higgins *et al*., 2004; Martini *et al*., 2006). The mechanical stress model (Kleckner *et al*., 2004) postulates that chromosomes are under mechanical stress, which can be locally relieved by the production of a CO subsequently making it less likely for another CO to form in the vicinity, assuming that the mechanical stress is required for the production of the CO. In other words, the first CO event is easily performed under stress on each chromosome. This event incurs an inhibitory signal resulting from the stress relief, in a bi-directed spread from a CO site. Multiple events which could be performed on the same chromosome in any location would be always evenly spaced. This model supported by the statistics of the distribution and number of meiotic COs/chiasmata in *D. melanogaster* and *C. elegans* (Kleckner *et al*., 2004). In addition, Joshi *et al*., 2009 proposed that the mechanical stress model could be added one more layer in order to explain Pch2 dependent CO-interference in terms of reconciliation in short-range. This is known as the one-CO module hypothesis (Joshi *et al*., 2009). The hypothesis proposes that Pch2 is involved in the establishment of a layer on the chromosome axis to create modules, and that mechanical stress within each module could be relieved by performing a single CO. The one-CO module has been proposed to involve an association of Zip3 and Hop1 hyper-abundance that is mediated by Pch2. The one-CO module hypothesis shows

that, for example, each chromosome of *C. elegans* could be encompassed to one module (Joshi *et al*., 2009). The third model of CO interference is the polymerization model which fit to CO data of *Drosophila* and budding yeast (King and Mortimer, 1990). This model proposes that the early recombination structures that are distributed independently of each other have an equal opportunity to perform and spread a bi-directional polymerization event. This polymer is referred to as interference which can inhibit additional early structures under the condition that the interference is strongest nearest to the initiated events, which would be subsequently referred to as COs (King and Mortimer, 1990). The fourth model is the chromosome oscillatory movement (COM) model which fit to CO data of human and mouse (Hulten, 2011). During prophase I, oscillatory movements will occur through the process along homologous chromosome. This hypothesizes that chiasma are formed via the proximity of homologous chromosomes at the nodal regions of the waves along the length of chromosome pairs that are created by the oscillatory movements from the telomeres and the kinetocores (Hulten, 2011).

1.4.3 Interference sensitive and interference insensitive pathways

The genetical pathways of crossover formation in yeast, mammas and *Arabidopsis* can be divided into two classes. The first are class I COs which are responsible for the majority of COs and are subject to CO interference, and require the function of the ZMM proteins (see earlier). The second are class II COs which are insensitive to

interference and are partly dependent on the Mus81/Mms4 protein complex (de los Santos *et al.*, 2003; Osman *et al.*, 2009). In *S. cerevisiae*, the lack of Msh4 or Msh5 results in a reduction of COs to ~60% of wild-type levels, leaving only interference-insensitive COs, whereas deletion of Mus81 or Mms4 (Eme1) shows ~25% reduction in COs, with the remaining COs being interference-sensitive (de los Santos *et al.*, 2003, Argueso *et al.*, 2004). In *Arabidopsis*, in the same situation, ~80-85% of the total COs are class I, interference-sensitive COs and ~15-20% are the interference-insensitive class II COs, mediated by the Msh4-Msh5 and Mus81-Eme1 pathways respectively (Higgins *et al.*, 2004; Copenhaver *et al.*, 2002; Berchowitz *et al.*, 2007; Higgins *et al.*, 2008). However, *Schzosaccharomyces pombe* only produces COs via a Mus81-Eme1 pathway (Cromie *et al.*, 2006; Smith *et al.*, 2003). The inverse situation is seen in *C. elegans,* where all COs are mediated by Msh4-Msh5 (Meneely *et al.*, 2002). In *Arabidopsis*, during leptotene/early zygotene stages, 80-100 foci each of AtRAD51 and AtMSH4 colocalises with AtMUS81 foci (~115 AtMUS81 foci present during leptotene) on the chromosome axes (Higgins *et al.*, 2008). The number of AtMUS81 foci decrease rapidly to ~5 foci by early pachytene. This suggests that the majority of DSBs are repaired via the Msh4-Msh5 pathway, whereas the remaining may comprise of aberrant joint molecules that could not be resolved by Msh4-Msh5 heterodimers, and are subsequently resolved via the Mus81-Eme1 pathway (possible as COs or NCOs) (Jessop and Lichten, 2008; Oh *et al.*, 2008).

1.5 Early decision model

During meiotic recombination, after DSBs are initiated and resection of the 5'ends are processed, the 3'ends invade into the intact homologous chromatid resulting in formation of hybrid DNA with complementary strands from DNA donor (Lichten *et al.*, 1990; Goyon and Lichten, 1993). The 3'ends invading the hybrid DNA act as primers for repair synthesis (Sun *et al.*, 1991). Evidence from budding yeast reveals that strand invasion is the key control step in the CO/NCO decision making process (Borner *et al.*, 2004). In 2001, Allers and Lichten proposed that a major proportion of NCOs results not from dHJ-mediated recombination, but rather from synthesis-dependent strand annealing (SDSA) (Allers and Lichten, 2001; McMahill *et al.*, 2007). This came to be known as the early CO-decision model of meiotic recombination (Bishop and Zickler, 2004). SDSA is a mechanism of homology-mediated repair with a failure of formation and resolution of ligated dHJs (Resnick, 1976; Nassif *et al.*, 1994). During SDSA, success in DSB repair is achieved by invasion of a 3'single-strand end into the intact homologous chromatid. The invading end may be shortened due to mismatch repair providing joint formation, Following this opportunity, the mismatch excision occurred leading to repair synthesis can extend the invading end and anneals with intact partner. Eventually, repair synthesis and ligation of annealing product is then converted to an intact duplex (Paques and Haber, 1999; Allers and Lichten, 2001; Ferguson and Holloman, 1996; Paques *et al.*, 1998). To conclude, the double-Holliday junction is produced from the invasion, repair and ligation and its resolution results in either crossovers or noncrossovers (Bishop and Zickler, 2004).

1.6 Meiotic checkpoint control

Defects in recombination and synapsis during meiosis can lead to crossing over failure at the pachytene stage and consequently aneuploidy. In many organisms, including *S. cerevisiae, D. melanogaster, C. elegans* and mice, there is a surveillance system called the pachytene checkpoint, which responds to meiotic errors and causes meiotic arrest in cells containing unresolved problems to avoid production of damaging products (Ghabrial and Schupbach, 1999; Bhalla and Dernburg, 2005; Ashley *et al*., 2004). Pch2 (pachytene checkpoint 2) is a meiosis-specific AAA+ ATPase family member that performs important roles in meiotic control, recombination and chromosome axis/SC morphogenesis. The pachytene checkpoint in *S. cerevisiae* and *C. elegans* is known to monitor fidelity of meiotic chromosome machinery, DSB repair and chromosome synapsis (Bhalla, 2005; Wu and Burgess, 2006). In yeast, Pch2 has been analysed and has been shown to have important functions for normal meiosis. Firstly, Pch2 is involved in timely and efficient recombination, with *pch2* mutants displaying extended time of DSBs longer than in wild type (Hochwagen *et al*., 2005). Formation of both COs and NCOs is delayed in the *pch2* mutant (Borner *et al*., 2008; Wu and Burgess, 2006). Interestingly, the yeast *pch2* mutant appears to show a delay at the DSB stage that is dependent on Rad17, an unrepaired DSBs checkpoint factor (Wu and Burgess, 2006). Pch2 is also required for maintaining the 'obligate crossover'. This is the reliable formation of at least one CO per pair of homologous chromosomes, even in spo11 hypomorphs, which show a reduction in DSB formation. *Pch2* mutants are defective in formation of obligate crossovers, and sometimes show the presence of

univalents at metaphase I (Joshi *et al*., 2009, Zanders and Alani, 2009). Thirdly, Pch2 is required to coordinate recombination and the progression of meiotic chromosome axis morphogenesis (Borner *et al*., 2008; Joshi *et al*., 2009; Zanders and Alani, 2009). Pch2 appears to control the assembly of chromosome axis protein Hop1 at sites designated to become COs. Hop1 and its binding partner, Red1, are prominent components of the axial element and preferentially associate with future crossover sites. Thus, crossover resolution and axis remodeling are linked via Pch2 (Joshi *et al*., 2009). Two results from *S. cerevisiae* studies reveal that *pch2* mutants have significantly weakened interference at many loci (Joshi *et al*., 2009, Zanders and Alani, 2009). However, there are incongruent results in terms of CO frequency. Joshi *et al*., 2009 present that the CO frequency in any loci is not significant altered (Joshi *et al*., 2009), whereas Zanders and Alani present that there are significant increases on medium and large chromosomes (Zanders and Alani, 2009). Furthermore, *pch2* mutants display increased CO:NCO ratios, though without any change in the number of DSBs, suggesting that Pch2 is required to repress the CO resolution at the CO/NCO decision step in the recombination pathway (Zanders and Alani, 2009). In addition, not all loci of *pch2* mutants are affected by the interference defect, with this defect sometimes being alleviated at lower temperatures (Joshi *et al*., 2009). In *C. elegans,* SC component defective mutants require *pch2* for apoptosis of oocytes (Bhalla and Dernburg, 2005), and the *pch2* mutant of *D. melanogaster* results in a delay in oocyte selection that is also seen in mutants of certain crossover-promoting factors (Joyce and McKim, 2009).

Trip13 (thyroid hormone receptor interacting protein) is the mouse *PCH2* ortholog. TRIP13 is not conserved in checkpoint functions in mammals. It is required for recombination pathways that lead to NCOs, but is not necessary for COs (Li and Schimenti, 2007). Roig *et al*., 2010 revealed that TRIP13 is required for efficient synapsis between homologues, and functions in the early stages of the DSB repair process, prior to RAD51 carrying out its function. Moreover, TRIP13 is required for normal number and distribution of COs.

1.7 Chromatin-modifying machinery

1.7.1 The nucleosome remodeling complexes of SWI/SNF family

Modification of nucleosome structure has been accepted as a principal regulatory mechanism. The mechanisms of dynamic chromatin modification are divided into two kinds. The first one involves covalent modifications to the histone N-terminal tails, without requiring the hydrolysis of ATP (Strahl and Allis, 2000). The second mechanism utilizes the hydrolysis of ATP to move the histone octamers, called nucleosomes, to facilitate access to particular DNA sites for various proteins (Becker and Horz, 2002). Recently, analysis has found that the various nucleosome remodelling complexes inside the cell share a common mechanism for nucleosome mobilization (Gangaraju and Bartholomew, 2007). SWI/SNF family is one of at least four families of ATP remodelling families, the others are ISWI family, CHD family,

INO80 and SWR1 family (Gangaraju and Bartholomew, 2007). SWI/SNF in *S. cerevisiae*, *Drosophila* and Humans, is present in two complexes, SWI/SNF and RSC. RSC is available in larger quantities within the cell than SWI/SNF, and is crucial for cell growth, whereas SWI/SNF is not. Discoveries have been made showing that SWI/SNF and RSC conform in non- overlapping roles. The Swi2 or Snf2 proteins form the catalytic subunit of yeast SWI/SNF and the Sth1 subunit is its paralog in RSC (Du *et al*., 1998). In yeast, the SWI/SNF complex functions in an early process of homologous recombination (HR), whereas RSC functions later, in single strand invasion (Chai *et al*., 2005, Huang *et al*., 2005). Moreover, RSC has been implicated in sister chromatid cohesion and segregation of chromosomes (Huang *et al*., 2004a; Huang *et al*., 2004b; Chang *et al*., 2005). SWI/SNF makes nucleosomal DNA accessible to proteins by forming DNA bulges on the surface (Fan *et al*., 2003). From their original position, nucleosomes are moved 52 bps. There are two steps in the process, starting with the loss of contact between histone H_2B and DNA, which is then shifted 52 bps from their previous positions (Kassabov *et al*., 2003; Kassabov *et al*., 2002). This suggests that SWI/SNF may remove the DNA segment from the surface of nucleosome and create a large DNA bulge, followed by movement of the bulge along the nucleosome surface. Consequently, the contact between H_2B and DNA can be restored again at another site of DNA (Gangaraju and Bartholomew, 2007).

Analysis of some of SWI2/SNF2 members with gene silencing revealed that they affected both mitosis and meiosis in various ways. Mutation to *DDM1* for example, led to gradual demethylation and the release of DNA in *Arabidopsis* genome (Jeddeloh

et al., 1999). RNA-directed DNA methylation also required DRD1 (Kanno *et al*., 2004, 2005). Cell transition from the embryonic to vegetative state required the gene PICKLE (GYMNOS) (Ogas *et al*., 1999), and differentiation of the carpels in *Arabidopsis* was also affected (Eshed *et al*., 1999), while the SPLAYED gene affected reproductive development (Wagner and Meyerowitz, 2002).

1.7.2 Histone acetyl-transferase (HAT) complexes

The chromatin-modifying machinery also includes histone acetyl-transferase (HAT) complexes, which modify histones through the addition of acetyl groups to specific residues, and histone de-aceylation complexes (HDACs), which remove them. Analysis in yeast found high levels of histone acetylation around meiotic recombination hotspots during meiosis (Yamada *et al*., 2004; Merker *et al*., 2008; Mieczkowski *et al*., 2007). A histone acetyl-transferase, M26 hotspot-specific hyperacetylation resulted in the frequency of DSBs reductions (Yamada *et al*., 2004). In contrast, loss of a HDAC leads to activate HIS4 hotspot activity (Merker *et al*., 2008). Factors of the meiotic recombination machinery might be recruited directly or indirectly by the function of histone acetylation (Hirota *et al*., 2008).

There are some studies which indicate a role for histone acetylation in chromatin decondensation, such as by inhibiting the formation of compact chromatin fibres (Shogren-Knaak *et al*., 2006). Most histone H4 is acetylated at lysine 16 in

decondensed chromatin (Smith *et al*., 2003). Modification to the interactions between histones by histone acetylation can affect chromatin structure (Kouzarides, 2007; Strahl and Allis, 2000). Histone de-acetylation is indicated to be vital for chromosome segregation in mammalian oocytes (Akiyama *et al*., 2006; Wang *et al*., 2006). Studies in plant meiosis show that the *Arabidopsis* genome has 18 genes encoding HDACs and 12 genes encoding histone HATs (Pandey *et al*., 2002). The HDAC T-DNA knockout lines and its antisense RNA lines present a variety of somatic tissue abnormalities and a reduction in seed set (Tian *et al*., 2003), induced seed abortion in *AtHD$_2$A* mutant (Wu *et al*., 2000), and reduced fertility in the first flowers in the *AtHDA6* mutant (Aufsatz *et al*., 2002). Mutation to AtGCN5, a HAT gene member, appears to result in reduction of fertility (Bertrand *et al*., 2003; Vlachonasios *et al*., 2003).

1.8 Methods for analysing plant meiosis

1.8.1 The transcriptomics and proteomics

There are many proteins involved in meiosis. In *Arabidopsis* for example, we have identified the proteins implicit in recombination pathways , AtSPO11-1/2 (Hartung and Puchta, 2000, 2001; Grelon *et al*., 2001; Stacey *et al*., 2006), AtDMC1, AtRAD51(Sanchez-Moran   *et al*., 2007) and the chromosome axis proteins, AtASY1(Caryl *et al*., 2000; Shin *et al*., 2010), AtASY3 (Ferdous *et al*., 2012), AtMSH4 and AtMSH5 (Higgins *et al*., 2004; Osman *et al*., 2009; Higgins *et al*., 2008a; b), AtMLH1 (Jean *et al*., 1999) etc. Recently, technical advances in

cytogenetics and immunocytology, as well as sequencing and annotation of the *Arabidopsis* genome, as well as the generation of libraries of T-DNA insertion mutants,   has improved the ability of researchers to investigate the sophisticated mechanisms of meiosis among higher plants (Bhatt *et al*., 2001; Caryl *et al*., 2003). However, there are several obstacles that have still confronted researchers in genetical identifications. A large number of genes involved during meiosis are poorly conserved between species, especially genes encoding proteins that serve important roles in sister chromatid cohesion, chromosome synapsis, and establishment of the synaptonemal complex (SC) (Sánchez-Morán *et al*., 2005). In addition, due to the *Arabidopsis* genome being duplicated, approximately 60% of nucleotides (AGI, 2000), result in creation of some small families of genes, and some of their gene sequences have been diverged. Eventually, this process might create functional redundancy in meiosis as well as the difficulties in their identification, as is the case with ASY1/ASY2 and the SYN1/SYN2/SYN3 gene families. Moreover, certain genes expressing moderate activity during the meiotic process, such as ZIP1 (Tung and Roeder, 1998), may not be detected by cytological methods in the mutants (Sánchez-Morán *et al*., 2005). Thus, identification of those genes clearly requires more suitable methods to underpin and extend the range of genes that can be identified. Proteomics is another powerful strategy, with improved methods providing success in the past few years for investigating proteins in several plant structures, such as chloroplasts (Taylor *et al*., 2003), the cell wall (Chivasa *et al*., 2002), and comparing mutants against wild- type *Arabidopsis* (Gallardo *et al*., 2002). The crop *Brassica oleracea,* shares ~80% its

genes with *Arabidopsis* (Cavell *et al*., 1998), and their stages of meiotic cell division are highly similar. Furthermore, an advantage of studying *Brassica oleracea* over *Arabidopsis* in term of preparing plant tissues for cytogenetic works and molecular genetics due to its phenotype is larger. Gaining meiotic material from this plant is therefore, much easier (Armstrong *et al*., 2002; Caryl *et al*., 2003). This property also makes *Brassica oleracea* more suitable for use in proteomic studies to identify meiotic proteins.

As variation in the expression of traits can be analysed between individuals, using transcript variation to identify the genes can provide the comprehension of phenotypic variation and serve a good candidate for gaining a meiotic function (Cubillos *et al*., 2012). Transcriptomic approach is performed through RNA isolation from meiocytes providing a high quality transcriptomics data, seen in *Arabidopsis* studies such as Libeau *et al*., 2011; Yang *et al*., 2011; Chen *et al*., 2010 and Cubillos *et al*., 2012 (Crismani and Mercier, 2013).

1.8.2 Bioinformatic methods

Bioinformatics is the combination of information technology and biology to analyse data from genome sequencing, gene and protein expression data, comparative genomics, etc. The formal and practical problems resulting from the management and analysis of large quantities of biological data can be resolved by bioinformatics. Bioinformatics allows the utilization of large amounts of advantageous biology

information that has been produced by the combination of genomic research technologies and information technologies (Kirschner, 2005).

1.9 Research aims

Progression through prophase I of meiosis leading to crossover (CO) formation is accompanied by, and dependent on extensive remodelling of the chromosome axes. This project will focus on the function of AtPCH2 (Pachytene Checkpoint 2) and AtSWI2/SNF2 during meiosis in *Arabidopsis*. In the past decade, study into the role of these meiotic proteins has been carried out in other model organisms and suggests that they are required for remodelling of the chromosome axes and essential for normal CO control. However, the roles of these proteins have not yet been analysed in *Arabidopsis* meiosis.

The aims of this project are to:

1. To determine if CHR24 a homologue of the SWI2/SNF2 chromatin remodelling gene family identified during the proteomic analysis of *Brassica oleracea,* and *Arabidopsis* meiocytes plays a role in meiosis.

2. To functionally characterize a potential orthologue of Pch2/TRIP13 in *Arabidopsis* identified using a bioinformatics approach, and investigate the role it plays in the formation of meiotic COs.

Chapter 2

Materials and methods

2.1 General information

2.1.1Bacterial strains

2.1.1.1 ElectroMAX™ DH5α-E™ Competent Cells (Invitrogen™):

supE44ΔlacU169(ϕ80LacZΔM15)hsdR17 RecA1 gyrA96 thi-1 recA1.

2.1.1.2 One Shot® BL21(DE3) Chemically Competent E. coli (Invitrogen™):

F⁻ompT gal dcm lon hsdSB(r$_B$⁻m$_B$⁻) λ(DE3 [lacI lacUV5-T7 gene 1 ind1 sam7 nin5]).

2.1.2 Cloning vectors

2.1.2.1 pET-21b cloning vector (Novagen)

A 5.4 Kb plasmid contains multiple cloning sites downstream of a T7 promoter. T7 promoter is under the expression of the Lac operator (*lacl*) which is under the control of isopropyl B-D-1-thiogalactopyranoside (IPTG) induction. The six repeats of CAC codon located at downstream of the multiple cloning site, encodes the hexahistidine (His-Tag sequence) attached to the C-terminal of the recombinant protein and provides the advantage for efficient protein purification (**Figure 2.1**).
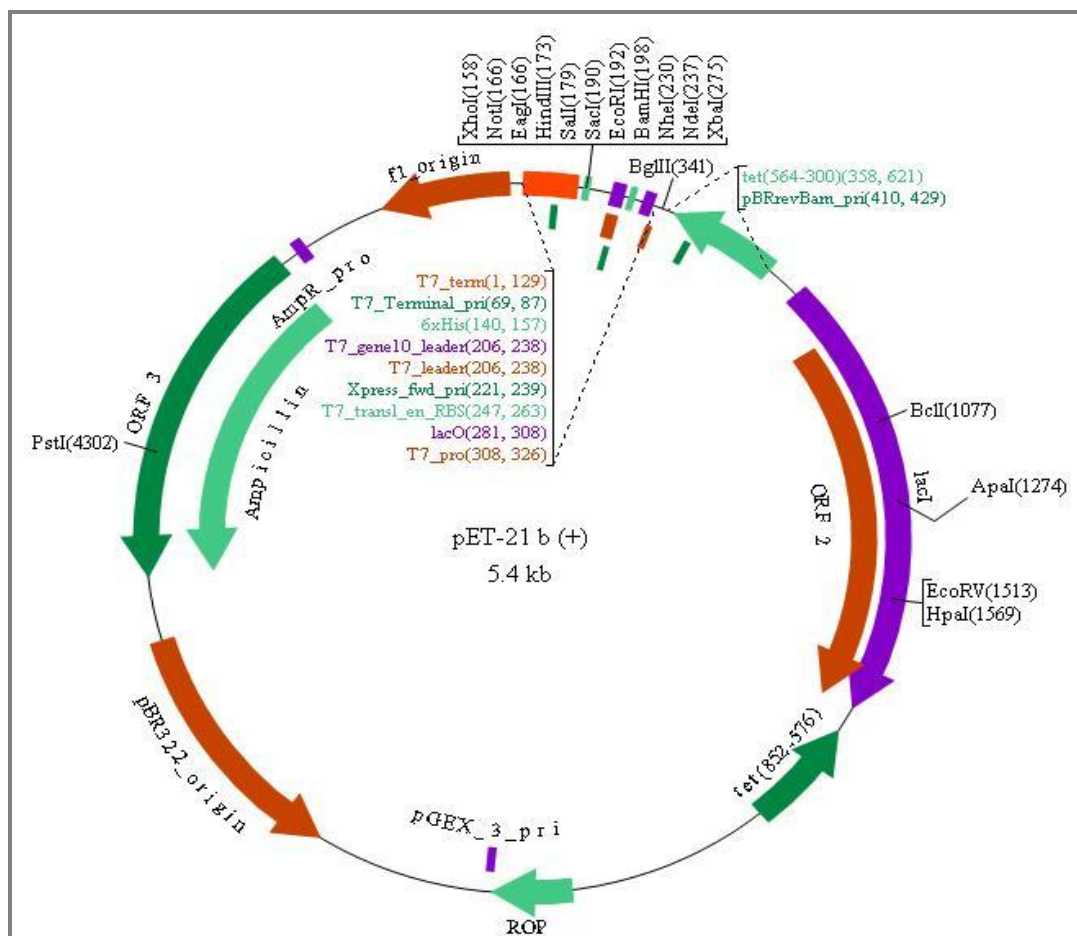
Figure 2. 1: The pET21b vector map.
The insertion site between *Nde1* and *Xho1* restriction enzymes is used to insert *AtPCH2* fragments that HIS-tag sequence located to the N-terminal of the expressed protein within T7 promoter.T7 primer was used for sequencing. (http://www.biovisualtech.com/bvplasmid/pET-21_b_%28+%29.htm)

2.1.2.2 pDrive cloning vector (Qiagen)

A 3.85 plasmid with multiple cloning sites locates within the LacZ inactivation marker. This plasmid contains ampicillin and kanamycin resistance (**Figure 2.2**).
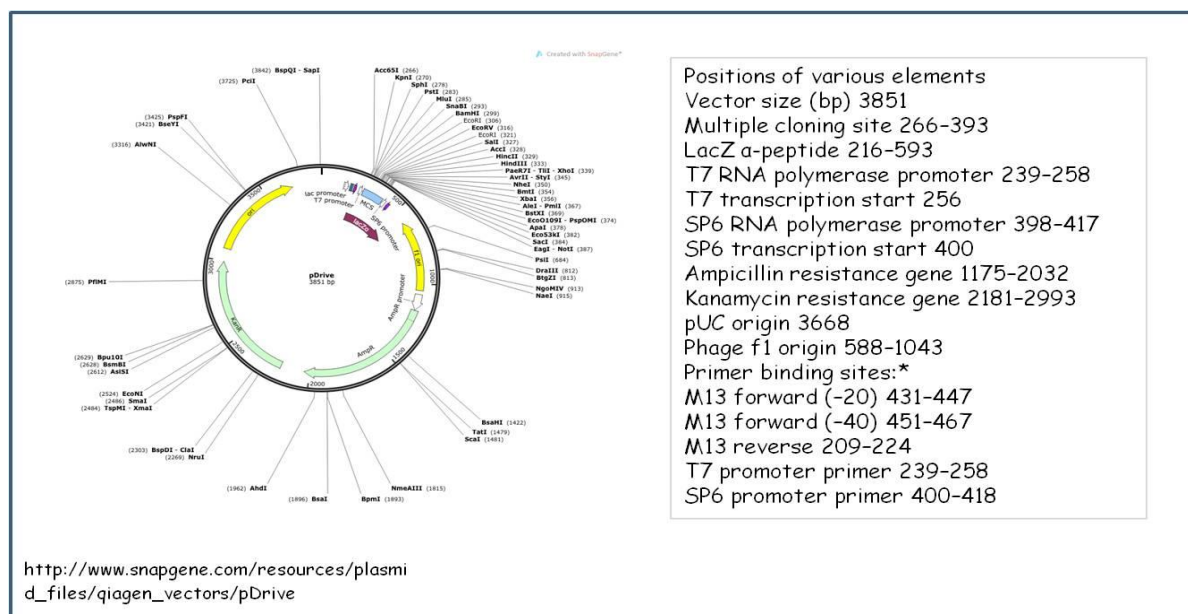
Figure 2. 2: pDrive cloning vector
The insertion site between the 2 *EcoRI* sites is used to insert *AtPCH2* fragments within T7 promoter. M13 primers were used for sequencing the RT-PCR products from *Atpch2*.

2.1.3 Oligonucleotide primer design

All primers were supplied by Eurofins MWG operon.

Primer types	**Primer sequences**	**Tm (ºC)**
cDNA AtPCH2 forward primer (P1)	CTCATTGAAGAAGGACCATGTGAGG	63.0
cDNA AtPCH2 reverse primer (P2)	CCATCTTCCTCCACCATCTCTTGG	64.4
GAPD forward primer (P3)	CTTGAAGGGTGGTGCCAAGAAGG	64.2
GAPD reverse primer (P4)	CCTGTTGTCGCCAACGAAGTCAG	64.2
DNA-free RNA checking forward primer (P5)	CGGTCTTTATAGCTGTTATTATACTGCG	62.2
DNA-free RNA checking forward primer (P6)	CGACTGTTCTTATCTTCTCACTTACC	61.6
Before *Atpch2.1* T-DNA insertion site primer (P7)	CAGTGCAAATAGCCGTCGCTGAG	64.2
After *Atpch2.1* T-DNA insertion site primer (P8)	CTCACATGGTCCTTCTTCAATGAGC	63.0

AtPCH2 recombinant protein forward primer	TTCTACCCGCAAAGGAGTTTGATGGC	64.8
AtPCH2 recombinant protein reverse primer	ACAAGACCTTAATATTTCATAACGAA	55.3
Atpch2.1 SAIL_1187_C06 forward primer	CAGTGCAAATAGCCGTCGCTGAG	64.2
Atpch2.1 SAIL_1187_C06 reverse primer	CTCACATGGTCCTTCTTCAATGAGC	63.0
Atpch2.2 SALK_031449.39.50 forward primer	CAATCCGGTGCAACTCCAGGTC	64.0
Atpch2.2 SALK_031449.39.50 reverse primer	CCATCTTCCTCCACCATCTCTTGG	64.4
Atpch2 SALK_130138 forward primer	GGATTATTCTTTTGCACGGACCACC	63.0
Atpch2 SALK_130138 reverse primer	GTCCGATCACTTCACAACTATTGGTG	63.2
SALK line T-DNA left boarder primer	TGGTTCACGTAGTGGGCCATCG	64.0
SAIL line T-DNA left boarder primer	TGGTTCACGTAGTGGGCCATCG	64.0
M13 forward primer	GTAAAACGACGGCCAGT	52.8
M13 reverse primer	CAGGAAACAGCTATGAC	50.4
T7 promoter primer	TAATACGACTCACTATAGGG	53.2
SALK_007071 (*Atchr24*) forward primer	CGGTCTTTATAGCTGTTATTATACTGCG	62.2
SALK_007071 (*Atchr24*) reverse primer	CGACTGTTCTTATCTTCTCACTTACC	61.6
SALK_047650c forward primer	GTGTACCACATCGGATGTTCTTG	60.6
SALK_047650c reverse primer	GTCATATCCATCAGCTTCGTCTTCC	63.0
SALK_152488 forward primer	GAAGCTAACACTGAGCTGGCTG	62.1
SALK_152488 reverse primer	TTGGCGTTATAAGACCGAGCTG	60.3

Table 2. 1: Oligonucleotide primers

2.1.4 Bacterial growth media

All media were prepared under sterilization conditions (autoclave at steam pressure 15 psi, 121 ºC for 20 minutes)

Lysogeny Broth (LB) media: 10g/L bacto-tryptone, 5 g/L bacto-yeast extract, 10 g/L NaCl.

Lysogeny Broth (LB) agar: LB medium, 15 g/L bacto-agar.

Incubations for cell cultures were performed under aseptic condition. In order to culture in selective agents, the final concentration of ampicillin was 100 µg/ml; for kanamycin it was 50 µg/ml.

2.1.5 Plant cultivation

The mutant lines were obtained from the Nottingham *Arabidopsis* Stock Centre (NASC) (**Table 2.2**). Seeds were sowed in John Innes No.1 potting compost and grown at 18 ºC with 16 hours white light and twice watering per day. *Arabidopsis* Columbia 0 (Col 0) ecotype was utilized as a control.

Mutant lines	Locations	T-DNA insertions
Atpch2.1	At4g24710	SAIL_1187_C06
Atpch2.2	At4g24710	SALK_031449
Atpch2.3	At4g24710	SALK_130138
Atchr24	At5g63950	SALK_007071
Atchr24 (N683449)	At5g63950	SALK_047650c
Atchr24 (N652488)	At5g63950	SALK_152488

Table 2. 2: List of T-DNA insertion lines in this project

2.2 Cytology

2.2.1 Fixation of buds

Buds were placed into ice cold fixative solution, ethanol and acetic acid at a ratio of 3:1, and the fixative was changed after 2-3 hours and again after 14-16 hours. The fixed buds were stored at room temperature.

2.2.2 Preparation of slides for basic cytology (modified from Armstrong and Osman, 2013)

The fixed buds were placed in a watch glass with 4-5 ml of fixative solution. Generally 6-8 buds ranging in size 0.3-0.4 mm. were chosen for spreading slides. After washing buds with citrate buffer (445μl 0.1M citric acid and 555μl 0.1M Na citrate and made up to 10 ml with dH_2O) for 2 minutes 3 times, were incubated in 0.3% enzyme mix (Cellulase, Cytohelicase and Pectolase in citrate buffer) for 1 hour and 30 minutes at 37 ºC in moist box. A microscope slide (Super Frost VWR) was used for spreading by placing a drop of 2μl water on the slide and a bud was added. After that, the bud was broken by a brass rod, followed by 5μl of 60% acetic acid twice then the blended sample was stirred with a needle and marked on slide by diamond marker. The slide was placed on a hot plate at 48 ºC for 1 minute, 100 μl of fixative solution was pipetted to fix the material on the slide and this was dried from the back by a hair dryer.

2.2.3 DAPI staining

DAPI stain (4', 6-diamidino-2 phenylindole) was dropped on the slide for 7 µl (1mg/ml stock in vectashield mounting medium (Vector laboratories)) and then covered with a cover slip. The excess of DAPI was removed by pressing on a cover slip gently with tissue. Slides were viewed with a Nikon T600 fluorescence microscope. Smart capture 2.0 software supported by Digital Science was used for image analysis.

2.2.4 Immunolocalisation on PMCs spreading (modified from Armstrong and Osman, 2013)

Anthers which containing meiosis stage of chromosome were dissected out off buts on wet filter paper for around 10 buds per slide. EM digestion solution (containing; Cytohelicase 0.1 g, Sucrose 0.375 g, SDW 25 ml, Polyvinyl pyrollidone (Mw 40,000) 0.25 g) 12 µl were dropped on slide prior to transfer anthers to the solution. Slides were incubated in a humid box at 37 ºC for 10 minutes after that anthers were then tapped with a brass rod for releasing meiocytes and put 12 µl of EM digestion solution more as well as 10 µl of 1% lipsol each slide, then mix and spread well by a needle on slide so that meiocytes can be separated. Slides were placed on a hot plate at 37 ºC for 4 minutes, keep dropping some more 1% lipsol in order to do not allow drying. The chromosome spreading area on slides was then fixed with 20 µl of 4% paraformaldehyde pH 8, the final concentration would be 2% paraformaldehyde and then left slides to completely dry at room temperature. The slides were washed with

PBS buffer (Phosphate tablet 1 tablet per SDW 100 ml, 0.1% Triton) three times for 5 minutes each, after which covered the chromosome spreading area on slide by EM block (1% Bovine Serum Albumin in 1% PBS, 0.1% Triton) 50ul for 10 minutes using parafilm. Primary antibody in EM block such as AtASY1 1: 5,000, AtZYP1 1: 500, AtDMC1 1: 500 was applied and incubated in a humid box over night at 4 ℃. Slides were washed in PBS buffer for 5 minutes three times and then 50 ul of secondary antibody in EM block such as Texas red 1: 200, FITC 1: 50 which specified to primary antibody, was applied to the slides using parafilm to cover. Slides were incubated in a dark humid box at 37 ℃ for 30 minutes after which the slides were washed in PBS buffer three times for 5 minutes each in a dark box prior to put 7 µl of DAPI/vectashield on each slide for labeling chromatin and reducing fading of fluorescent probes.

2.2.5 Silver staining on surface spreading of meiotic prophase in PMCs for EM

The slides were coated with a plastic film using plastic solution (0.75% petridish dissolved in chloroform) and then removed any charge by exposure to UV light at 0.1 torr. The PMCs were prepared same as the immunolocalisation experiment on a cavity slide after which 1-2 µl of digested PMCs were dropped on a drop of 10-12 µl of 1% lipsol, a mixed drop was dropped on a coated slide and spread out. The spread slides were left to allow the chromatin start spilling out (using phase contrast microscope to monitor) and then fixed the materials on the slides with 10 ul 4% paraformaldehyde pH 8, left them for drying. The dried slides were fixed with 4% paraformaldehyde for

10 minutes and briefly rinsed with 0.01% Photoflox2 and left them dry. 50% silver nitrate solution was dropped to soak a square of mesh which covered on each slide after that the slides were incubated at 60 ºC until the mesh was turned to golden brown, removed the mesh and briefly rinsed with SDW. The slides were marked with ink-marker the meiocyte under phase contrast microscope and then floated off the plastic film on water. The film was placed on EM copper grids and left them for drying in order to keep all until viewing with electron microscope (EM).

2.2.6 BrdU labeling for a meiotic time-course (Armstrong *et al*., 2003)

Under standard green house condition, stem with young inflorescences were cut under water in a length around 6 cm and then transferred to BrdU (Bromo-deoxyuridine) solution (0.01 M), left for 2 hours in order to uptake in of BrdU into cells in s-phase. The flowering stems were removed to tap water after which inflorescences were cut off from the stems and fixed in fixative solution (3:1 of 100% ethanol : glacial acetic acid) at following time points; 0 hour, 5, 10, 20, 24, 30, 35, 40, 45 hours after 2 hours of BrdU uptake. The individual fixed bud was prepared same as preparation of slide for basic cytology. BrdU was detected using an anti-BrdU kit (Roche) followed by the manufacturer's instructions and eventually was counterstained by DAPI.

2.2.7 Fluorescent tetrads assay (Berchowitz and Copenhaver, 2007)

The genotypes in this experiment were created and prepared as showed in the **Figure 3.26**. The fifth to the thirtieth flowers of the primary stem were only used for analysis. An opened flower was placed down into the 20 µl of PMG on a slide (17% (w/v) sucrose, 2 mM $CaCl_2$, 1.625 M boric acid and 0.1% (v/v) Triton-x) and a tapping motion was performed in order to release the pollen into the solution. The PMG with pollen was covered with cover slip and then viewed under fluorescence microscope through eCFP, eYFP and DsRed2 filters. Pollen from both mutant and wild type genotypes classified into 12 patterns were scored (**Figure 3.27**). The statistical analysis used Stahl Lab Online Tools:http://molbio.uoregon.edu/~fstahl/.

2.2.8 Alexander staining

Mature flowers were fixed in 10% alcohol. The anthers were isolated and put on slide. 2 drops of water were added then cut the anther to release the pollen into water. 2 drops of Alexander stain were added and then covered with cover slip. After that, sealing the slide with glue and plated the slide on hot plate at 50 ºC for 1 hour 30 minutes. The slide was observed under a light microscope.

2.2.9 Fluorescence *in situ* hybridisation (modified from Armstrong, 2013)

Chromosome spreading slides were made from pollen mother cells. The slides were washed in 2xSSC (diluted from 20xSSC; 3 M NaCl, 3 M tri-sodium citrate) for 10 minutes at room temperature followed by digestion with pepsin (0.01 pepsin in 0.01 M HCl) for 90 seconds at 37 ℃. The pepsin-digested slides were washed in 2xSSC for 10 minutes and fixed with 4% paraformaldehyde for 10 minutes after which briefly rinsed with sterile distilled water (SDW). The slides were then dehydrated with a series of alcohol concentrations: 70%, 85%, 100% respectively for 2 minutes each concentration and then left slides for drying. The first solution was applied on slides for 20 µl each slide (the first solution contains; 3 µl of each desired probe, made up to 20 µl with hybridization mix) and then covered with a cover slip. Rubber solution was used to seal the cover slip; the sealed slides were left on a hot plate at 75 ℃ for 4 minutes and then incubated in a humid box at 37 ℃ for 2 days. The incubated slides were cover slip replaced. The slides were washed with: 50% formaldehyde 2xSSC at 45 ℃ three times for 5 minutes each; 2xSSC at 45 ℃ once for 5 minutes; 4T (4xSSC + 0.05% Tween 20) at 45 ℃ once for 5 minutes; 4T at room temperature once for 5 minutes. The slides were applied the secondary solution (the secondary solution contains; BIO (1:200 Milk block) or DIG (1:50 DIG block) for 50 µl each slide in order for detecting probes with fluorescent labeling (**Figure 2.3**), and then incubated at 37 ℃ for 30 minutes in a dark humid box. All slides were washed three times for 5 minutes each in 4T at room temperature after that left them for drying, eventually stained with 7 µl of DAPI.
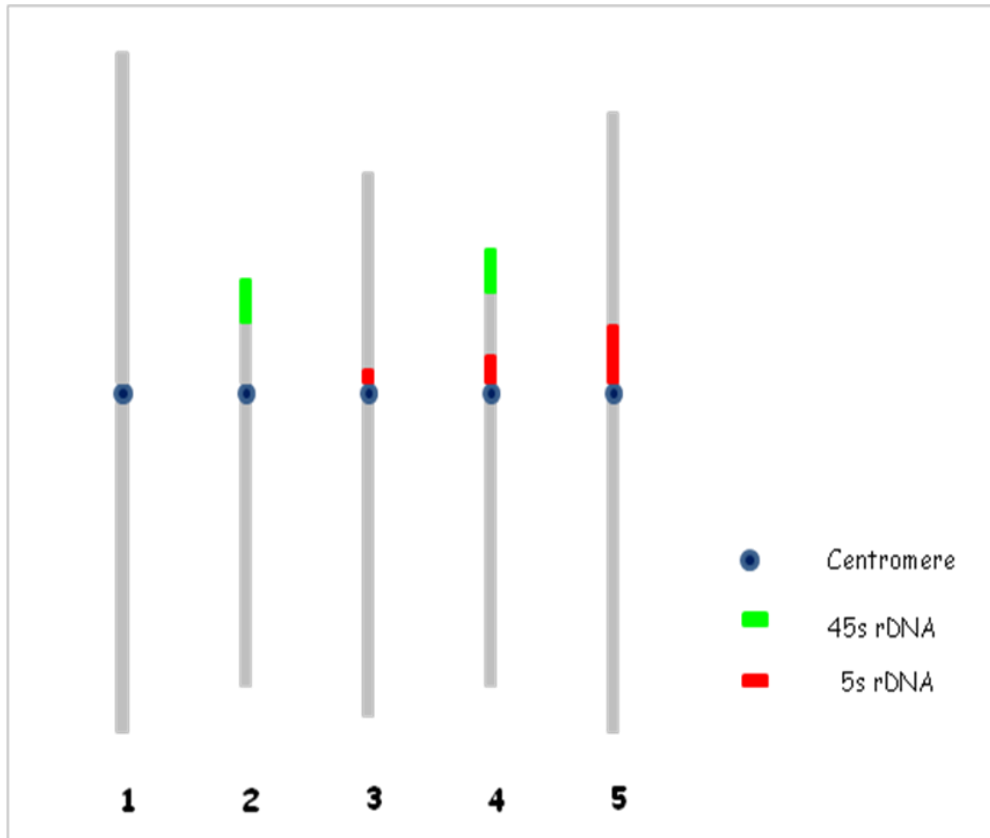
Figure 2. 3: Schematic diagram of *Arabidopsis* chromosomes with positions of probes labeled. A haploid set of *Arabidopsis* chromosomes shows positions of probes labeled on each chromosome number. Dark ring shape represents centromere position; green and red bars present 45s and 5s rDNA position respectively.

2.3 Molecular biology

2.3.1 DNA and RNA manipulation

2.3.1.1 Plant DNA extractions

Extract'n'Amp Plant PCR kit (Sigma) was used for leaf DNA extractions. 0.5 ml microfuge tube was used to cap a small disc of leaf after that 50 µl of extraction buffer was applied and then broke cells and mixed well in the buffer using the tip of pipette. All samples were incubated in a PCR machine for 10 minutes at 95 ℃ after which the samples were cooled down on ice prior to blend with 50 µl of dilution buffer. The samples were centrifuged to spin down the crude plant tissue. DNA samples were stored at -20 ℃ for genotyping experiments which used 1 µl of supernatant for a 25 µl reaction.

2.3.1.2 Plant RNA extraction

Plant tissues weighting around 100 mg were used for extracted using the method described in the RNeasy mini handbook (Qiagen) protocol for purification of total RNA from plant cells. All microfuge tubes and plastic rods used in this experiment were soaked overnight in diethyl pyrocarbonate (DEPC) 1: 1000 in SDW prior to being autoclaved.

2.3.1.3 Polymerase Chain Reactions (PCR)

Reaction mixes were undertaken in a Thermo Hybaid PCRS print termo-cycler or ThermoHybaid Omnigene. The gene specific primers used depend upon the T-DNA

insert genes from stock. 12.5 μl of Reddymix Taq polymerase (Invitrogen), 9.5 μl of BPC grade water and 1 μl of forward and reverse primer was put to each reaction (concentration of 10 uM). 1μl of extracted DNA from leaf was used for each reaction. The PCR cycle was; 93 ºC for 2 minutes at the first cycle for preparing denaturation followed by 35 cycles of 93 ºC for 1 minute, 54 ºC for 1 minute for annealing (generally being around 4 ºC below the lowest of the primer Tm) and 72 ºC for 1 minute 30 seconds for extension. Eventually, 1 cycle of 72 ºC for 10 minutes with a final prolonged extension stage was performed.

2.3.1.4 Agarose Gel electrophoresis for DNA

1% agarose gel with 0.5 mg/ml ethidiumbromide was set in Hybaid electrophoresis kits. 0.5x TBE (5x TBE: 0.45M Tris, 0.45M Orthoboric acid, 12.5 mM EDTA) was used as the electrolyte. The size of PCR products were compared with aliquot of 1 kb ladder (15 μl 1kb ladder (Invitrogen), 50 μl DNA Loading Buffer (40% (v/v) glycerol, 0.25% (w/v) bromophenol blue, 0.25% (w/v) xylene cyanol, 135 μl SDW). PCR products were visualized using QuantityOne Software.

2.3.1.5 Agarose Gel electrophoresis for RNA

Each RNA sample required RNA loading dye (Invitrogen) at 1:1 ratio prior to incubate at 65 ºC and then loaded on gel that was prepared same as DNA gel.

2.3.1.6 One-Step RT-PCR (QIAGEN)

The volume of each sample contains:

~500 ng	RNA sample
10 µl	5x QIAGEN OneStep RT-PCR buffer
2.0 µl	dNTP mix (10 mM of each dNTP)
2.0 µl	QIAGEN OneStep RT-PCR enzyme mix
1.0 µl	RNasin (Promega)
0.6 µM	Forward primer
0.6 µM	Reverse primer
X µl	RNase-free water up to 50 µl

Reaction mixes were undertaken in a Thermo Hybaid PCRS print termo-cycler or ThermoHybaid Omnigene. The PCR cycle was; 50 ºC for 30 minutes at the first cycle to allow reverse transcription performing the first strand cDNA, followed by 95 ºC for 15 minutes for reverse transcriptase inactivating and cDNA denaturing. The first strand cDNA was then amplified by 35 cycles of 94 ºC, 55 ºC and 72 ºC respectively for 1 minute each step, eventually, finished reaction with a prolonged extension stage by 1 cycle of 72 ºC for 10 minutes.

2.3.2 Cloning procedure

2.3.2.1 Colony PCR

Colonies were tested by colony PCR experiment using one primer specific to vector and another specific to the insert. Colonies were picked up by sterile pipette tips under

aseptic conditions and mixed in the PCR reaction mixture consequently the mixtures were carried out as described in **Polymerase Chain Reactions (PCR) (2.3.1.3).**

2.3.2.2 Extraction of amplified DNA from agarose gels

DNA bands were visualised and excised from gels under weak UV light. DNAs were extracted using QIAquick Gel Extraction Kit Protocol (QIAGEN).

2.3.2.3 Quantification of nucleic acid concentration

Due to absorbency of nucleic acid concentration 40 mg/ml at OD 260 nm is 1 unit, measuring concentration of nucleic acid. Samples could be estimated by converting absorbency of 100 fold diluted samples at OD 260 nm from absorbency reading. Alternatively, nucleic acid concentrations of samples can be estimated by running on gel with known concentration of DNA for comparison (Bioline HyperLadder I).

2.3.2.4 Ligation of DNA fragments into pET-21b, pDrive vectors

The DNA ratio was 2:1 or 3:1 (insert : vector) were incubated at 16 ºC overnight with 2 µl of 5x ligation buffer (0.5 M Tris-HCl pH 7.6, 100 mM MgCl2, 100 mM dithiothreitol, 500 µg/ml bovine serum albumin), 0.5 µl T4 DNA ligase (Invitrogen) and then made up to 10 µl with SDW.

2.3.2.5 Transformation of competent *E. coli* cells by heat-shock

50 µl competent cells of *E. coli* DH5α or BL21 stored at -80 ºC was gently applied with 2-4 µl of ligation reaction at start melting of competent cells in order to avoid

damaging of the competent cells. The transformation reaction was then incubated on ice for 20-30 minutes after which the competent cells were heat shocked at 42 ℃ for 45 seconds and suddenly incubated on ice for 2-3 minutes for cooling down. The transformed cells were re-covered by adding 600 µl of Lysogeny broth (LB) gently and incubated in 15 ml tube at 37 ℃, 200 rpm shaking for 1 hour. The recovered cells were spread onto an 8 cm LB-agar plates which contained the appropriate selective agents. Plates were then inverted for incubation at 37 ℃ for 16 hours.

2.3.2.6 Purification of plasmid DNA

Wizard plus SV minipreps DNA purification system (Promega) was used for plasmid DNA purification from bacterial cultures. The microcentrifuge protocol was followed by manufactures guidelines.

2.3.2.7 Sequencing of plasmid DNA

The plasmid DNA sequencing was performed by the Functional Genomics Laboratory in the University of Birmingham.

Generally, plasmid DNA sequencing reaction contains:

200-600 ng   Plasmid DNA templates (Wizard prep kit purification)

1 µl   Primer (3 pmol/µl)

x µl   Biological performance certified (BPC) grade water (sigma), up to 10 µl.

2.3.2.8 Sequencing analysis

Chromas software was used to analyse the DNA sequencing. The BLAST functions of WWW.ncbi.nlm.nih.gov (National Centre for Biotechnology Information) web site was used to homology searches. WWW.bioinformatics.org/sms/rev_comp.html was carried out to reverse complementation. WWW.web.expasy.org/translate using ExPASy translation tool for *In silico* translation of DNA to protein sequence.

2.3.2.9 DNA digestion with restriction enzymes

Restriction enzymes were obtained from New England Biolabs or Fermentas. Digestions were performed in appropriate buffers supplied with the enzymes. The length of digestion for plasmid DNA was between 1 hour and 16 hours at 37 °C; for plant genomic DNA was 16 hours at 37 °C. Heat denaturation at 65 °C for 20 minutes was used to inactivate the restriction enzymes in the reactions.

2.3.2.10 DNase I treatment of RNA (Promega)

DEPC water	13 µl
10x DNase I buffer	4 µl
RNasin (RNase inhibitor)	2 µl
Extracted RNA products	20 µl

Mixed all above in RNase-free tube and then added DNase I 1 µl. 40 µl in total reaction was then incubated for 15 minutes at room temperature prior to add 2 µl of 25 µM EDTA and incubated for 10 minutes at 65 °C in order to inactivate DNase I.

2.3.2.11 RNA phenol-chloroform extraction

1 volume of DNase I-treated RNA was added to 1 volume of phenol pH 4.3 and mixed thoroughly in order to move out the remaining proteins. The mixture was then centrifuged at 13,000 rpm for 5 minutes, removed the top layer to a new tube and added 200 µl of chloroform to remove phenol, mixed and spun at 13,000 rpm for 5 minutes and collected the top layer. RNA was precipitated with 1 µl of glycogen in 250 µl of 100% ethanol at -70 ℃ for 30 minutes and then spun down to RNA pellet, washed RNA pellet with 70% ethanol twice eventually left it for drying. The RNA pellet was then resuspended in 20 µl DEPC water.

2.3.3 Protein manipulation

2.3.3.1 Protein extraction from plant tissues

100 mg plant tissue was collected in 50 µl extraction buffer (1% SDS, 50 mM Tris-HCl, 5% β-mercaptoethanol, 1 complete mini EDTA-free protease inhibitor cocktail tablet (Roche) per 10 ml) and snap-frozen in liquid nitrogen. The sample was thawed and homogenized using a pipette tip. The sample was then added 2 µl of 5x protein loading buffer before boiling in a water bath for 5 minutes in order for loading onto SDS-PAGE gel.

2.3.3.2 Protein extraction from *E. coli*

In order to analyse recombinant protein expression, 6 µl recombinant *E. coli* was incubated in 10 ml LB medium containing appropriate antibody at 37 ℃ overnight on

shaker at 200 rpm. The culture was diluted equal volume with LB medium and divided into two flasks, only one flask was applied with 1 mM of isopropylthio-β-D-galactosidase (IPTG) (Sigma) and then incubated both flasks for 6 hours at 37 ℃ on 200 rpm shaker. Each culture was collected 1 ml, centrifuged and the cell pellet was resuspended with 75 μl of Bugbuster Master Mix (Novagen) after which incubated for 30 minutes at room temperature on a rotor. The cell cultures were centrifuged for collecting pellets and supernatants. The pellets were resuspended with 75 μl of SDW; each sample was added 2 μl of 5x protein loading buffer before boiling in a water bath for 5 minutes in order for analysing by SDS-PAGE.

Note: For large scale of protein extractions, it was scaled up.

2.3.3.3 SDS-PAGE gel electrophoresis of proteins

Proteins were analysed using the BioRad self-assembly electrophoresis kits. Gels were prepared in two kinds, the Resolving and the Stacking gel which was on top.

Resolving gel	7.5%	10%	15%
SDW	7.3 ml	6.1 ml	3.6 ml
Tris resolving buffer pH 8.8 (1.5 M Tris)	3.75 ml	3.75 ml	3.75 ml
10% Sodium dodecyl sulphate (SDS)	150 μl	150 μl	150 μl
Acrylamide (Protogel)	3.8 ml	5 ml	7.5 ml
15% (w/v) Ammonium per sulphate (APS)	75 μl	75 μl	75 μl
N,N,N', N'-Tetramethylethylenediamine (TEMED)(Sigma)	15 μl	15 μl	15 μl

In order to remove air-bubbles and level before pouring stacking gel on top, butanol was added to the resolving gel before setting. Butanol was removed by water washing after gel setting and then stacking gel was poured.

> Stacking gel

SDW	3 ml
Tris stacking buffer pH 6.8 (0.5 M Tris)	1.25 ml
10% Sodium dodecyl sulphate (SDS)	50 µl
Acrylamide (Protogel)	625 µl
15% (w/v) Ammonium per sulphate (APS)	25 µl
TEMED (Sigma)	5 µl

N.B. APS was prepared for fresh and TEMED was mixed immediately before pouring.

A gel comb was inserted in the stacking gel and left in the gel for setting. The comb was removed and gel tank was assembled as described in the kit's instructions. Protein samples which were prepared using protein loading buffer and boiled, were loaded in the gel and then run in 1xELFO buffer (25 mM tris, 192 mM glycine, 0.1% SDS, final pH 8.3) at 50 V in stacking gel and 100 V in resolving gel.

2.3.3.4 Coomassie staining

Gels were stained for 1-2 hours with Coomassie Blue (0.1% (w/v) Coomassie R250, 45% (v/v) methanol, 45% (v/v) glacial acetic acid, 10% (v/v) SDW) and de-stained by

de-staining solution (20% methanol, 7% glacial acetic acid in SDW). The visible gels were dried and preserved between cellophane sheets.

2.3.3.5 Isolation of HIS-tagged proteins using Ni-NTA resin (QIAGEN)

The cell pellet sample was thawed and resuspended in 1.35 ml lysis buffer (50 mM Tris, 300 mM NaCl, 20 mM Imidazole, final pH 8), transferred to 2 ml microfuge tube and 150 µl of 10 mg/ml fresh lysozyme was added after which vortexed and incubated on ice for 30 minutes. The lysate was pulse sonicated for 10x5 seconds at 10 units on ice and then centrifuged lysate at 13,000 rpm, 4 ℃ for 15 minutes. As the recombinant proteins were found in insoluble fraction, the inclusion body pellet was retained. The inclusion body pellet was resuspended with 1.4 ml Denaturing lysis buffer (6 M guanidine-HCl, 500 mM cysteamine (2-mercaptoethylamine)) and incubated for 45 minutes at room temperature on rotating wheel.

The translucent slurry was then centrifuged at 13,000 rpm for 20 minutes. The supernatant was transferred to a fresh tube (50 µl was retained for gel analysis as 'before binding') and then 350 µl of Ni-NTA resin slurry was added for 1 hour at room temperature using the rotating wheel. The sample was spun for 2 minutes at 13,000 rpm and the supernatant was removed (50 µl was retained for gel analysis as 'after binding'). Resin-bead sample was washed for three times with 1.4 ml of wash buffer (Denaturing lysis buffer pH 6.3) for 5 minutes at room temperature using rotating wheel followed by a 2 minutes spin at 13,000 rpm (50 µl was retained for gel analysis as 'bead washing'). The HIS-tag attached proteins that were carried by Ni-

NTA resin would be eluted; using 175 µl of elution buffer A (Denaturing lysis buffer pH 5.9) 4 times for 5 minutes on rotating wheel followed by a 2 minutes spin at 13,000 rpm (50 µl was retained for gel analysis as monomer proteins), using 175 µl of elution buffer B (Denaturing lysis buffer pH 4.5) as described in elution buffer A and retained 50 µl as multimer and aggregated proteins.

2.3.3.6 Protein refolding (for denaturing method only)

Protein refolding was required the volume of refolding buffer 100 times greater than the volume of protein. Refolding buffer was: 0.1 M Tris, 2mM EDTA, 0.5 M Arginine HCl, 10 mM Cystamine di-hydrochloride, 5% Glycerol, final pH 8.0. The monomer, multimer and aggregated proteins were pooled and divided to two parts; 50% mixed protein was added very slowly to refolding buffer on a stirrer in the 15 ºC room, allowed to mix for 1 hour before adding the remaining 50% (do not allow the protein to start precipitation) and then left to stand overnight without stirring.

2.3.3.7 Refolding protein analysis

In order to remove of guanidine and any reagents in the refolded protein, refolded protein was added to dialysis tubes and then dialysed against the dialysis buffer (5 L of 50 mM Tris-HCl pH 8, 100 mM NaCl, 2 mM EDTA at 4 ºC), the buffer was changed after 2-3 hours and then left overnight.

2.3.3.8 Reduction dialysed protein volume to final concentration

Dialysis tubes were transferred to a clean plastic tray, sprinkled with PEG 6000 on a shaker at room temperature. PEG was kept adding more in order to be dissolved in liquid being drawn out of the tubing. When the required volume had been reached, the protein was removed from the tubing and aliquots was checked by gel analysis with known concentration of BSA and BioRad assay to ensure it is sufficiently concentrated for raising antibody (the final concentration should be around 1 mg/ml).

2.3.3.9 Quantification of protein using spectrophotometry

Protein was estimated the concentration by the BioRad assay. Protein samples were added with the protein assay reagent (Coomassie Brilliant Blue G-250) and analysed with 595 nm absorbance using a spectrophotometer (Jenway 6305). The protein Ovalbumin 20 µg/ml was used as a standard assay.

2.3.3.10 Antibody production

The protein was frozen in liquid nitrogen and sent to BIOGENES (Germany) for immunizing two rats.

2.3.3.11 Western transfer analysis

The stacking gel part was cut off from SDS-PAGE gel and the resolving gel was transferred onto the same size of 3M paper soaked in electrode buffer (20% methanol, 0.01 M sodium hydrogen carbonate, 3.0 mM sodium carbonate). A nylon membrane (Hybond-C extra (Amersham)) and another 3M paper were cut as same size as

resolving gel and then laid on top the gel respectively. All steps were performed under electrode buffer soaking and removing air bubbles between layers. The stack was sandwiched between two electroblotting pads and clasped in the holder before insertion into the electroblotting tank that was full of electrode buffer. BioRad power packs were used and the proteins were transferred at 400 mA for 1 hour. The membrane was removed to a clean plastic box and blocked with blocking buffer (5% skimmed milk powder (w/v), 0.1% Tween 20 in 10x TBS) on a shaker over night at 4 °C.

2.3.3.12 Antibody probing

The western membrane which was blocked overnight was then incubated in primary antibody (1:1,000 in blocking buffer) for 2 hours at room temperature. Three times washing with blocking buffer for 10 minutes each were carried out with the membrane after which incubated with secondary antibody (1:5,000 in blocking buffer of horse radish peroxidase (HRP)) for 1 hour at room temperature. The probed membrane was washed with blocking buffer for 10 minutes followed by three times washing with TBST (1xTBS, 0.1% Tween 20) for 10 minutes each.

2.3.3.13 Enhanced chemilluminescence (ECL) detection

ECL western blotting detection reagents (Amersham) were used to detect the antibody probed membrane; 1:1 of reagent A and B were mixed and poured immediately over the membrane followed by wrapping the membrane with cling film. The blotted membrane was exposed to photographic film using AGFA CURIX 60 Xograph.

2.3.3.14 Purification antibody using Melon Gel IgG Spin Purification Kit (Thermo scientific number 45260)

500 gel slurry was added into a spin column placed in a micro centrifuge tube and centrifuged at 700 rpm. The gel was washed with 300 µl of purification buffer twice after which added 100-500 µl diluted antibody (1:10 in purification buffer) to the washed column and incubated by end-over-end mixing for 5 minutes at room temperature. The column placed in the centrifuge tube was spun for 1 minute at 700 rpm and then the purified antibody was collected for immunolocalisation.

Chapter 3

Analysis of *Atpch2* mutants

3.1 Introduction

Despite a century of research important aspects of meiosis are not yet understood. In the past decade *Arabidopsis* and rice have become important systems for studying meiosis in flowering plants. The identification of meiotic mutants has provided an important approach to studying plant meiosis. In addition, the availability of the *Arabidopsis* genome sequence together with developments in bioinformatics provides an additional route for the identification of meiotic proteins and analysis of their functional interrelationships. We have used a combination of these approaches to identify candidate meiotic genes and proteins in *Arabidopsis*. As the first stage in their analysis we are conducting a systematic survey of the corresponding T-DNA insertion mutants. Pch2 (Pachytene Checkpoint 2) is a meiosis specific AAA+ ATPase family member. In budding yeast, Pch2 is involved in chromosome axis organisation and regulation of CO formation and distribution (Zanders and Alani 2009). TRIP13 is the mouse Pch2 orthologue and is vital for proper synaptonemal complex formation. In the absence of TRIP13 the frequency of COs and chiasmata is reduced and their distribution is altered (Roig *et al.,* 2010). PCH2 has been studied in many model organisms, e.g. budding yeast (San-Segundo and Roeder, 1999; Mitra and Roeder, 2007; Borner, 2008), *C. elegans* (Bhalla and Dernburg, 2005), *D. melanogaster* (Joyce and McKim, 2009), TRIP13/PCH2 in mouse (Roig *et al*., 2010; Li and Schimenti, 2007). At the start of this project, PCH2 had not previously been studied in plant meiosis. We utilized a bioinformatics approach to identify At4g24710 as a potential

orthologue of Pch2/TRIP13 in the plant model, *Arabidopsis.* We have investigated the meiotic roles of AtPCH2 in *Arabidopsis thaliana*, using T-DNA insertion lines.

3.2 Identifying *Atpch2* mutants

There are many approaches to compromise gene function in various organisms, such as by generating mutations using x-rays or chemical mutagenic agents, like methyl methane sulphonate (MMS). However, these mutations may be not specified to the target gene and require more complicated methods to identify the mutated-gene location and their sequences. T-DNA (transfer DNA) insertion is an alternative approach to generate gene mutation by insertion of mobile DNA elements within a gene. Moreover, these DNA inserts carry a known DNA sequence that can provide a direct route to identify the position of the insertion. One advantage of using the T-DNA insert lines is that the homozygous alleles can be maintained in the form of heterozygous alleles in the plant population (Krysan *et al.*, 1999). The individual plants that are inserted by a particular T-DNA finally can be easily isolated by polymerase chain reaction (PCR) methods. *Agrobacterium tumefaciens* is one of species of bacteria that can infect the host plant by transferring the T-DNA from Ti plasmid to plant genome. The infected cells then form a tumor (called crown gall disease) and produce an essential food as a source of growth and energy for the bacteria. In the same way, researchers can utilize the T-DNA insertion mechanism to disrupt a particular gene of interest.

The SAIL (Syngenta *Arabidopsis* Insertion Library) has produced a population of T-DNA lines that comprises three institutes; Torrey Mesa Research Institute, Syngenta Biotechnology Incorporated and Syngenta Seeds Incorporated, all located in the United States. Researchers can access the database and search for T-DNA insertion lines of a gene of interest at website: www.*Arabidopsis*.org.
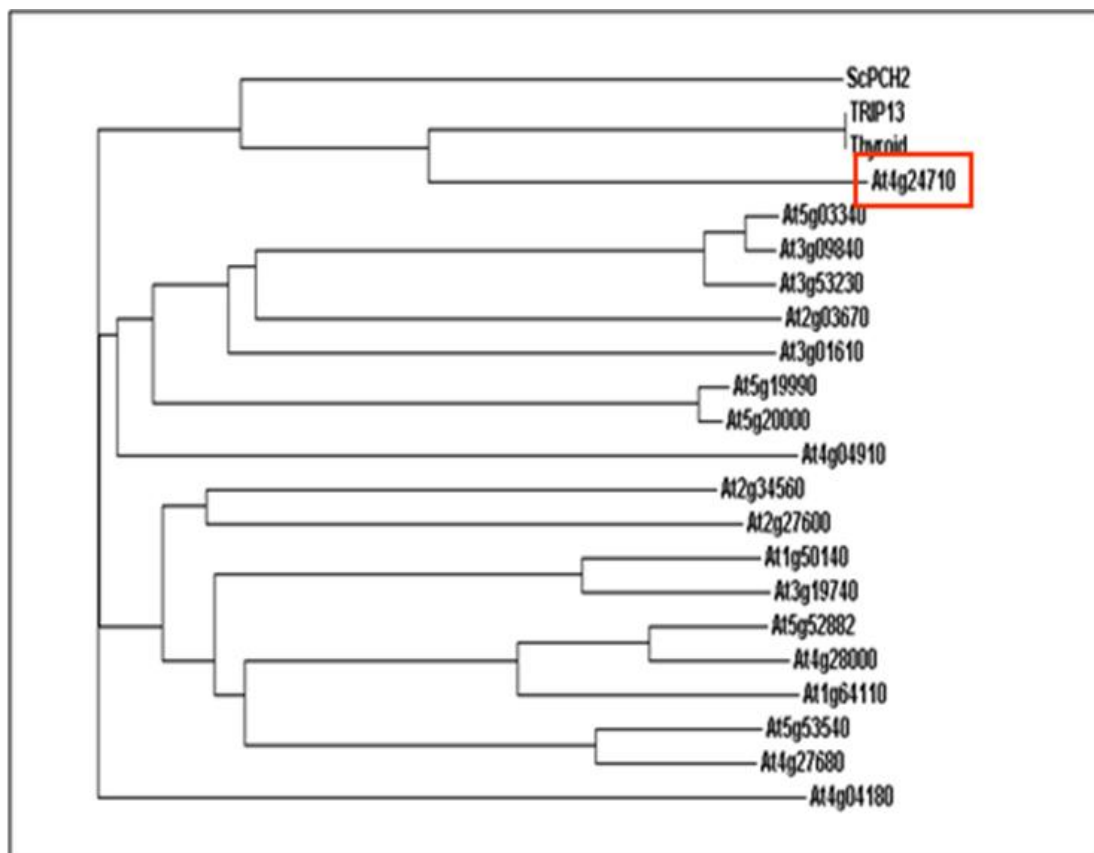
Figure 3. 1: Phylogenetic tree of *Arabidopsis* PCH2/TRIP13-like proteins (ClustalW2).
Pch2 (Pachytene Checkpoint 2) is a meiosis specific AAA+ ATPase family member in budding yeast. TRIP13 is the mouse Pch2 orthologue. At4g24710 (Red box) was identified as a potential orthologue of Pch2/TRIP13 in *Arabidopsis* (Roig *et al*., 2009).

A bioinformatics approach was used to identify At4g24710 as a potential orthologue of Pch2/TRIP13 in *Arabidopsis* (**Figure 3.1**). In a parallel study we identified 10

peptides giving 25% coverage (124/490 amino acids) using mass spectrometry of a putative PCH2 orthologue (Bra 013827) from *Brassica oleracea* as a co-precipitating component of a meiotic complex pulled-down by the axis-associated protein, ASY1 (K. Osman unpublished data). Comparison of the Brassica gene and *Arabidopsis* PCH2 orthologue revealed that they were 87% identical and 91% similar at the amino acid level. We identified T-DNA insertion lines that will be referred to as *Atpch2* in this project. Three T-DNA insertions were identified in At4g24710: *Atpch2.1* (N843942, SAIL_1187_C06) is inserted downstream from the putative start codon ATG ~500bp in the third exon; *Atpch2.2* (N531449, SALK_031449) is inserted downstream from the start codon ~1,900bp in the intron; *Atpch2.3* (N630138, SALK_130138) is inserted downstream from the start codon ~1,700bp in the intron (**shown in Figure 3.2**). These inserted lines were screened and confirmed using PCR for genotyping of individual plants prior to analysing their fertility and chromosomal behaviour compared to that of wild type.
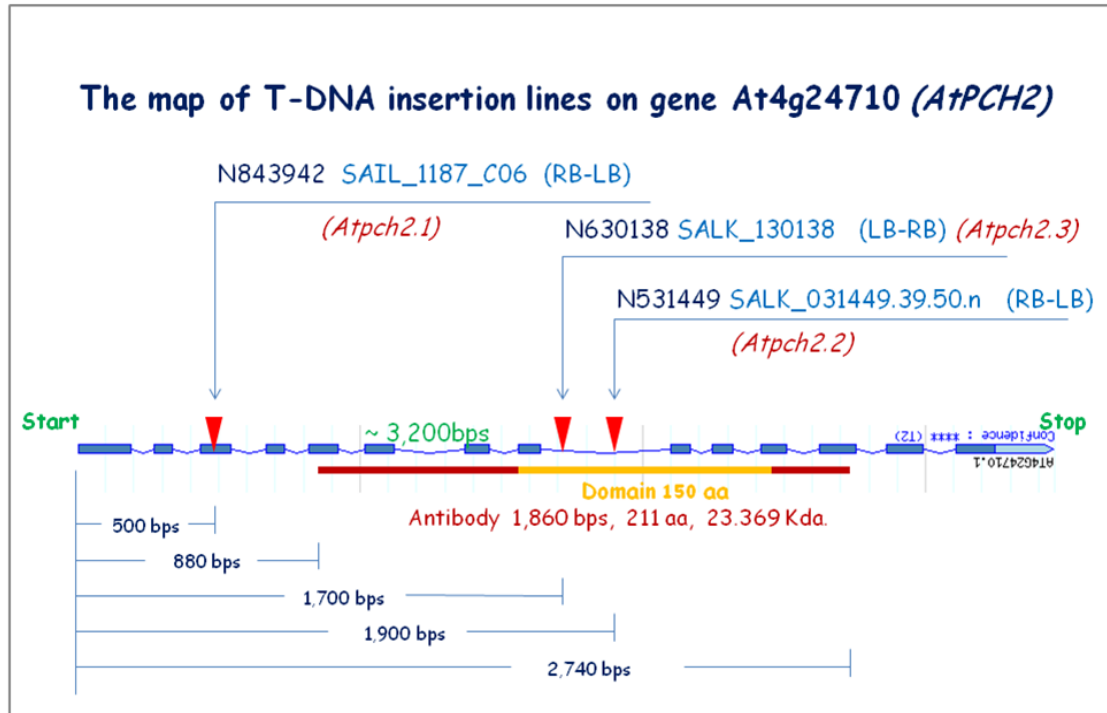
Figure 3. 2: The map of T-DNA insertion lines on gene At4g24710 *(AtPCH2).*
The map shows three positions of T-DNA insertion(orange triangle) on At4g24710 (blue bar) as well as the position of AAA+ATPase domain (yellow bar) and the region that used to perform antibody production (red bar). The gene structure is taken from SALK website.

3.3 Characterisation of *Atpch2* T-DNA insertion lines

Under standard greenhouse conditions, all alleles of *Atpch2* mutants and wild type were sown in the pots at the same area. The vegetative growth of *Atpch2.1* was normal compared to wild type (data not shown). However, the siliques of *Atpch2.1* showed a large number of gaps inside and their length was obviously much shorter than those of wild type with 1.41 ± 0.06 cm.(mean $\pm$ sd) and 1.66 ± 0.05 cm. (mean $\pm$ sd) in wild type. As a result, the number of seeds per silique was reduced to around a half, 34.60 ± 4.22 (mean $\pm$ sd) compared to 67.82 ± 3.40 (mean $\pm$ sd) in wild type (**Figure 3.3**).

These phenotypic characteristics were very similar for *Atpch2.2* and *Atpch2.3* in all individual plants (data not shown). The defects of both silique length and fertility in *Atpch2* indicate that *AtPCH2* is required for reproductive process in *Arabidopsis*.
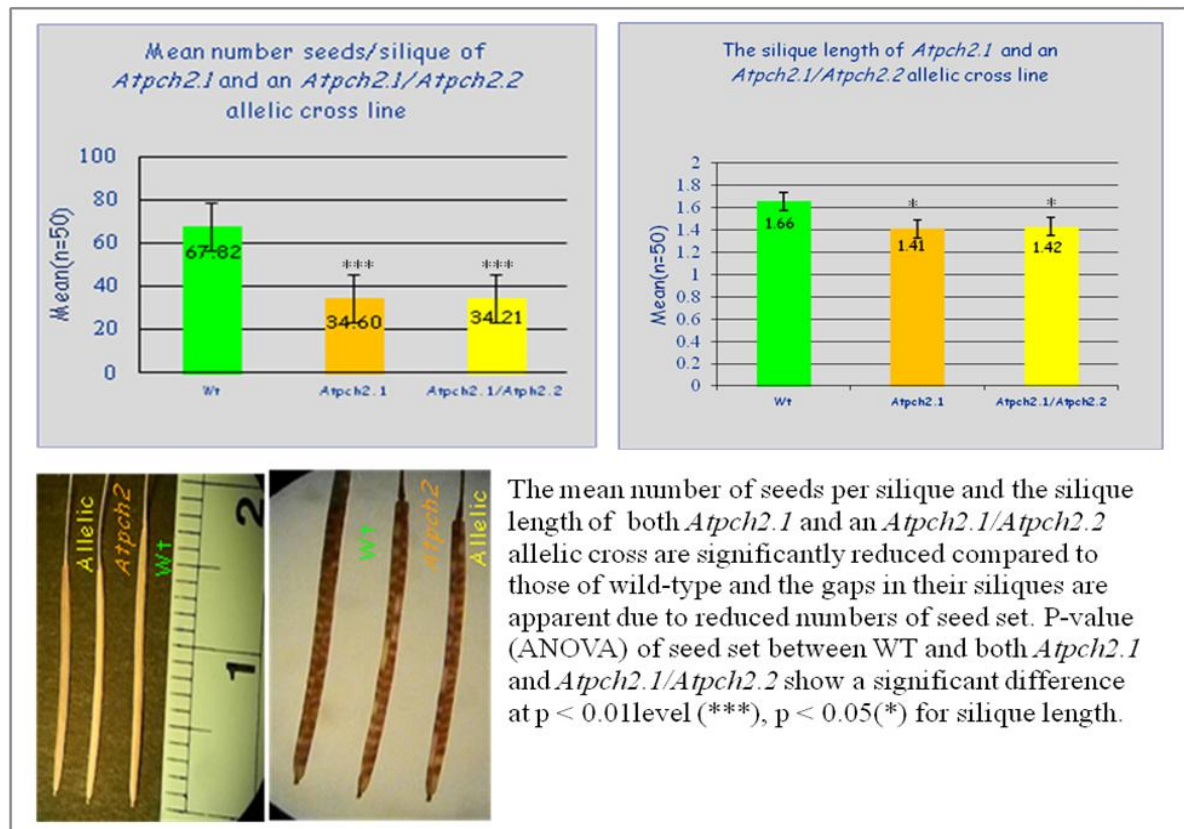
Figure 3. 3: The reduction of fertility and silique length in *Atpch2*.

3.4 Cytological Characterisation of *Atpch2* mutants

As the T-DNA insertion lines analysed, N843942, N630138 and N531449, were shown to be very similar in terms of fertility and cytogenetic phenotype. The detailed analysis presented here in focuses on line N843942. A meiotic atlas of DAPI- stained

pollen mother cells (PMCs) of *Arabidopsis* wild-type was obtained to compare the

pattern of normal chromosome behaviour against that of the mutant lines (**Figure 3.4**).
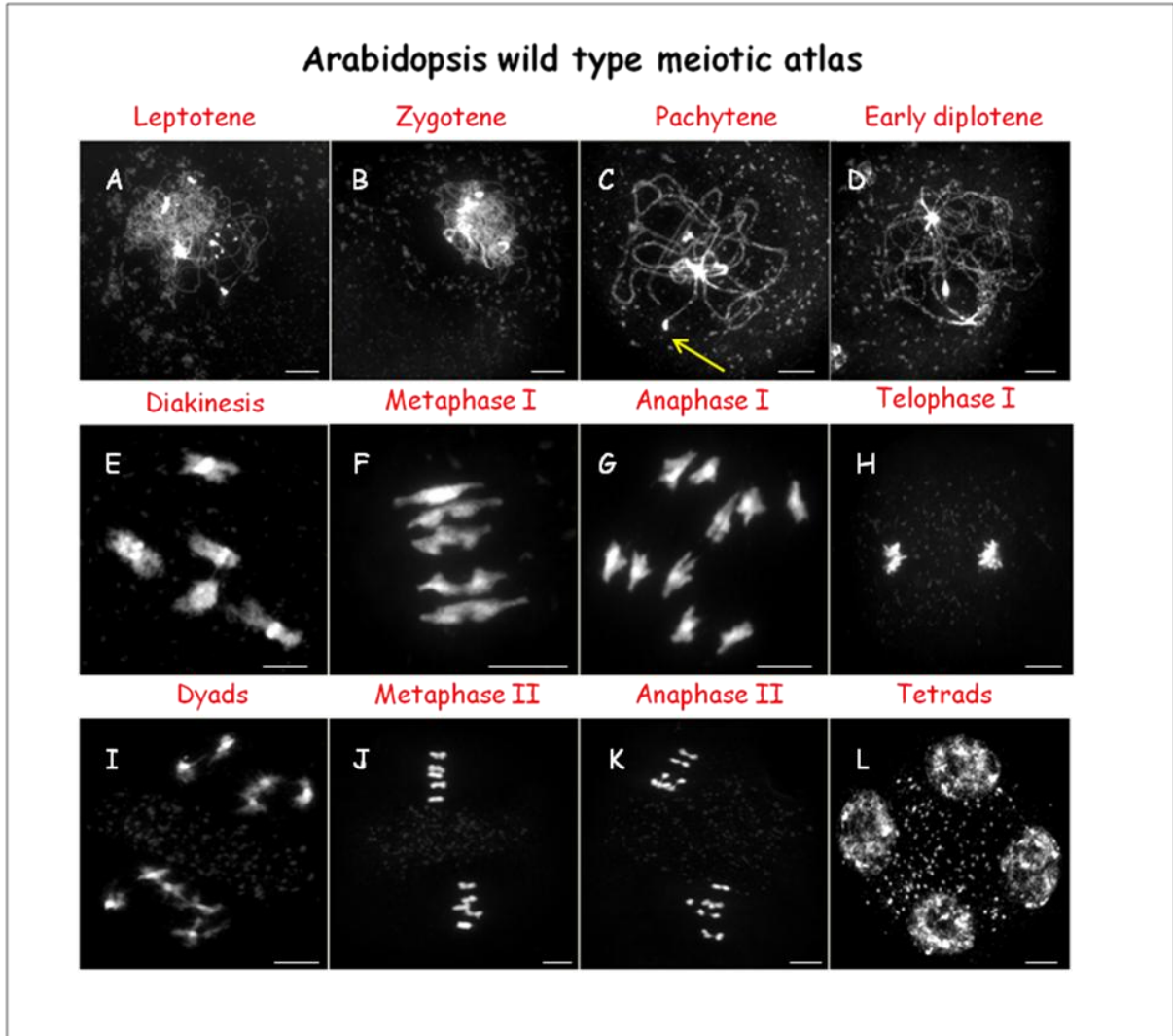
Figure 3. 4: An atlas of meiotic chromosome behaviour in wild-type *Arabidopsis*.
Meiotic atlas from spread and DAPI-stained pollen mother cells of *Arabidopsis* Col 0
(2n=10) has been used to as standard pattern of normal chromosomal behaviours in
Arabidopsis meiosis for characterizing the mutant lines. (**A**) At leptotene, the
chromatin is seen as thin line and scatters out of the nucleus. The nucleolus is
unstained and occupies the nuclear volume around a third. (**B**) During zygotene,
chromosomes appear clumpy and are located at one side of nucleus. Homologous
chromosomes initiate pairing and partially synapsed chromatin can be visualized. (**C**)
At pachytene, chromosomes are more condensed as completely synapsed structures.
As a result, all chromosomes are obviously visible and traced. The yellow arrow
shows nucleolar organizing regions (NORs), the association of two NORs, which are
located on the subtermini of the short arms of chromosome 2 and 4 (Armstrong and
Jones, 2002). All chromosomes appear to be desynapsed at early diplotene (**D**) and

75

gradually condensed at late diplotene, and then they become fuzzy bivalents at diakinesis (**E**). At this stage, chromosomes condense continually to give the highest condensed bivalents at metaphase I (**F**). The metaphase I bivalents line up on the spindle equator. (**G**) During anaphase I, homologous chromosomes separate from each other and move to the opposite poles becoming telophase I (**H**). At this stage, sister chromatids of each chromosome still associate together at centromere regions (Armstrong and Jones, 2002). On either side of band of cytoplasmic organelles, there are five condensed chromosomes co-oriented on the spindle equator at metaphase II (**J**). Subsequently, (**K**) anaphase II shows sister chromatids separation in progress. The four polar groups of five chromatids at telophase II gradually decondense and re-form into tetrads of haploid nuclei (**L**). Scale bar = 5 µm.

By comparison with wild-type, DAPI- stained pollen mother cells of *Atpch2* appeared

normal at interphase and leptotene (data not shown). However, a variety of defects was

identified in male meiocytes cytogenetic analysis. The homologous chromosome pairs

of *Atpch2* at pachytene presented defects with some regions apparently remaining

unpaired (**Figure 3.5**). This defect leads to a high frequency of univalents to be

observed from diplotene to metaphase I (**Figure 3.6**) and eventually chromosome

missegregation (**Figure 3.7**).
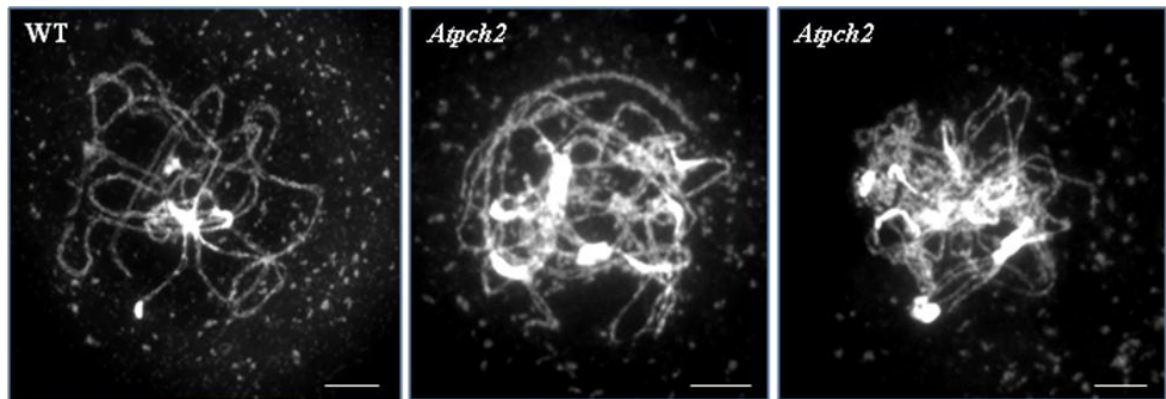
Figure 3. 5: Some regions of homologous chromosomes were unpaired at pachytene. Scale bar = 5 µm.
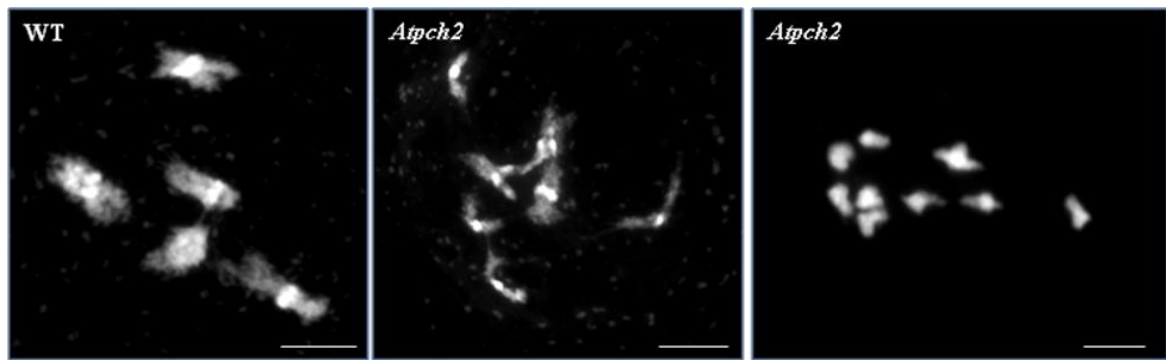
Figure 3. 6: Examples of univalents were observed at Diplotene and MI.
At diplotene and MI a high frequency of univalents is observed. Scale bar = 5 µm.
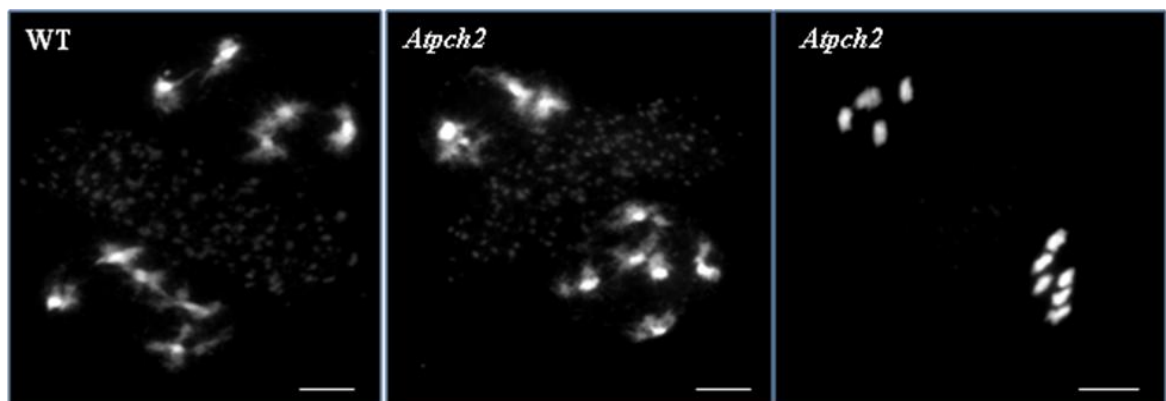
Figure 3. 7: Reduced numbers of COs lead to chromosome mis-segregation
Chromosome mis-segregations were observed in *Atpch2* during meiosis II. Scale bar = 5 µm.

3.5 Chiasma frequency in *Atpch2* mutants

To determine the effect of the *Atpch2* mutation on CO formation, chiasma counts were conducted at metaphase I. Fluorescence *in situ* hybridization (FISH) using 45s and 5s rDNA probes reveals that the univalents found in *Atpch2* meiocytes were not restricted to any one chromosome. Each chromosome was observed to be affected to different degrees (**Figure 3.8**). Univalents of specific chromosomes could be identified using FISH, and the number of chiasmata scored (**Table 3.1**). This table shows that the P-values (ANOVA) of chiasma frequency per chromosome of *Atpch2* are significantly less than the wild-type at the 1% level, except chromosome IV, and reduced to around 70% in total (9.60 in wild-type and 6.94 in *Atpch2*). Although the P-value of Chromosome IV between wild-type and *Atpch2* is not a significant difference at the 5% level, univalents were observed at metaphase I in 2 out of 50 meiocytes (**Table 3.1**). Furthermore, the chiasma distribution along *Atpch2* chromosomes was analysed and appeared to be altered (**Table 3.2**). In chromosome I, while the chiasma frequency of *Atpch2* was reduced to around a half of the wild-type at distal sites, it was a similar frequency at interstitial sites. In chromosome II, the chiasmata of *Atpch2* were reduced along the long arms, whereas they were in similar number on the short arms compared to the wild-type. In chromosome III and V seemed to be parallel in terms overall of a chiasma frequency reduction. Though the chiasmata of *Atpch2* chromosome III and V at distal sites were decreased to 3 out of 4, they were reduced with a same level to a half at interstitial sites compared to the wild-type, and also displayed similarity in the number of univalents (3 and 4 univalents in chromosome III and V respectively).

Interestingly, on chromosome IV, the chiasma frequency on the long arms of *Atpch2* was the same as wild-type at distal sites but reduced by ~50% at interstitial sites. In contrast, the chiasma frequency was increased at distal sites on the short arms from 25 in wild-type to 38 in *Atpch2*.
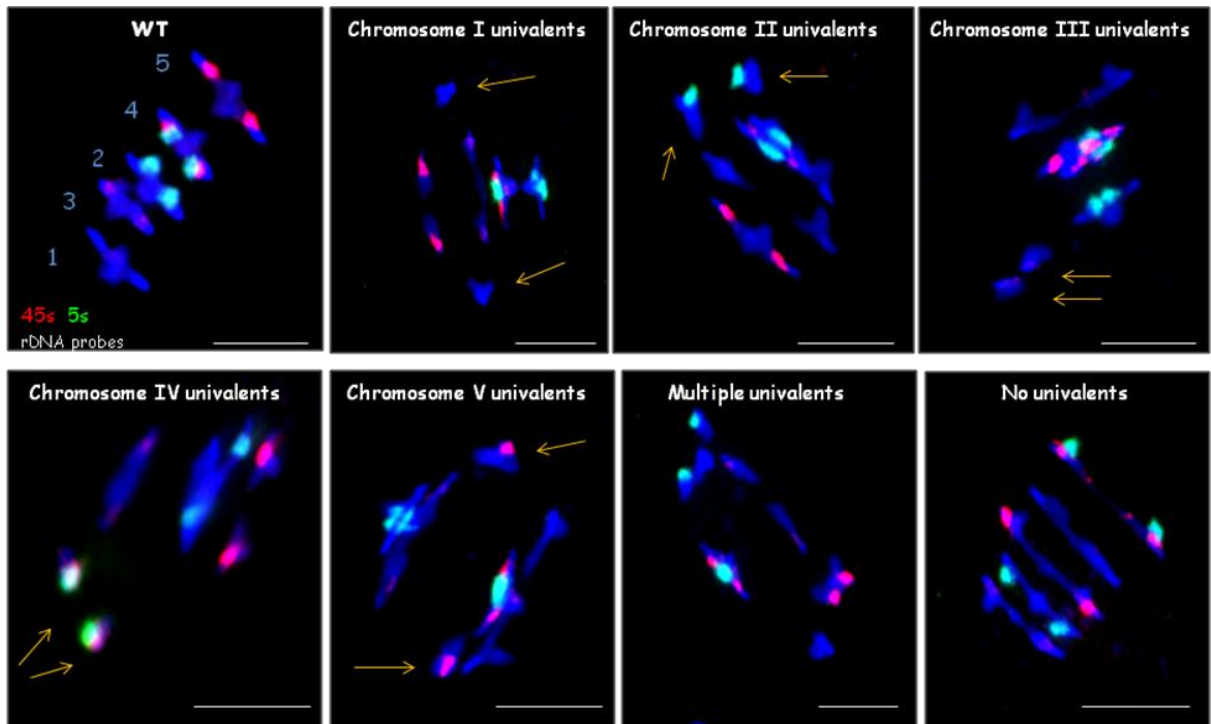
Figure 3. 8: FISH analysis shows univalents in *Atpch2*.
Fluorescence in situ hybridization using 45s and 5s probes reveals a failure of crossover formation in chromosome spread preparations of meiocytes from an *Atpch2* mutant. The univalent defect was not specific to any chromosome (yellow arrows show the univalents of each chromosome), moreover, the defect showed varying degrees such as one univalent, multiple univalents and no univalents in individual meiocytes. Scale bar = 5 μm.

Chiasma Scoring using FISH to identify chromosomes						
	Chrm I (mean)	Chrm II (mean)	Chrm III (mean)	Chrm IV (mean)	Chrm V (mean)	Total
WT 50 cells	2.12	1.74	2.02	1.80	1.92	9.60
Atpch2 50 cells	1.24	1.24	1.36	1.76	1.34	6.94
P-value (ANOVA)	(***) 4.2E-11	(***) 3.6E-4	(***) 6.9E-9	N.S. 0.76881	(***) 7.7E-6	(***) 2.0E-3

Table 3. 1: Chiasma scoring using FISH to identify chromosomes
P-value (ANOVA) of all chromosomes between wild-type and *Atpch2* show a significant difference at $p < 0.01$ level except chromosome IV: (***) is significant difference at $p < 0.01$ level, N.S. is non-significant difference (n=50).

	WT (50 cells)	***Atpch2* (50 cells)**
Chromosome I	d = 83 , i = 23 Uni = 0 Mean = 2.12	d = 42, i = 20 Uni = 7 Mean = 1.24
Chromosome II	S d = 23, i = 0 L d = 37, i = 27 Uni = 0 Mean = 1.74	S d = 22, i = 0 L d = 21, i = 19 Uni = 9 Mean = 1.24
Chromosome III	d = 80, i = 21 Uni = 0 Mean = 2.02	d = 57, i = 11 Uni = 3 Mean = 1.36
Chromosome IV	S d = 25, i = 0 L d = 33, i = 32 Uni = 0 Mean = 1.80	S d = 38, i = 0 L d = 33, i = 17 Uni = 2 Mean = 1.76
Chromosome V	d = 79, i = 17 Uni = 0 Mean = 1.92	d = 58, i = 9 Uni = 4 Mean = 1.34

Table 3. 2: The chiasma distribution along chromosome wild-type and *Atpch2*
The chiasma distribution was scored at MI using FISH analysis (n=50). All *Atpch2* chromosomes appeared to be altered in chiasma distribution to different degrees.
Note: i = interstitial, d = distal, S = short arm, L = long arm, Uni = univalents.

3.6 Bridges at anaphase/telophase I on chromosome IV in *Atpch2* may indicate the specific defects

Although chromosome IV of *Atpch2* exhibited a non-significant difference in chiasma frequency compared to wild-type, the chiasma distribution was altered on the short arms in the opposite way to the other chromosomes mentioned above. Moreover, a large proportion (8/21) of chromatin bridges was observed on chromosome IV in male meiocytes at anaphase I/telophase I (**Figure 3.9**). These were restricted to this chromosome.
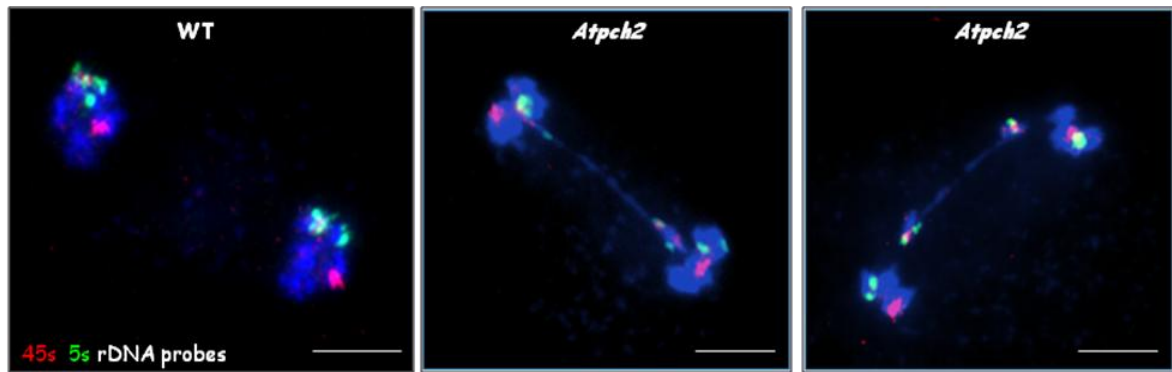
Figure 3. 9: Bridges at anaphase/telophase I in *Atpch2*
Fluorescence *in situ* hybridization revealed a large proportion of bridges of chromosome IV at anaphase/telophase I in *Atpch2*. Scale bar = 5 µm.
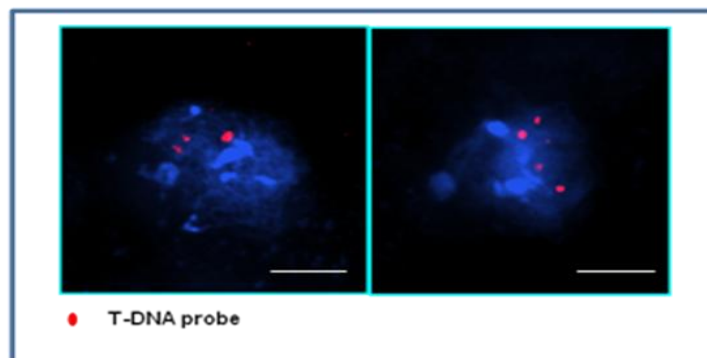
Figure 3. 10: Multiple T-DNA insertions in *Atpch2*

FISH analysis using T-DNA probes (red signals) revealed that *Atpch2.1* line has more than one site of T-DNA insertion in the genome. Scale bar = 5 µm.

3.7 Allelic cross line of *Atpch2* mutants

FISH analysis using T-DNA probes showed multiple signals revealing that there was more than one site of T-DNA insertion within *Atpch2* genome (**Figure 3.10**). In At4g24710 (*AtPCH2*), PCR determination using gene specific primers and T-DNA insertion primers found three homozygote T-DNA insertion lines, N843942 (SAIL_1187_C06) , N531449 (SALK_031449) and N630138 (SALK_130138) (**Figure 3.2**). All lines presented the appearance of phenotype, fertility and chromosome behaviours in meiosis consistent with the original line, N843942 (SAIL_1187_C06). However, to verify that the defects in the original line occur because of mutation to At4g24710 by T-DNA insertion, an allelism test was performed. An allelism test is a cross between two different T-DNA insertion alleles of the gene under investigation. If the allelic cross *(Atpch2.1/Atpch2.2)* has the same phenotype as the individual parents then it confirms the observed phenotype is due to loss of function within the gene (*AtPCH2*). This experiment used *Atpch2.1* (SAIL_1187_C06) line and *Atpch2.2* (SALK_031449) line to do an allelism test (**Figure 3.11**). The chromosomal behaviour of an *Atpch2.1/Atpch2.2* allelic cross in meiosis confirms that the observed phenotypes of the original line *Atpch2.1* is a direct result of an *AtPCH2* defect.
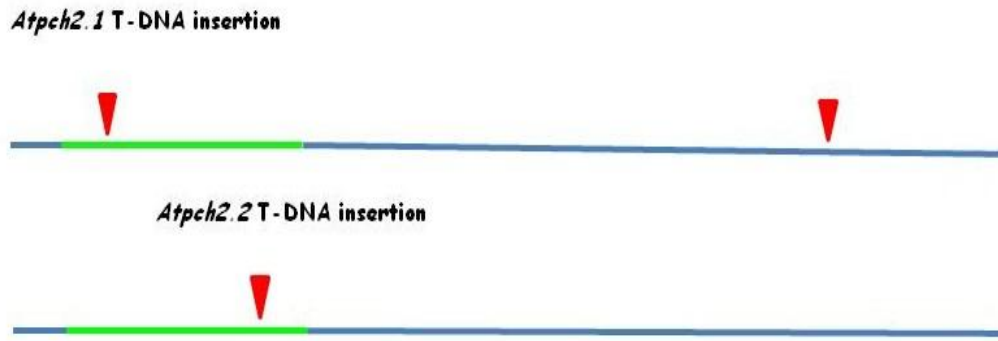
Figure 3. 11: An allelic cross model
An allelism test was performed by crossing two different T-DNA insertion alleles *Atpch2.1* and *Atpch2.2* on At4g24710 (green bars). Both chromosomes carry different T-DNA insertions in an *Atpch2.1/Atpch2.2* line.
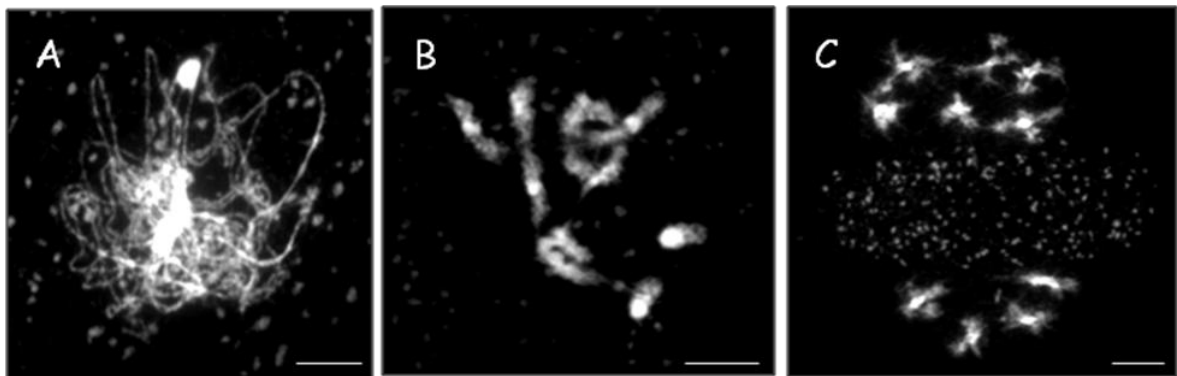
Figure 3. 12: Chromosomal behaviours of an *(Atpch2.1/Atpch2.2)* allelic cross in meiosis. DAPI stained pollen mother cells of the Atpch2.1/Atpch2.2 allelic cross show the same phenotype as the individual parents. Homologous chromosomes are unpaired in some parts at pachytene (A) and a high frequency of univalents was observed at diplotene (B) and chromosome mis-segregation at meiosis II (C). Scale bar = 5 μm.

3.8 RT-PCR: Transcriptional analysis of the *Atpch2* mutant

Reverse transcription polymerase chain reaction (RT-PCR) is one of many techniques used to detect RNA expression levels in various tissues (Freeman *et al.*, 1999). RNA was extracted from *A. thaliana* wild-type bud, leaf, stem and root as well as *Atpch2* bud and leaf (**Figure 3.13**). Using primers specific to the region downstream from T-DNA insertion (*Atpch2.1*) on *AtPCH2* (P1 and P2, **Figure 3.17**), RT-PCR was performed using a one-step RT-PCR kit (Qiagen$^{®}$) that the first strand cDNA is synthesized prior to the amplification of the cDNA template is continuously performed in one reaction. *AtGAPD* (glyceraldehydes-3-phosphate dehydrogenase) is a house-keeping gene that is expressed at the same levels in all *Arabidopsis* tissues (Agashe *et al.*, 2002), and primers for *AtGAPD* were in a parallel RT-PCR to *AtPCH2* for assessing the amount of RNA in each interesting tissues. To eliminate DNA contamination that would be amplified at the cDNA amplification step, DNase1 was used to treat the extracted RNA. The DNase1 was finally inactivated by EDTA at 65 ℃ for 10 minutes. All proteins and other reagents can be eliminated by phenol pH 4.3 in DEPC-SDW and the phenol was removed by chloroform. Treated RNA was then precipitated with glycogen and cold ethanol. The purified RNA from all tissue samples of wild-type and *Atpch2* were first checked to be DNA free by standard PCR with primers (using P5, P6; shown in Materials and methods). The result suggested that the RNA was DNA-free (**Figure 3.14**) and RT-PCR was performed with *AtGAPD* primers. These reactions were run simultaneously in the same thermal cycler with *Atpch2* primers and AtGAPD primers. 10 ul of all RT-PCR products were run on a 1%

agarose-TBE gel and relative band intensities were compared (**Figure 3.15**). The expression analysis showed that *AtPCH2* is transcribed in both reproductive and vegetative tissues. This result indicates a potential role during reproduction for AtPCH2. In theory, RT-PCR products of *Atpch2* should not be amplified from *Atpch2* RNA, due to the T-DNA insertion. In this experiment, however, the expression of P1, P2 specific region was observed in *Atpch2,* producing 2 products, (**Figure 3.15, blue arrows**) are the same size as the wild-type product and an extra band which was roughly 100 base pairs larger.

To investigate this result, sequence analysis was performed. The RT-PCR product from *Atpch2* bud was ligated into the pDrive vector and transformed to DH5α competent *E. coli* cells following by spreading onto x-gal treated agar plates. Colony PCR and gel electrophoresis were used to screen the bacterial colonies that could be carrying the P1P2 specific region and the extra region. Prior to sequence analysis, plasmid DNA from 4 colonies was extracted using a Wizard miniprep kit (Promega). **Figure 13.16 (A)** shows that colonies 1, 2 and 4 were carrying the P1P2 specific regions of *Atpch2*, whereas colony 3 was carrying the extra region. **Figure 13.16 (B)** shows the products that EcoRI used to restriction digest miniprep DNA. The plasmid DNA of colonies 1 and 3 were sequenced with M13 forward and M13 reverse primers. The result of the sequence analysis reveals that the P1P2 specific region on *Atpch2* can transcribe two kinds of mRNA. The first mRNA is (**show sequence in 13.18**) the same size as the wild-type mRNA (422 nt) and the second one is wild-type mRNA plus the

first intron of At4g24710 (422+93 nt) which is consistent with the observed band sizes

of them on 1% agarose-TBE gel (**Figure 3.15**). Although T-DNA-inserted At4g24710

produces RNA products, these are part of a region downstream from the T-DNA

insertion site (**Figure 3.17**). To further investigate the expression of *Atpch2*, P7 and P8

were designed upstream and downstream of the T-DNA insertion site respectively, to

perform RT-PCR using purified RNA from bud and leaf tissues of *Atpch2*, and bud

tissue of wild-type as a control reaction (**Figure 13.17**). This result clearly shows that

this region of *Atpch2* has no RNA products, in other words, T-DNA insertion prevents

transcription of full-length *AtPCH2*. In terms of protein function, the fertility and

meiotic chromosome behaviour defects in *Atpch2* are good evidence to support the

failure of protein function of *AtPCH2* in *Atpch2.1*. The RNA expressed from P1P2

specific region may be promoted by a promoter within the T-DNA or an enhancer

located elsewhere, however these RNA products may be confronted by frame shifted

reading of nucleotides within the sequence caused by loss or gain of nucleotides.
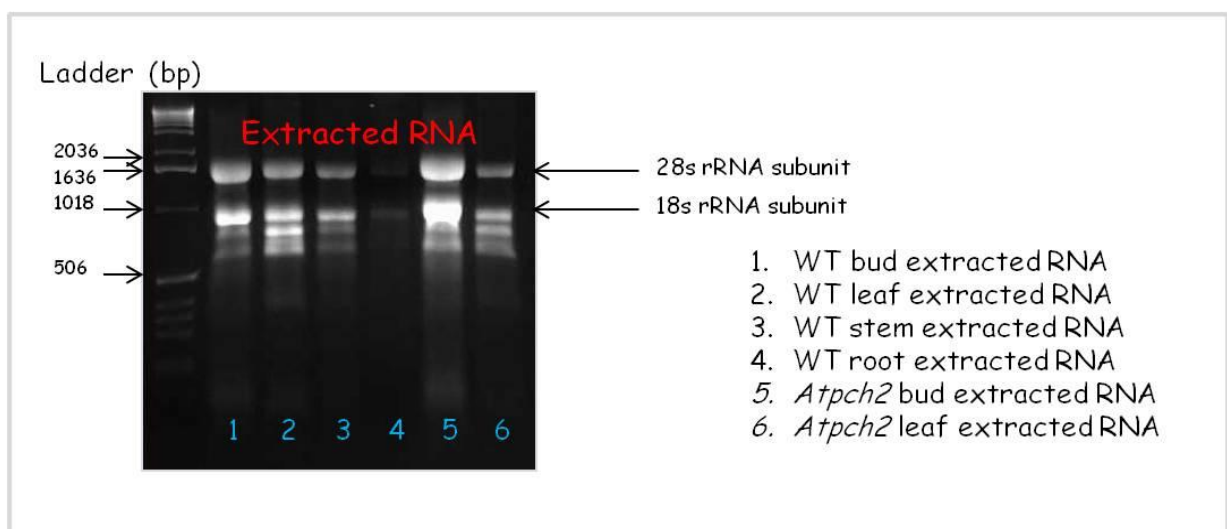
Figure 3. 13: Extracted RNA from 6 different tissues.

The success of RNA extraction from wild-type and *Atpch2* tissues was confirmed by the size of bands of extracted RNA samples corresponding to 28s and 18s rRNA subunits in 1% agarose-TBE gel electrophoresis. Each well shows different tissue samples numbered 1-6.
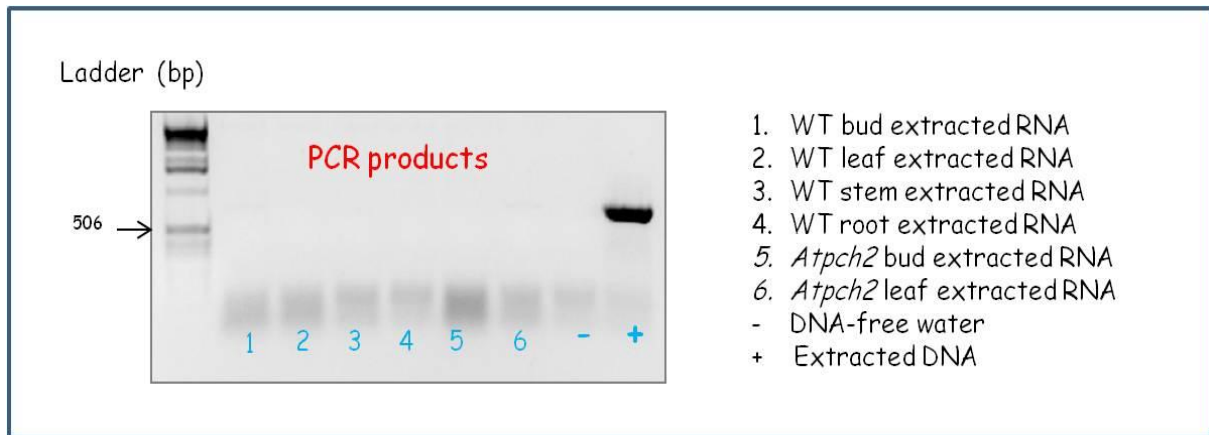
Figure 3. 14: Extracted RNA confirmed to be DNA free.
PCR products using P5P6 primers presented negative results with all extracted RNA samples as well as negative control, whereas the positive control exhibited positive result. This can verify that all extracted RNA samples are DNA-free.
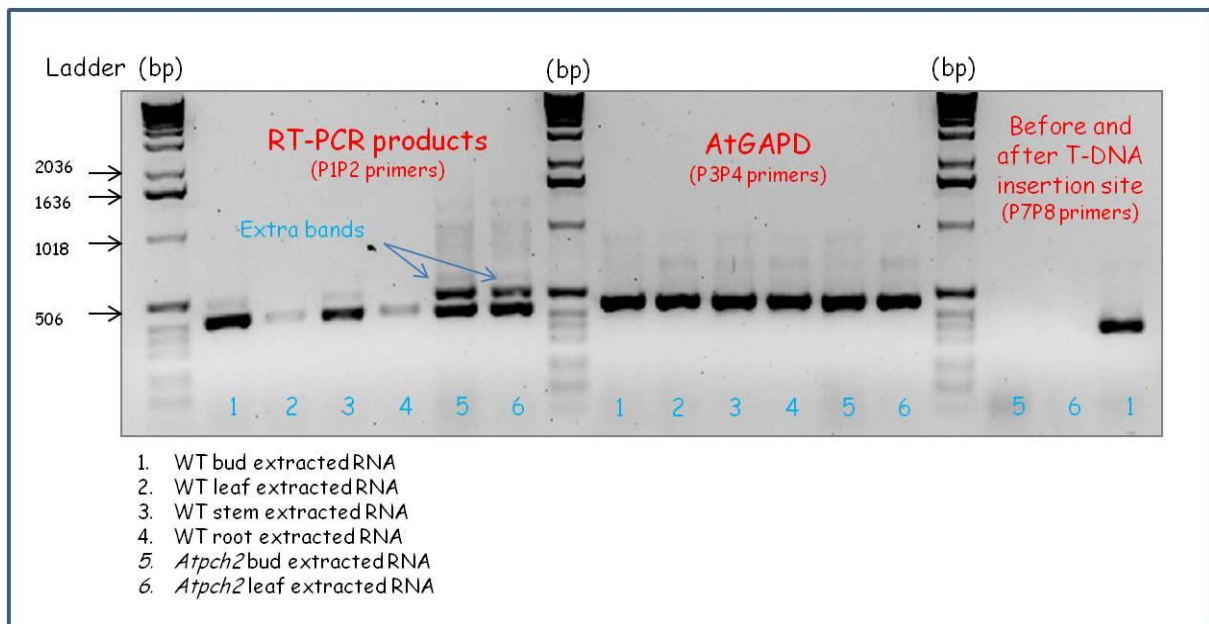
Figure 3. 15: RT-PCR
RT-PCR products using P1P2 primers presented amplified bands at the expected size, 422bps, in all sample tissues except *Atpch2* bud and *Atpch2* leaf which presented extra bands of around 500 bps (blue arrows). RT-PCR products using *AtGAPD* primers (P3P4) exhibited equal band brightness all sample tissues. RT-PCR products using

specific primers (P7P8) for upstream and downstream of the T-DNA insertion site, presented negative results with *Atpch2* bud and *Atpch2* leaf extracted RNA, while presented positive results with wild-type bud extracted RNA.
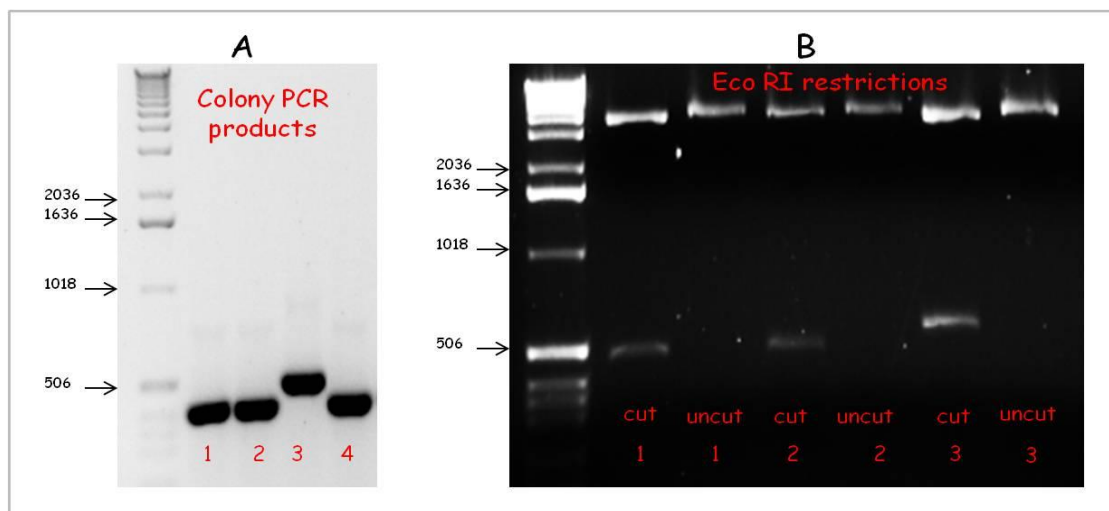
Figure 3. 16: Colony PCR products and EcoRI restriction products
(**A**) Colony PCR products from 4 colonies of DH5α transformed with pDrive containing the RT-PCR products showed amplified bands of the expected size in colonies 1, 2 and 4, while colony 3 presented an extra band. (**B**) *EcoRI* was used to restriction digest miniprep DNA.
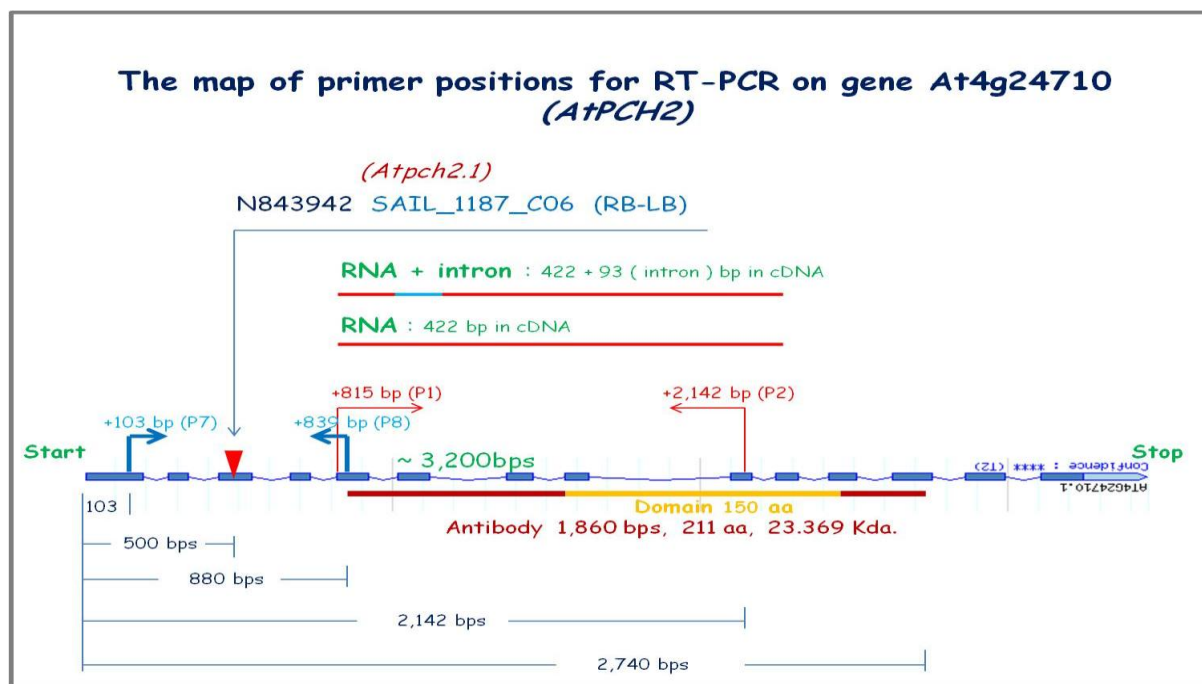
Figure 3. 17: Primer positions for RT-PCR on gene At4g24710 *(AtPCH2)*

The map shows primer positions of P1P2 and P7P8, and also the positions of 2 RT-PCR product sequences which were amplified from a part of *AtPCH2* detected by P1P2 primers. Sequencing analysis revealed that one RT-PCR product sequence consists of all exonic sequence (P1P2, 422 bps), while another RT-PCR product sequence comprises the same sequence plus the first intron of the gene (P1P2, 422+93 bps).

Figure 3. 18: The positions and details of primers and products in At4g24710 sequence involved in RT-PCR experiment.

The full sequence of gene At4g24710 *(AtPCH2)* shows T-DNA insertion site SAIL_1187_C06 (RB-LB) in red arrow, P7 in green box, P8 in yellow box, P1 in blue

letters, P2 in purple letters, the RT-PCR product sequence from colony 1 is presented in red letters plus P1P2, while the RT-PCR product sequence from colony 3 comprises of RT-PCR product sequence from colony 1 plus intron which is presented in green letters.

3.9 Immunolocalisation: functional analysis of *Atpch2* mutants

3.9.1 ASY1 and ZYP1 organization altered in *Atpch2*

To investigate the axis defects of chromosomes in prophase I in *Atpch2*, immunolocalisation on spread chromosomes of *Arabidopsis* wild-type (WT) and *Atpch2* PMCs were carried out for comparison. Immunolocalisation was performed using antibodies raised against the chromosome axis protein, AtASY1 (Caryl *et al*., 2000), and the synaptonemal complex (SC) central element protein, AtZYP1 (Higgins *et al*., 2005). Immunolocalisation of AtASY1 and AtZYP1 in *Atpch2* appeared abnormal compared to wild-type (**Figure 3.19**). In wild-type, AtZYP1 starts localizing as small foci prior to SC polymerization and then extends between the axes of homologous chromosomes during zygotene, juxtaposing them. At pachytene, SC polymerization is complete and AtZYP1 is continuous along the length of homologous chromosomes (Osman *et al*., 2011). The occurrence of AtASY1 is presented earlier than AtZYP1 foci. At early leptotene, AtASY1 foci are observed on the axial elements and then present on both sides of AtZYP1 at pachytene (Ma, 2006). The association between AtASY1 and AtZYP1 in wild-type, AtASY1 seemed diffuse where AtZYP1 had localized along chromosomes at pachytene. In contrast, AtASY1 persisted to co-localise with AtZYP1 in *Atpch2* (**Figure 3.19**). This suggests that AtASY1 and

AtZYP1 organization was altered in *Atpch2*. Furthermore, AtZYP1 polymerized continually along homologous chromosomes until full length at late pachytene in wild-type, whereas in *Atpch2*, AtZYP1 polymerization was observed in small patches and complete AtZYP1 polymerization was not observed, suggesting *Atpch2* may be defective in chromosome synapsis.
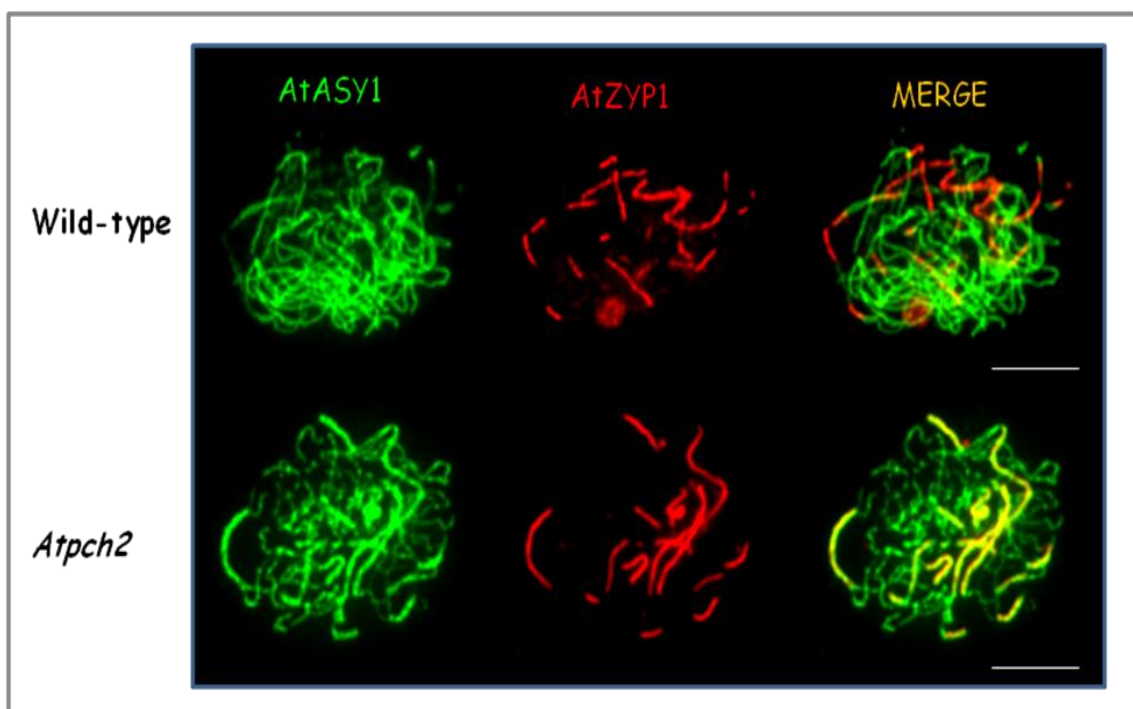
Figure 3. 19: Immunolocalisation of AtASY1 and AtZYP1.
Scale bar = 5 µm.
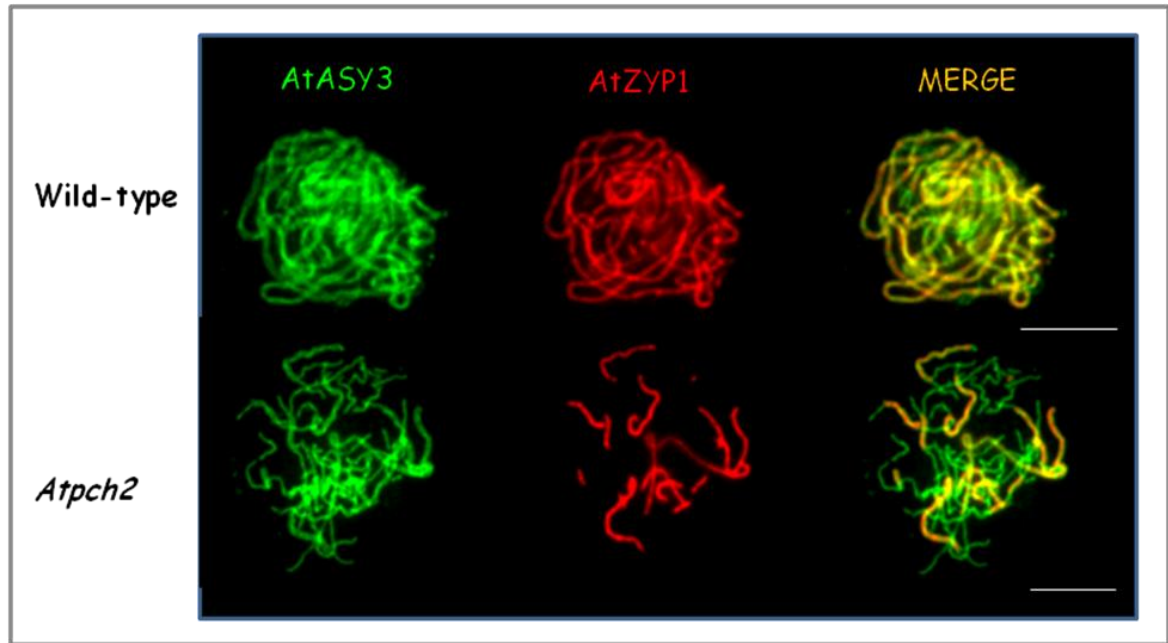
Figure 3. 20 Immunolocalisation of AtASY3 and AtZYP1.
Scale bar = 5 µm.
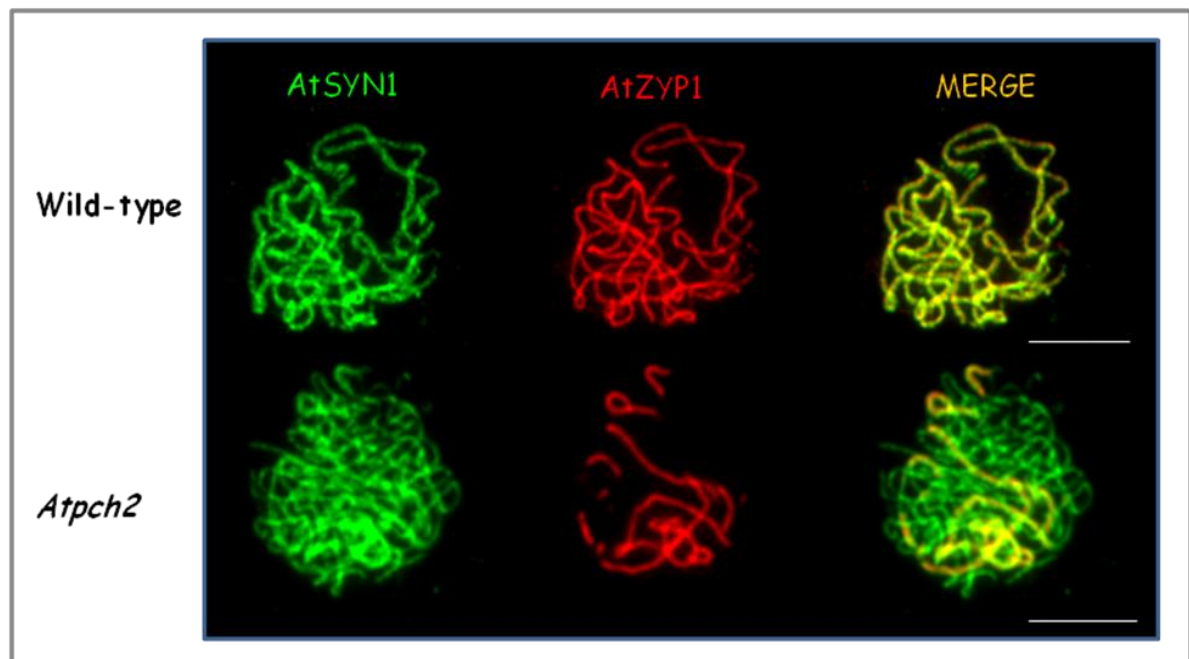
Figure 3. 21: Immunolocalisation of AtSYN1 and AtZYP1.
Scale bar = 5 µm.
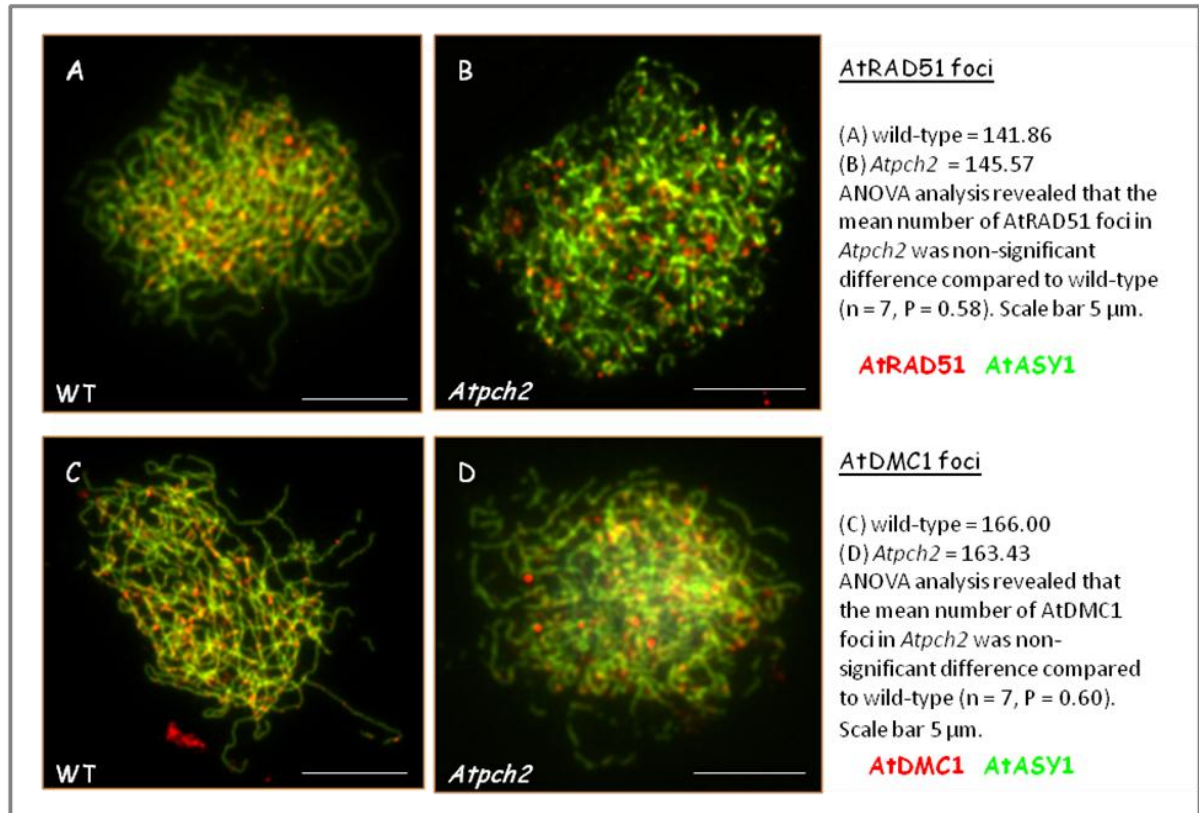
Figure 3. 22: Immunolocalisation of AtASY1 co-localizes with AtRAD51and AtDMC1. Scale bar = 5 µm.
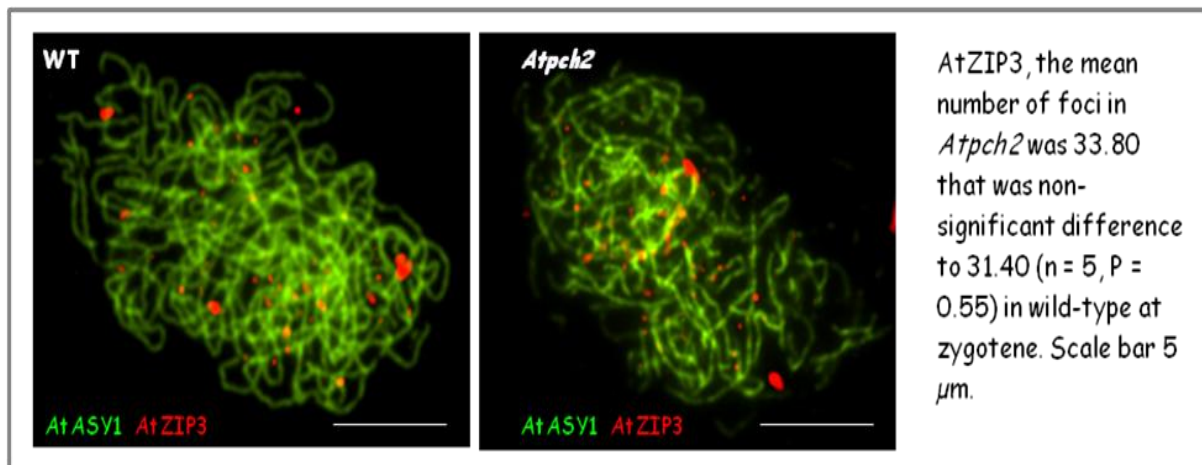
Figure 3. 23: Immunolocalisation of AtASY1 and AtZIP3.
Scale bar = 5 µm.

AtMSH4, the mean of foci in *Atpch2* at leptotene was 152.20 (n = 5) that has non-significant difference to the wild-type at the same stage, 151.40 (n = 5, P = 0.89). AtMSH4 foci were steadily decreased through zygotene eventually observed at early pachytene around 10 foci in both *Atpch2* and wild-type. Scale bar 5 μm.
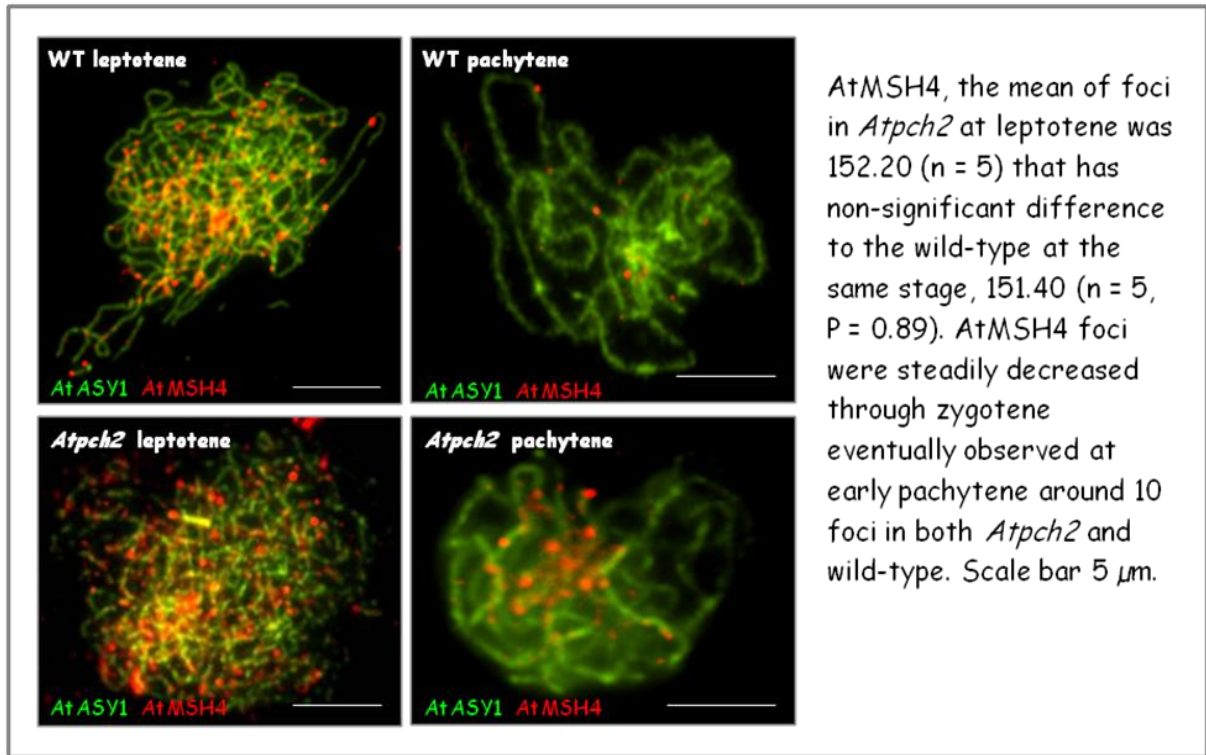
Figure 3. 24: Immunolocalisation of AtASY1 and AtMSH4
Scale bar = 5 μm.

The distance between adjacent MLH1 foci (which mark COs) appears reduced compared to wild-type. This may indicate a defect in CO interference in *Atpch2*. The mean number of AtMLH1 foci in wild-type was 9.71, while in *Atpch2* were reduced to 6.71 foci which is significant difference (n = 7, P < 0.01). Scale bar 5 μm.
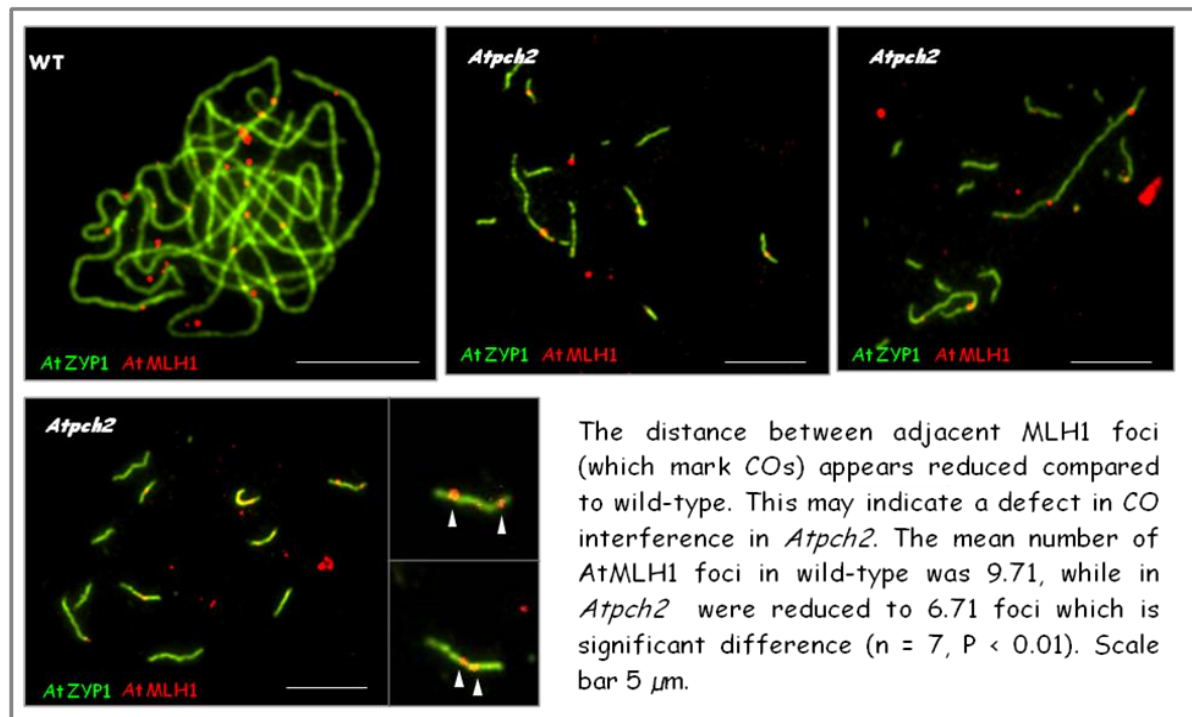
Figure 3. 25: Immunolocalisation of AtZYP1 and AtMLH1.
Scale bar = 5 μm.

3.9.2 Localisation of AtASY3 in *Atpch2* appears normal

AtASY3 is a protein that is involved in axial organization and appears to be a functional homolog of Red1 in *Arabidopsis* (Ferdous *et al*., 2012). Co-localisation of AtASY3 and AtZYP1 on spread preparations of *Atpch2* PMCs showed that AtASY3 localisation was similar to the wild-type (**Figure 3.20**). AtASY3 protein localised linearly along chromosome axial elements from leptotene to pachytene, suggesting that AtASY3 function may not be required for *Atpch2* mutant.

3.9.3 Localisation of AtSYN1 in *Atpch2* appeared similar to wild-type

AtSYN1 is the *Arabidopsis* homologue of the budding yeast meiotic cohesin, Rec8 (Bai *et al*., 1999). Dual immunolocalisation of AtSYN1 and AtZYP1 on chromosome spread preparations of PMCs from *Atpch2* and wild-type, showed that AtSYN1 formed linear chromosome axis-associated signals throughout prophase I in both wild-type and *Atpch2* (**Figure 3.21**). This result reveals that sister chromatid cohesion may still function normally despite loss of AtPCH2 during meiosis.

3.9.4 The number of AtRAD51 and AtDMC1 foci in *Atpch2* appeared similar to wild-type

AtRAD51 and AtDMC1 (Klimyuk and Jones, 1997; Li *et al*., 2004) function at the 3'single-stranded DNA ends, that are generated by the cooperation of SPO11 and the

MRX complex to catalyse invasion of the intact recombination partner (Anderson *et al.*, 1997; Bishop *et al.*, 1992). Based on the specific function of AtRAD51 and AtDMC1 during prophase I, the number of their immunolocalisation foci can indirectly reflect the number of DSBs in *Arabidopsis* meiosis. Immunolocalisation of AtRAD51 and AtDMC1 were observed at leptotene in both *Atpch2* and wild-type. ANOVA analysis reveals that the number of AtRAD51 and AtDMC1 foci in *Atpch2* was not significantly different compared to wild-type. In the case of AtRAD51, the figures for *Atpch2* and wild-type were 145.57 and 141.86 (n = 7, P = 0.58) respectively (**Figure 3.22 (A)**). For AtDMC1, the mean number of foci for *Atpch2* was 163.43 compared to the wild-type 166.00 (n = 7, P = 0.60) (**Figure 3.22 (B)**).

3.9.5 The number of AtZIP3 and AtMSH4 foci in *Atpch2* appeared similar to wild-type

ZIP3 is a member of ZMM protein group involved in formation of class I, interference-sensitive COs, which also includes AtMSH4 and AtMSH5. In budding yeast, Zip3 functions upstream of the other SIC components (Synapsis Initiation Complexes) and is proposed that it facilitates the localisation of Zip2, Zip4 and Spo16 (Chelysheva *et al.*, 2012). In plants, at early prophase I, these proteins co-localise with DMC1/RAD51 foci with most sites being resolved as non-crossovers. As the number of these foci gradually reduce through zygotene, at early pachytene the remainder of MSH4/MSH5 foci may be interacting with MLH1-MLH3 heterodimer and are eventually resolved as COs (Chelysheva *et al.*, 2012). In *Arabidopsis*, AtZIP3 is

proposed to be epistatic to AtMSH4/AtMSH5 (Osman *et al.*, 2011). Immunolocalisation of AtZIP3 and AtMSH4 were investigated in *Atpch2* compared to the wild-type. For AtZIP3, the mean number of foci at zygotene in *Atpch2* was 33.80, displaying a non-significant difference to 31.40 (n = 5, P = 0.55) in wild-type (**Figure 3.23**). In the case of AtMSH4, the mean foci number in *Atpch2* at leptotene was 152.20 (n = 5), also sharing a non-significant difference to the wild-type at the same stage, 151.40 (n = 5, P = 0.89). The number of AtMSH4 foci was steadily decreased through zygotene, until at pachytene only around 10 foci were observed in both *Atpch2* and wild-type (**Figure 3.24**).

3.9.6 The distance between adjacent AtMLH1 foci of *Atpch2* appears reduced compared to wild-type

Immunolocalisation of AtMLH1, the MutL homologue which is proposed to be the marker protein of class I COs (Jackson *et al.*, 2006) and AtZYP1 on spread preparations of *Atpch2* PMCs, was compared to wild-type. The mean number of AtMLH1 foci which co-localised with AtZYP1 in wild-type was 9.71 (n = 7) at pachytene. In *Atpch2*, AtMLH1 foci per meiocyte was reduced to 6.71 foci (n = 7, P < 0.01); this corresponds to the reduction of the *Atpch2* chiasma frequency (**Figure 3.25, top**). Interestingly, some of the distances between adjacent AtMLH1 foci which co-localised with the AtZYP1 signals that remained in stretches along *Atpch2* chromosomes, appeared to be shorter than expected in the wild-type (**Figure 3.25, bottom**). This may indicate a defect in CO interference in *Atpch2*.

3.10 Crossover interference analysis of *Atpch2*

CO interference is a poorly understood CO control mechanism that prevents COs forming close together along each chromosome pair (Bishop and Zickler, 2004; Pawlowski and Cande, 2005). As the distance between adjacent AtMLH1 foci of *Atpch2* appeared reduced, and chiasma distribution was altered along *Atpch2* chromosomes, fluorescent pollen tetrads were used to assay CO interference in a region between three transgenic markers, at two intervals on chromosome 5 (**Figure 3.26**). This assay is performed in the quartet (*qrt*) mutant background where the 4 pollen products of each meiocyte are held together. This can be used to measure the recombination history of a set of progeny in *qrt* mutants carrying a set of fluorescent markers which are expressed in pollen. A collection of *A. thaliana* transgenic FTLs lines carrying the transgenes were kindly donated by G.P.C. (Berchowitz and Copenhaver, 2008). This experiment used *A. thaliana* (Col) carrying three fluorescent-tagged markers with identification numbers: FTL1273 (A); FTL1659 (B) and FTL993 (C), on chromosome 5 (known as I5aI5b interval, **Figure 3.26**) in the *qrt* mutant background, to assay CO interference in wild-type and *Atpch2* mutant. The map of the three linked markers and crossing diagram to create FTL lines in *Atpch2* background is shown in **Figure 3.26**. The meiotic recombination patterns based on three fluorescent transgenic markers and *qrt* background can be classified to 12 different patterns presented in models A-L, as well as images obtained using an epi-fluorescence microscope with three different filters, DsRed2, eYFP and eCFP (**Figure 3.27**). This method can be used to measure CO interference, as explained by Malkova *et al*., 2004,

is where R: R1 represents the interference ratio of wild-type and R2 represents the interference ratio of *Atpch2*. Definitions in this experiment are shown in **Table 3.4 and table 3.3 as well as the raw data**. The map distance and variance were determined by the Perkins equation (Perkins, 1962) and the statistical significance of ratios compared between sample populations were calculated by Stahl Lab Online Tools: http://molbio.uoregon.edu/~fstahl/ (**Table 3.4**). The value of the interference ratio produces a value between 0 and 1 with R = 1 being no interference and R = 0 being complete interference. Comparing wild-type with the *Atpch2* mutant, shows that the interference ratio of wild-type within I5aI5b intervals was 0.4124, while the ratio of *Atpch2* was 0.9762. This result indicates that the *Atpch2* has significantly weaker interference than the wild-type. As mentioned above, this result is clearly consistent with the reduction in the distance between adjacent AtMLH1 foci, the CO marker protein, observed in dual-immunolocalisation of AtMLH1 and AtZYP1 in *Atpch2*. Although the I5aI5b intervals are just a small region on chromosome 5 of *Arabidopsis*, it could be representative of the whole genome. In support of this proposal, the fluorescent pollen tetrads assay showed that the CO frequency of *Atpch2* within the I5a interval was 0.3002 Morgans (0.1483+0.1519), whereas the CO frequency of wild-type at the same interval was 0.4861 Morgans. This shows that the CO frequency of *Atpch2* was reduced to ~62% compared to wild-type, similar to the result from the FISH analysis which showed the chiasma frequency (**Table 3.1**) was reduced to 72% of wild-type levels.
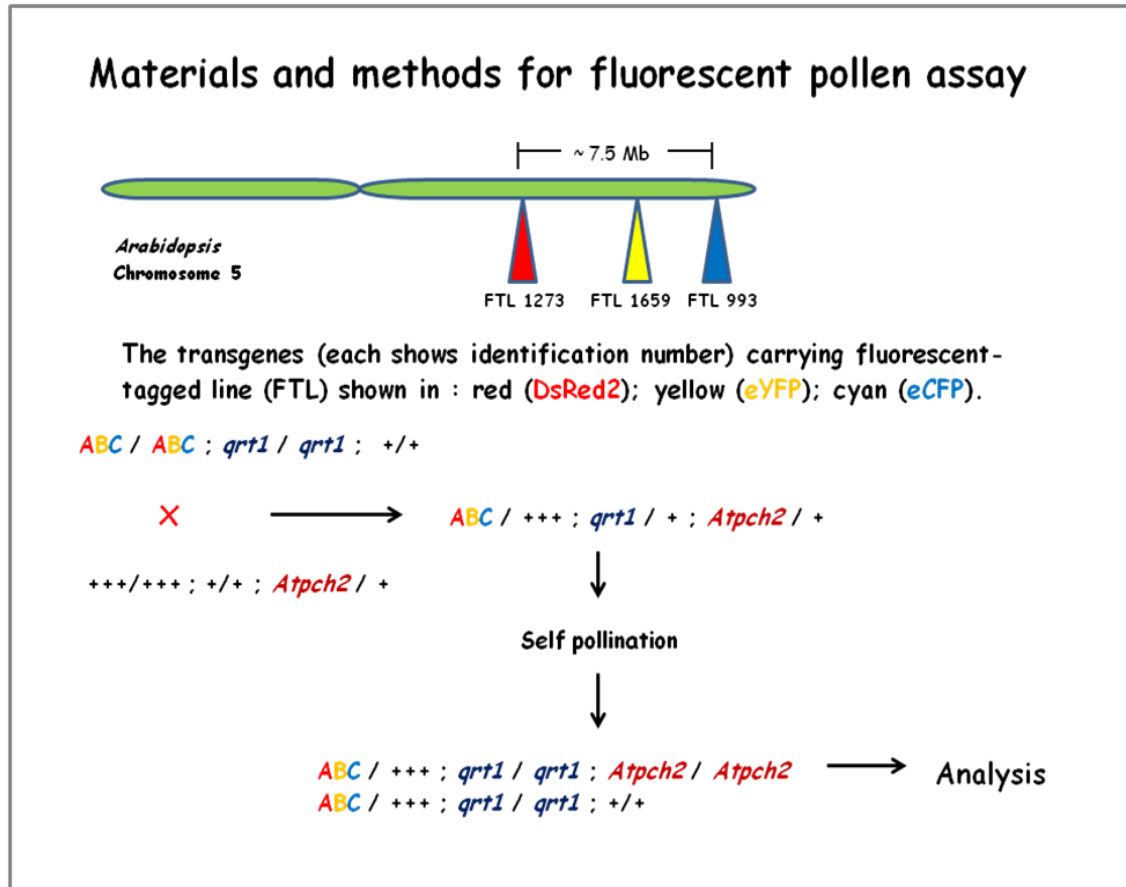
Figure 3. 26: Materials and methods for fluorescent pollen assay
Chromosome 5 was three FTLs sites on the long arm which provides two genomic intervals (I5aI5b). This figure explains the crossing procedure in brief to produce the ABC / +++ ; *qrt1 / qrt1* ; *Atpch2 / Atpch2* and ABC / +++ ; *qrt1 / qrt1* ; +/+ lines. Due to the *Atpch2 / Atpch2* genotype plants presenting a high frequency of univalents in meiosis, to avoid aneuploidy we used *Atpch2*/+ genotype plants to cross with ABC / ABC; *qrt1 / qrt1* ; +/+ instead of *Atpch2 / Atpch2* genotype at the first step of procedure.
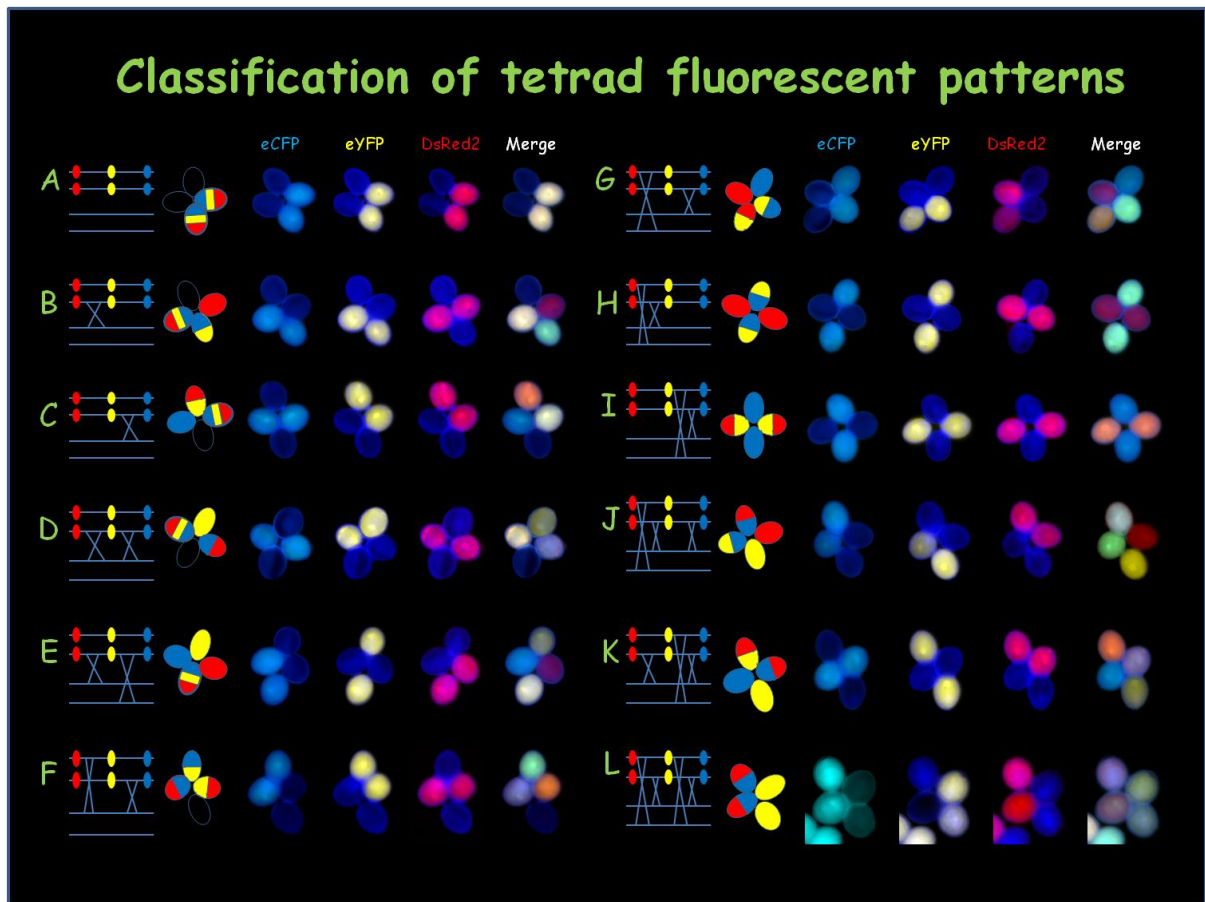
Figure 3. 27: Classification of tetrad fluorescent patterns

12 recombination patterns within I5aI5b intervals (A-L) present each model of tetrad fluorescent patterns in the same position of the multicolor fluorescent tetrads from plants that can be visualized through three different fluorescent filters (eCFP, eYFP and DsRed2). Note: in this figure, the dark blue color in the blank FTLs pollen is DAPI in order for the complete tetrads to be visible.

Genotype : ABC / +++ ; qrt1 / qrt1 ; +/+

Plant	Screen date	Flower	A	B	C	D	E	F	G	H	I	J	K	L	Total
2	3/1/2013	12	15	33	17	2	1	0	0	1	0	0	0	0	69
11	3/1/2013	10	32	54	31	2	1	1	1	0	0	0	0	0	122
9	3/1/2013	9	36	60	41	3	4	2	1	0	0	0	0	0	147
9	5/1/2013	15	115	170	94	4	11	9	13	7	2	1	0	1	427
9	7/1/2013	21	101	159	97	4	4	5	8	2	2	1	0	0	383
12	3/1/2013	11	72	126	89	4	6	3	5	3	0	0	0	0	308
12	5/1/2013	18	119	178	95	13	9	4	6	4	0	4	1	0	433
25	7/1/2013	18	100	165	126	9	14	6	8	4	1	2	0	0	435
		Total	590	945	590	41	50	30	42	21	5	8	1	1	2324

Genotype : ABC / +++ ; qrt1 / qrt1 ; Atpch2 / Atpch2

Plant	Screen date	Flower	A	B	C	D	E	F	G	H	I	J	K	L	Total
6	4/1/2013	19	141	37	64	2	8	13	3	3	6	0	0	0	277
27	4/1/2013	12	80	30	60	3	5	6	5	0	3	0	0	0	192
27	6/1/2013	19	183	80	88	13	8	10	6	1	4	4	1	0	398
27	7/1/2013	23	239	61	117	5	5	8	9	3	5	2	0	0	454
23	4/1/2013	20	143	48	73	3	7	5	7	3	4	0	3	0	296
30	4/1/2013	14	138	64	106	6	9	10	9	2	8	0	0	0	352
30	6/1/2013	20	170	51	87	16	10	7	5	1	3	1	1	0	352
		Total	1094	371	595	48	52	59	44	13	33	7	5	0	2321

Table 3. 3: Fluorescent tetrad data divided to 12 recombination patterns
The data were scored from 5 plants in wild-type background (ABC / +++; *qrt1 / qrt1* ; +/+) and 4 plants in *Atpch2* background (ABC / +++ ; *qrt1 / qrt1* ; *Atpch2 / Atpch2*), in addition, each flower was selected between the fifth to the thirtieth flowers of the primary bolt (Berchowitz and Copenhaver, 2008). A-L patterns are the recombination patterns within I5aI5b intervals.

	A	B	C	D
CO frequency (Morgans)	0.1419	0.3442	0.1483	0.1519
Variance	0.00018061	9.952E-05	0.00013574	8.041E-05
Standard Error	0.01343924	0.00997608	0.01165084	0.00896704

	R1	R2
Ratios	0.4124	0.9762
Variance	0.00166783	0.00920464
Standard Error	0.04083913	0.09594081

Definitions
A : CO frequency of wt with adjacent CO
B : CO frequency of wt without adjacent CO
C : CO frequency of *Atpch2* with adjacent CO
D : CO frequency of *Atpch2* without adjacent CO
R1 : Interference ratio of wt = A/B
R2 : Interference ratio of *Atpch2* = C/D

(One Tailed) Is |R1-R2| > 1.65 x sqrt Var [R1-R2]
0.5638 > 0.172

(Perkins equation (Perkins, 1962); Stahl Lab Online Tools: http://molbio.uoregon.edu/~fstahl/)

Table 3. 4: The results of CO frequency and interference ratios of fluorescent pollen assay.

3.11 BrdU time-course of *Atpch2* mutant

We have previously shown that the proper association between AtASY1and AtZYP1 is required for successful meiotic recombination in plant meiosis (Osman *et al*., 2011). AtASY1 and AtZYP1 co-localisation was altered in *Atpch2*. We wanted to gain a better understanding of the possible role of AtPCH2 in chromosome axis remodeling and its effect on the progression of key molecular events of meiosis. We investigated the framework of the relative timing and duration of meiotic events in *Atpch2* in more detail using a meiotic time-course experiment. The meiotic time-course is based on BrdU pulse-labeling of the PMCs in meiotic S-phase (Armstrong *et al*., 2003). Labeled inflorescences were fixed in ice-cold ethanol/acetic acid fixative, at 5, 10, 20, 30, 35, 40 and 45 hours (hrs) after the BrdU pulse. Individual fixed buds were analysed immunologically using an anti-BrdU antibody and counterstained with DAPI (See **Materials and Methods**). The BrdU pulse-labeling of *Atpch2* revealed that the onset of zygotene/pachytene in both *Atpch2* and wild-type was observed at the same time at 20 hrs post S-phase. However, the percentage of BrdU-labeled meiocytes of *Atpch2* was much less than those of wild-type. The number of zygotene/pachytene meiocytes of *Atpch2* rapidly increased at 24 hrs and remained at high levels until 45 hrs, whereas the wild-type dropped to 0 meiocytes at 35 hrs. In terms of meiotic progression, *Atpch2* meiocytes progressed from zygotene/pachytene stage to diplotene significantly slower than in wild-type, as at 35 hrs only a few *Atpch2* diplotene meiocytes were observed, while the wild-type reached a peak by 30 hrs and some meiocytes had developed to dyads/MII (**Figure 3.28; Table 3.5**). In other words, *Atpch2* was held at

zygotene/pachytene stage for longer than the wild-type by at least 10 hrs, between 35

hrs (BrdU-labeled meiocytes of wild-type presented 0) and 45 hrs. This indicates that

the meiotic progression of *Atpch2* is delayed at pachytene stage at least 5 hrs compared

to wild-type.

Wild-type	Time 0	Time 5	Time 10	Time 20	Time 24	Time 30	Time35	Time 40	Time 45
Leptotene	0/20(0)	30/39(77)	23/23(100)	30/30(100)	17/62(27)	3/18(17)	1/13(8)	0/17(0)	0/7(0)
Zygo/Pachytene	0/24(0)	0/35(0)	0/43(0)	90/108(83)	31/50(62)	15/49(31)	0/34(0)	0/10(0)	0/10(0)
Diplotene	0/12(0)	0/12(0)	0/5(0)	0/21(0)	0/13(0)	43/63(68)	8/34(24)	3/20(15)	0/20(0)
Diakinesis/MI	0/10(0)	0/6(0)	0/5(0)	0/12(0)	0/28(0)	7/29(24)	16/18(89)	29/34(85.3)	11/15(73.33)
Dyads/MII	0/8(0)	0/12(0)	0/5(0)	0/8(0)	0/13(0)	0/25(0)	7/9(78)	31/31(100)	35/35 (100)

Atpch2	Time 0	Time 5	Time 10	Time 20	Time 24	Time 30	Time35	Time 40	Time 45
Leptotene	0/12(0)	27/35(77)	16/18(89)	20/21(95)	30/30(100)	11/16(69)	17/18(94)	16/16(100)	12/18(66.66)
Zygo/Pachytene	0/13(0)	0/34(0)	1/50(2)	16/102(16)	45/53(85)	70/95(74)	63/64(98)	30/32(93.75)	30/32(93.75)
Diplotene	0/10(0)	0/12(0)	0/11(0)	0/24(0)	0/17(0)	4/30(13)	2/9(22)	19/22(86.36)	33/33(100)
Diakinesis/MI	0/5(0)	0/8(0)	0/6(0)	0/9(0)	0/9(0)	0/13(0)	0/16(0)	12/22(54.54)	11/11(100)
Dyads/MII	0/5(0)	0/18(0)	0/3(0)	0/13(0)	0/6(0)	0/8(0)	0/8(0)	39/66(65)	72/91(79.12)

Table 3. 5: The BrdU pulse-labeling data of *Atpch2* and wild-type meiocytes
The table shows the proportions of BrdU-labeled meiocytes per the total numbers in wild-type (a top table) and *Atpch2* (a bottom table). The figures in the parentheses refer to their proportions as percentages. These percentages were used to plot the line graph for comparing and investigating the meiotic progression in both wild-type and *Atpch2* in **Figure 3.28**.
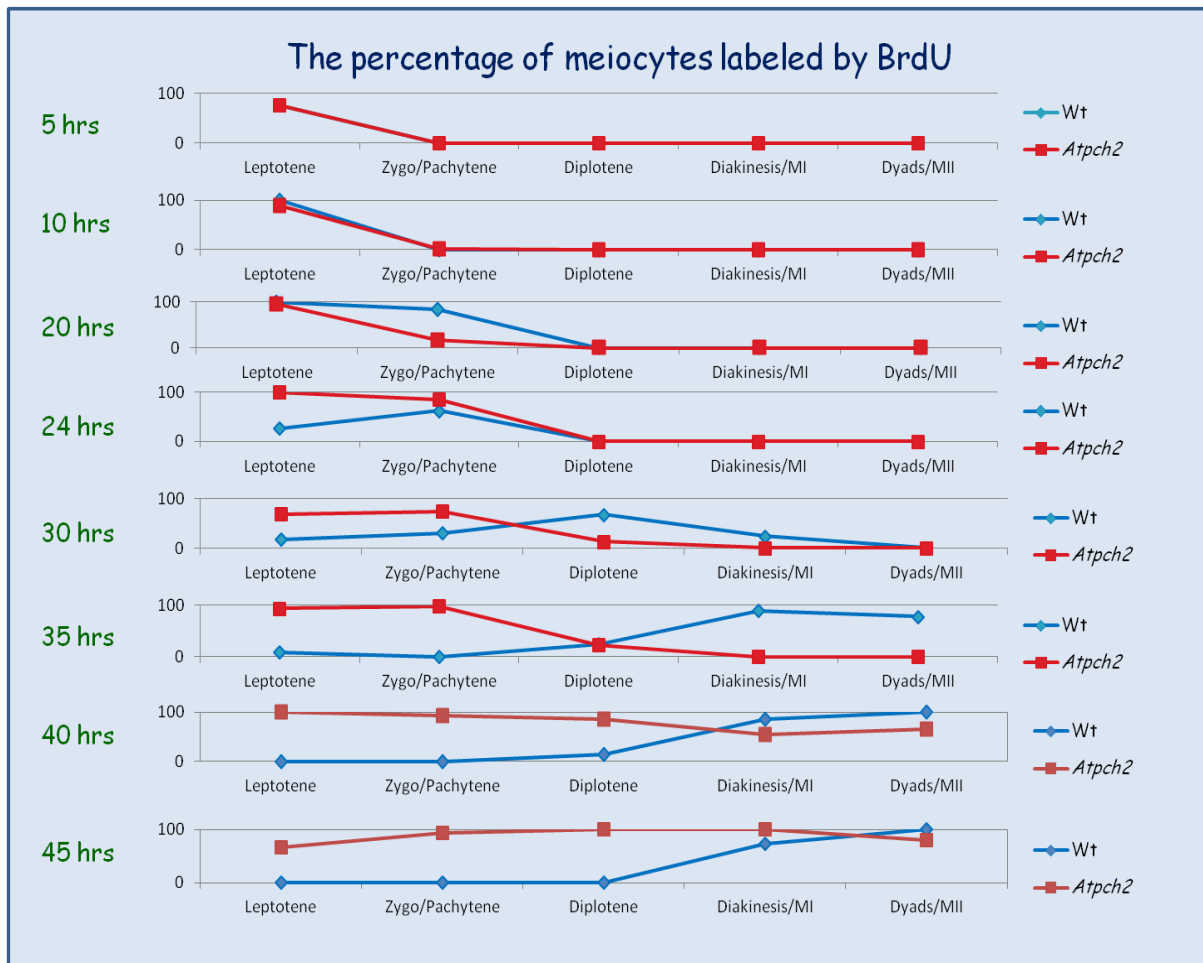
Figure 3. 28: Proportion of meiocytes labeled by BrdU
The 8 graphs show different time points from 5 to 45 hrs post-BrdU labelleling when samples were fixed. The progression of meiotic chromosomes between *Atpch2* and wild-type can be traced by percentage of BrdU-labeled meiocytes from leptotene to metaphase II (Dyads/MII). This result reveals that the meiotic progression of *Atpch2* is delayed at pachytene stage at least 5 hrs compared to wild-type.

3.12 Measuring the distance between chromosome axes in *Atpch2* by transmission electron microscopy

As AtASY1and AtZYP1 localisation in *Atpch2* meiosis may be affected due to loss of

AtPCH2 function, as AtASY1 persisted along axial elements of *Atpch2* chromosomes

until late pachytene and the polymerization of AtZYP1 was observed in patches

instead of along the full length of chromosomes. We hypothesized that loss of AtPCH2 function may disrupt the formation of the transverse filament protein that cross-link with the homologous chromosome axes in the context of the SC, and decided to investigate this in more detail. Electron microscopy was used to analyse silver-stained chromosome spread preparations, to allow measuring of the span of chromosome axes at synapsed regions of *Atpch2* compared to wild-type. The span measurement between axes of homologous chromosome synapse regions of wild-type and *Atpch2* using EM were presented equal in size as 140 nm. (**Figure 3.29**). However, this span measurement of *Atpch2* is come from a synapsed region of chromosomes, most regions are not paired. Therefore AtPCH2 may be involved in ensuring the SC efficient formation on homologous chromosomes.
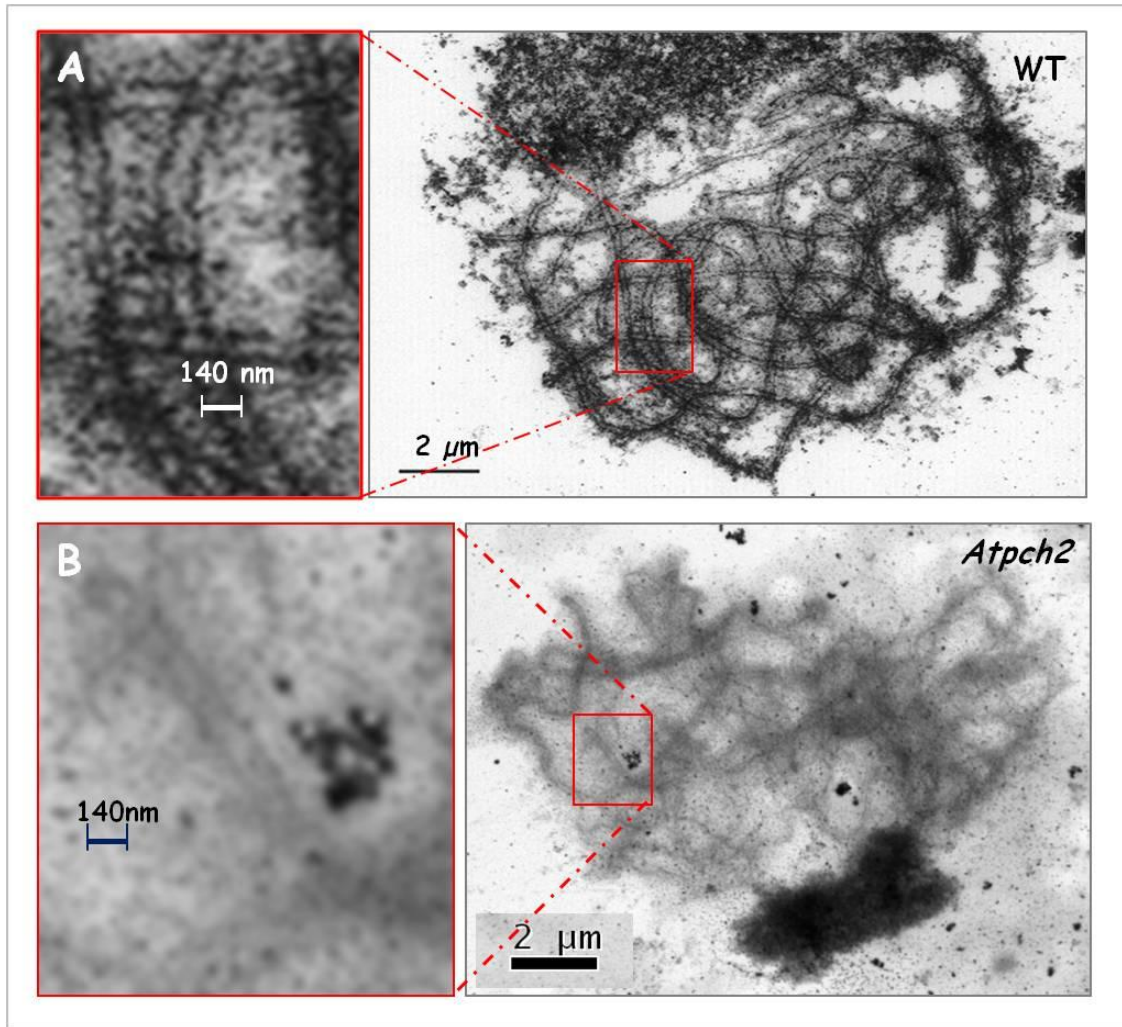
Figure 3. 29: The electron microscopy analysis in silver-stained chromosome spread preparations.
A cropped area is enlarged and shows a scale of the span measurement between axes of homologous chromosome synapse regions of WT **(A)** (Higgins *et al.*, 2004) and *Atpch2* **(B)**.

3.13 Discussion

In budding yeast, Pch2 (Pachytene Checkpoint 2) is a meiosis specific AAA+ ATPase family member involved in chromosome axis organisation and regulation of CO formation and distribution (Zanders and Alani, 2009). TRIP13 is the mouse Pch2 orthologue in mouse and is vital for proper synaptonemal complex formation. In the

absence of TRIP13, the frequency of COs and chiasmata is reduced and their distribution is altered (Roig *et al.,* 2009). Three homozygote T-DNA insertion lines were identified in At4g24710 (*AtPCH2*) and all lines presented defects in fertility and meiotic chromosome behaviour. An allelism test (*Atpch2.1/Atpch2.2*) clearly confirmed the loss of function within the gene. Although an RT-PCR experiment on *Atpch2* using P1P2 specific primers revealed the transcription of two mRNA products, these could be translated into non-fuctional *AtPCH2* proteins. Various defects in *Atpch2* are good evidence to verify this. Moreover, the RT-PCR experiment on *Atpch2* using P3P4 primers found that mRNA was not transcribed from the flank of the original (*Atpch2.1*) T-DNA insertion site, indicating that *AtPCH2* failed in transcription of the whole gene and most likely fails to produce a functional protein. Reduction of chiasmata in *Atpch2* presented in this experiment might result from a variety of defects during first meiotic cell division, eventually leading to reduced fertility. Some regions of homologous chromosomes are still not synapsed at pachytene stage, possibly causing the decrease of COs in *Atpch2*. This phenomenon predicts that AtPCH2 is required for CO interference and/or the efficiency of homologous synapsis completion consistent with the requirement of Pch2 for CO control in yeast (Joshi *et al*., 2009, Zanders and Alani, 2009) and the requirement of TRIP13 for normal numbers of COs in mouse (Roig *et al*., 2010). Homologous chromosome pairing disruption in *Atpch2* during zygotene/pachytene leads to exhibition of univalents at diplotene and more obviously at MI. Although every chromosome seemed to be affected by this problem of showing univalents, a high

frequency of univalents was markedly found on chromosome II with around three fold that of chromosome III and IV, and more than twice that of chromosome V. However, this does not mean that chromosome II is more sensitive to the deficiency of AtPCH2 than the others because all chromosomes presented chiasma distribution alteration and a significant difference in CO frequency compared to wild-type, except chromosome IV.

Bridges found on chromosome IV at anaphase/telophase I might be explained in terms of recombination and chromosome structure formation/organization. A high frequency of bridges suggests that chromosome IV chiasma (ta), especially on the long arm, could not be separated properly at this stage due to a structural organization problem. Defects in recombination of meiocytes and/or chromosome synapsis can lead to CO failure, missegregation and cause aneuploidy (Ghabrial and Schupbach, 1999; Bhalla and Dernburg, 2005; Ashley *et al.*, 2004). Missegregations were found in *Atpch2* meiocytes (**Figure 3.7**), confirming that AtPCH2 is required for normal levels/distribution of COs.

The SC influences chromosomal structure which changes markedly during meiotic recombination. The four chromatids of homologous chromosome are arranged in a particular structure in the SC. Each axial element (AE), holds and organizes one pair of sister chromatids. Once axial elements are organized into completely assembled SC, they are called lateral elements (Ma, 2006; Osman *et al.*, 2011). In *Arabidopsis*, the

ASY1 protein localizes to the axial/lateral elements (Armstrong *et al*., 2002), the *asy1* mutant cannot form SC in meiocytes (Ross *et al*., 1997; Caryl *et al*., 2000). Based on the interpretation of the immunolocalisation of AtASY1 and AtZYP1 in *Atpch2* showing that AtASY1 persists to co-localise with AtZYP1 until pachytene, we hypothesize that AtASY1 and AtZYP1 organization was altered due to a lack of AtPCH2 function. Furthermore, the defects of this organization may affect chromosome synapsis as AtZYP1 polymerization was observed in patches at pachytene in *Atpch2*. AtASY1 function in meiotic recombination may involve many proteins that associate in a proper position and time during meiosis. Association of proteins on chromosomes during meiosis is directly involved in chromatin remodeling, which allow the function of specific proteins at the right site along chromosome. This dynamic mechanism may result from hydrolysis of ATP or without the hydrolysis of ATP (Gangaraju and Bartholomew, 2007). The lack of AtPCH2 may cause the alteration of chromatin remodeling in *Atpch2*, and as a result the meiotic progression of *Atpch2* was delayed at pachytene at least 5 hrs compared to wild-type, and AtASY1 persisted to colocalise with AtZYP1 until pachytene stage. Although the organization between AtASY1 and AtZYP1 was altered, the span of chromosome axes using silver-stained chromosome spread preparations in *Atpch2* was not distorted compared to the wild-type. However, AtASY3 which is proposed to play a role in axial organization and performs a similar function to AtASY1 (Ferdous *et al*., 2012) was observed to display normal localisation in *Atpch2* immunolocalisation. Also, the meiotic cohesin protein, AtSYN1, appeared to show normal localisation in *Atpch2*. Based on these

results, we could conclude that AtASY3 and AtZYN1 may be not required for *Atpch2* mutant in order to function in meiotic recombination whether directly or indirectly. AtRAD51/AtDMC1 specifically functions on the single-stranded DNA and promote strand invasion such that they can indirectly reflect the number of DSBs in *Arabidopsis* meiosis (Anderson *et al*., 1997; Bishop *et al*., 1992). Immunolocalisation of AtRAD51 and AtDMC1 in *Atpch2* showed non-significant difference in their number of foci at leptotene compared to wild-type. This seems to be consistent with the number of AtZIP3 and AtMSH4 foci in *Atpch2* that also revealed non-significant difference. AtZIP3 and AtMSH4 foci co-localise with AtRAD51/AtDMC1 foci at leptotene and then reduce gradually through to pachytene, when AtZIP3 dissociates from chromosomes and some AtMSH4 foci associate with AtMLH1 (Chelysheva *et al*., 2012). These data indicate that AtPCH2 may be not required for DNA DSB repair during meiotic recombination pathways. However, AtPCH2 could be involved in CO resolution at pachytene as immunolocalisation of AtMLH1 revealed a reduction in the number of AtMLH1 foci, which corresponds with the observed chiasma frequency. The localisation of AtMLH1 foci seemed to be random and some of them appeared to show a reduced distance between adjacent foci; this could suggest that loss of AtPCH2 may affect CO interference. Moreover, this proposal could be confirmed by the chiasma distribution that was altered in *Atpch2* as well, as *Atpch2* has significantly weaker interference compared to the wild-type CO interference analysis using fluorescent pollen tetrads.

Chapter 4

Production and analysis of an AtPCH2 antibody

4.1 Introduction

TRIP13/Pch2 is a pachytene checkpoint protein that has been studied in many model organisms. Immunolocalisation in *S. cerevisiae* using an anti-Pch2 antibody reveals that Pch2 forms foci at early zygotene and the number of Pch2 foci reached a peak during pachytene. Most of Pch2 foci were co-localised with Zip1. In addition, some Pch2 foci/signals were detected in the nucleolar area during late zygotene and pachytene, but were not observed at earlier stages (San-Segundo and Roeder, 1999; Joshi *et al.*, 2009). In mouse spermatocytes, TRIP13 the functional homologue of budding yeast Pch2, was detected from leptotene to early pachytene stage and was absent in late pachytene spermatocytes (Li and Schimenti, 2007). To investigate the localisation of Pch2 in *Arabidopsis*, an antibody raised against Pch2 was produced. Production of a AtPCH2 antibody will provide a valuable tool to investigate meiotic recombination in *Arabidopsis*.

4.2 Cloning the AtPCH2 C-terminus in pET21b expression vector

The *AtPCH2* gene encodes a predictive protein of 475 amino acids with a molecular weight of 52.63 KDa. The genomic region comprising nucleotide from 491 to 1,116, corresponding to amino acids from 165 to 372 residues (23.37 KDa), was chosen to produce a recombinant protein that will be used for antibody production (**Figure 4.1**). In order to produce a PCH2 recombinant protein, RNA was extracted from *Arabidopsis* wild-type buds. RNA was then reverse-transcribed using SuperScript II RT (**see Materials and Methods**). The specific PCH2 cDNA sequence was amplified

with PCH2-ab forward and PCH2-ab reverse primers to give a PCR product of 624 bps

length.

Figure 4. 1: Nucleotide and amino acid sequence of *AtPCH2*
 (**A**) Nucleotide sequence of *AtPCH2* cDNA
T-DNA insertion site of *Atpch2.1* is indicated by red arrow, AtPCH2-ab forward primer is showed in red letters and the reverse primer in yellow letters.
(**B**) Amino acid sequence of AtPCH2
The AtPCH2 antibody-recognised site is in blue letters and the green letter region indicates the AAA-ATPase domain.

The amplified PCR product was visualised in a 1% agarose gel and was purified. The

purified PCR product was then ligated into pDrive. *E. coli* DH5α was then transformed

with recombinant pDrive. Plasmid DNA extraction was carried out from white colonies and the purified plasmid DNA was digested by *Eco*R1 to confirm the correct insertion size. The insert in the plasmid DNA then was sequenced with T7 promoter primer. The results exhibited 100% sequence identity with the target region (data not shown).

The extracted-plasmid DNA was digested by *Nde*1 and Xho1 restriction enzymes so that the target region could be ligated into the expression vector pET21b at the position such that a HIS-tag is located at the C-terminal of the insert. HIS-tag sequence provides an advantage for efficient protein purification (**see Figure 2.1 in Materials and Methods**). Transformation of *E. coli* DH5α with pET21b vector containing the insert was carried out. In order to confirm that no mutation had occurred during cloning, the recombinant pET21b vectors were extracted from *E.coli* DH5α cells and T7 primer was used to perform sequencing. The result presented 100% sequence identity with the target sequence (data not shown).

4.3 Induction of AtPCH2 recombinant proteins

Under the control of the T7 promoter and non-metabolisable isopropyl B-D-1-thiogalactopyranoside (IPTG), *E.coli* BL21 cells can express a recombination protein at high level. The pET21b vector containing the insert was transformed into *E.coli* BL21 cells. Both soluble and insoluble protein fractions were extracted from IPTG induced and IPTG non-induced cultures. To compare the expression of the AtPCH2 C-

terminal recombinant protein, a 15% SDS-PAGE denaturing gel was carried out. The

SDS-PAGE gel was then Coomassie Blue R-250 stained to visualize protein bands

(**Figure 4.2**). The protein gel showed an intense band of protein in the IPTG induced,

insoluble fraction at around the expected molecular weight of 23KDa. In contrast, the

other wells did not show a band at the same molecular weight.
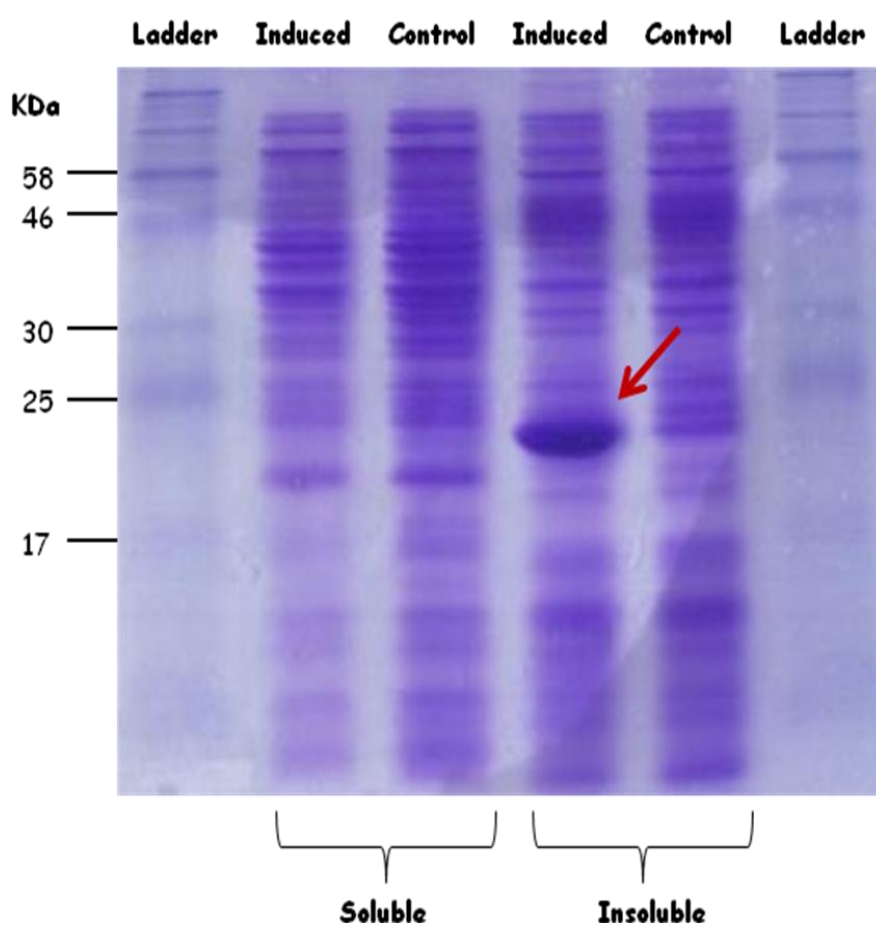
Figure 4. 2: The Coomassie Blue R-250 stained SDS-PAGE gel.
The stained gel compared the expression of AtPCH2 C-terminal recombinant protein
between IPTG induced and IPTG non-induced *E.coli* BL21 cultures. The control lanes
are crude extracts from IPTG non-induced culture; induced lanes are crude extracts
from IPTG induced cultures. The red arrow shows a band corresponding to the
expected molecular weight of PCH2 recombinant protein.

4.4 Purification of AtPCH2 recombinant protein

According to the protein gel, an intense band was visualised at the expected molecular weight of AtPCH2 recombinant protein. Therefore, a larger scale cell culture was performed. **Figure 4.3** shows western blot analysis of AtPCH2 recombinant protein probed by anti-HIS antibody (mouse) comparing IPTG induction and non-induction; this confirmed the presence of the ~23KDa protein attached to HIS-tag that will be isolated from insoluble fractions of cell culture. The protein purification from insoluble fractions was then carried out using nickel column affinity purification (Ni-NTA resin, Qiagen). The insoluble inclusion body pellet, containing the PCH2 protein, was resuspended in 6 M guanidine HCl to solubilise proteins.
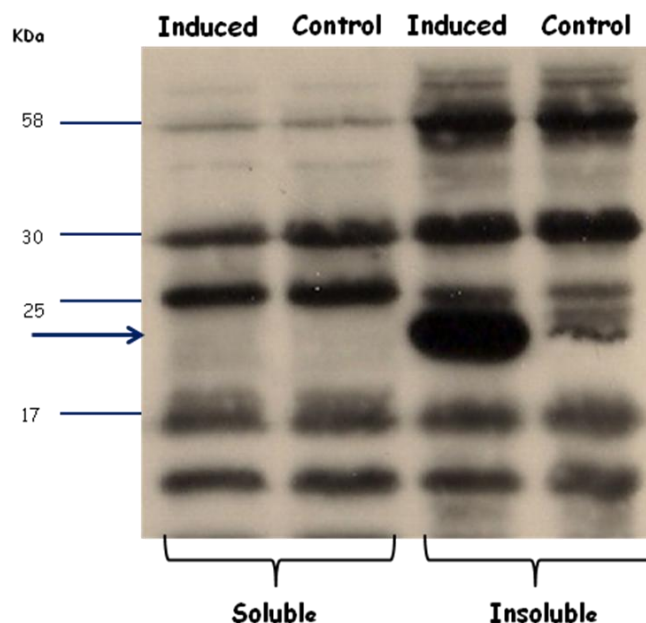
Figure 4. 3: Western blot analysis of PCH2 recombinant protein.

The arrow shows the PCH2 recombinant protein band at around 23 KDa after 5 minutes exposure time. The protein was probed by anti-HIS-antibody (from mouse).

Ni-NTA resin was then used to bond a large proportion of PCH2 recombinant protein and bound protein was washed and eluted with denaturing lysis buffer at different pHs: pH 6.3 for washing resin beads; pH 5.9 for monomer protein elution and pH 4.5 for multimer protein and aggregates elution. **Figure 4.4** shows the yield and purity of each elute compared to 'before' and 'after' binding to resin samples on 12.5% SDS-PAGE. The protein gel revealed that the abundance of AtPCH2 recombinant protein was reduced after incubation with the resin, suggesting successful binding to beads. The gel showed enrichment of a band at pH 4.5 in the eluted solution which represented the right molecular weight compared to the sample from the AtPCH2 recombinant protein in the first lane. However, the lane of washing resin beads also showed a faint band. This suggests that some proteins may have been lost during the washing steps. The eluted proteins were then refolded in refolding buffer at pH 8.0. In order to remove the guanidine and protein folding buffer, the refolded protein was dialysed against 50 mM Tris-HCl, 100 mM NaCl, 2 mM EDTA with a final step at pH 8.0 at 4 ℃. These proteins were then concentrated by dialysis against PEG 6000. The final concentration of protein was estimated at 0.66 mg/ml, using BioRad assay and spectrophotometry. The protein was frozen in liquid nitrogen and sent to BIOGENES (Germany) for immunizing two rats.
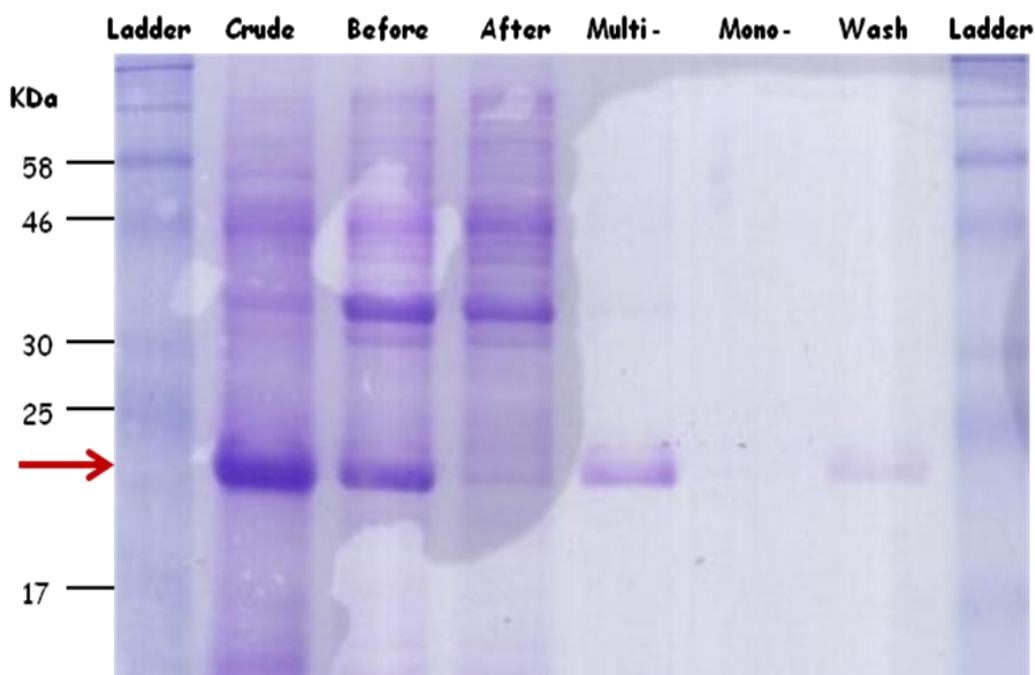
Figure 4. 4: Comparison of AtPCH2 recombinant protein yield at each step.
The yield and purity of each elute compared to the before and after binding resin beads solutions on 12.5% protein gel SDS-PAGE. The arrow shows expected size bands at around 23 KDa.

4.5 Specificity of AtPCH2 antibody

4.5.1 Western blot analysis of AtPCH2 test bleed antiserum on *E. coli* PCH2 recombinant protein

The AtPCH2 test bleed antiserum from two rats was tested for specificity of AtPCH2 recombinant protein from *E. coli* extract using western blot analysis. AtPCH2 recombinant protein was loaded onto a SDS-PAGE and probed with AtPCH2 antiserum at a dilution of 1:1,000 and 1:5,000. The pre-immune serum was used as a negative control with the same dilutions. Anti-rat HRP antibody was used at a dilution of 1:10,000 to detect the presence of AtPCH2 recombinant protein. AtPCH2 test bleed

antiserum from rat number 2 recognised a single band at around 23 KDa for the dilution of 1:5,000. However, the serum from rat number 1 seemed to also recognise other bands with higher intensity at the same dilution. Both pre-immune sera did not detect a band, at either dilution (**Figure 4.5**). This suggests that the AtPCH2 antiserum from rat number 1 may also recognise other *E. coli* proteins.
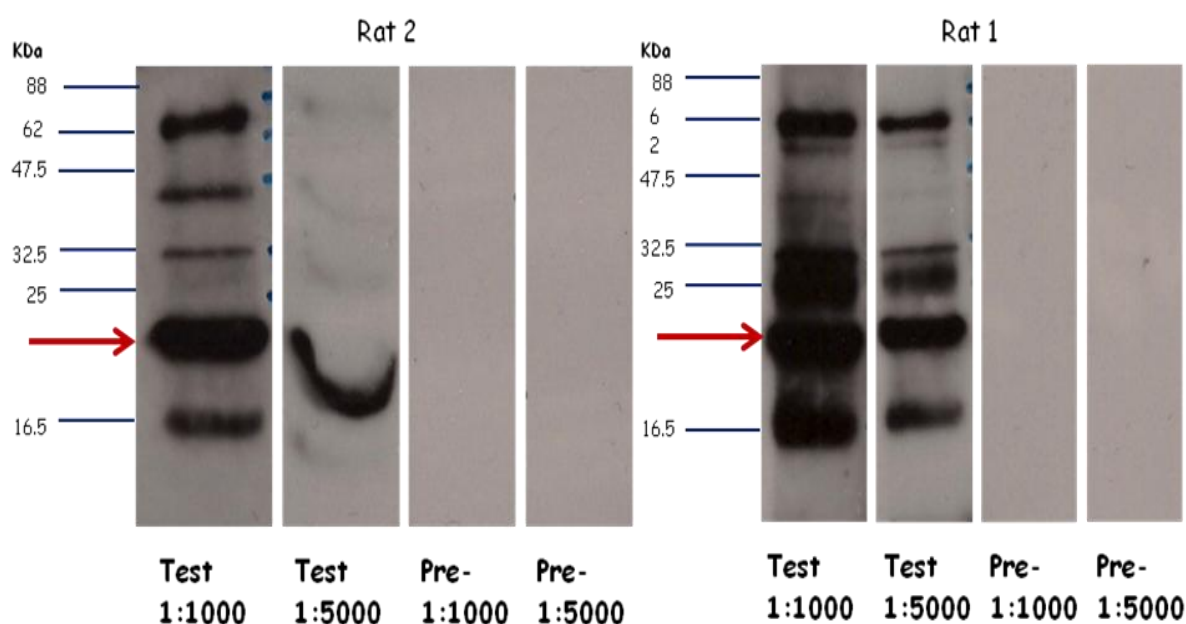
Figure 4. 5: PCH2 recombinant protein probed with AtPCH2 test bleed antiserum comparing to pre-immune serum.
PCH2 recombinant protein was probed with AtPCH2 test bleed antiserum from two rats using western blot analysis for specificity with 20 seconds exposure time. The arrow shows expected size bands at around 23 KDa, and the pre-immune sera did not detect anything.

4.5.2 Western blot analysis of AtPCH2 test bleed antiserum on plant crude extract.

To investigate the specificity of AtPCH2 antibody to plant protein, bud tissue from wild-type *Arabidopsis thaliana* (WT), *Atpch2* mutants and *Brassica oleracea*, a close

relative of *A. thaliana*, were extracted. Using 20 µl of Brassica, 10 µl and 25 µl of wild-type extracted proteins, a 7.5% SDS-PAGE gel was resolved and then transferred to nitrocellulose membrane. The electroblotted nitrocellulose was divided into three replicate parts, as shown in **Figure 4.6**, for probing with pre-immune serum, AtPCH2 antibody and AtASY1 antibody for a control. Anti-rat antibody conjugated to horseradish peroxidase (HRP) was used as the secondary antibody for detection. Using enhanced chemilluminescence (ECL) reagents, the X-ray films were developed. **Figure 4.6** showed an absence of the expected size band of AtPCH2 protein (52.63 KDa) using pre-immune serum probe. For AtPCH2 antibody probe, both *A. thaliana* wild-type protein lanes presented an expected size band which exhibited an intensity corresponding to the amount of extracted protein loaded. However, the recognition of AtPCH2 by the anti-serum was not shown intense band in the lane for both *Arabidopsis* and Brassica crude extract, whereas the AtASY1 antibody recognised the *Arabidopsis* wild-type proteins more intensive. This may result from the AtPCH2 antibody had not been cleaned. To resolve this problem, the AtPCH2 antibodies were then cleaned using Melon Gel IgG spin purification kit which removes non-antibody serum proteins, albumin and transferin with physiological pH selection (**see Materials and Methods**).
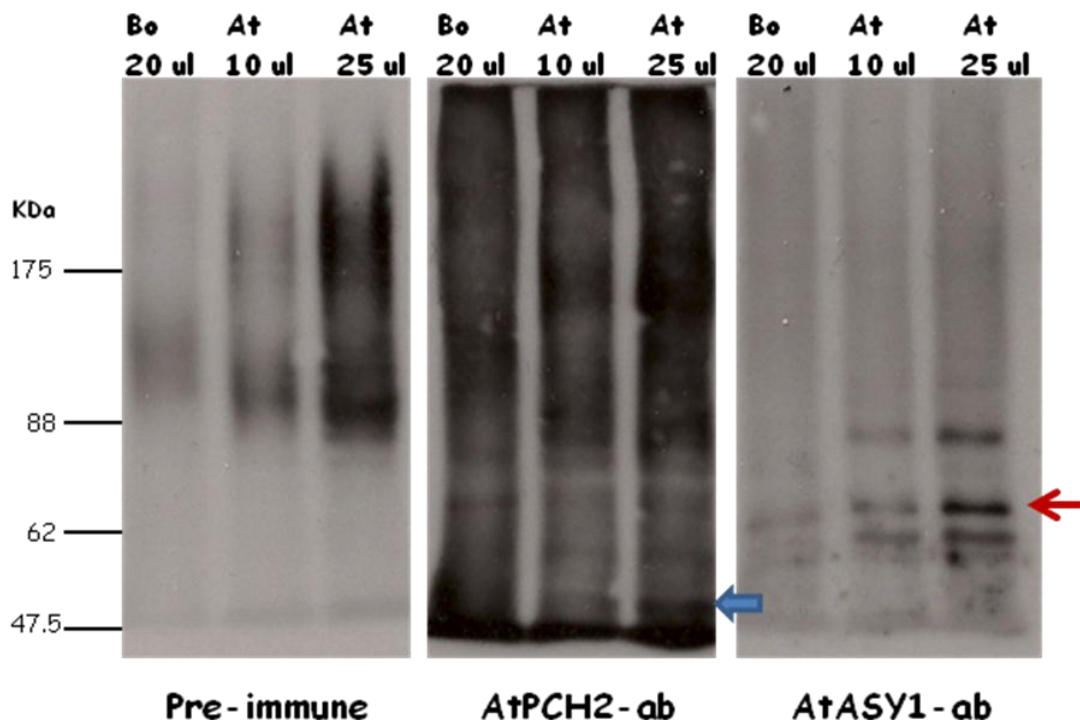
Figure 4. 6: Western blot analysis of plant crude protein extracts using pre-immune serum, uncleaned AtPCH2 antibody and AtASY1 antibody.
The blue arrow shows the expected size of AtPCH2 protein at around 52 KDa, the red arrow indicates the expected size of AtASY1protein (control); Bo= extracted protein from Brassica anthers; At= extracted protein from *Arabidopsis* wild-type buds.

Cleaned and uncleaned AtPCH2 antibodies were then used to probe the extracted protein from *Arabidopsis* wild-type (AtWT), *Atpch2.1, Atpch2.2* and Brassica. 25 µl of each extract was loaded onto a 10% SDS-PAGE gel followed by electro blotting to nitrocellulose. **Figure 4.7** showed clearly that a band corresponding to the expected size of AtPCH2 was recognised by the purified AtPCH2 antibody. However, the recognised bands were also observed in *Atpch2.1* and *Atpch2.2* extracted proteins with a less intensive band compared to the wild-type. This result is consistent with the RT-PCR experiment described in Chapter 3. *Atpch2* mutants may express a protein that is not functional. This is confirmed by the aberrant meiotic phenotype observed in

Atpch2 plants. In terms of AtPCH2 antibody specificity, the experiment presented a successful cleaning of the AtPCH2 antibody and confirmed the presence at higher intensity of the AtPCH2-sized band. In the Brassica anther extract, an intense band of ~ 90KDa was also observed. This is discussed further in **Section 4.7**.
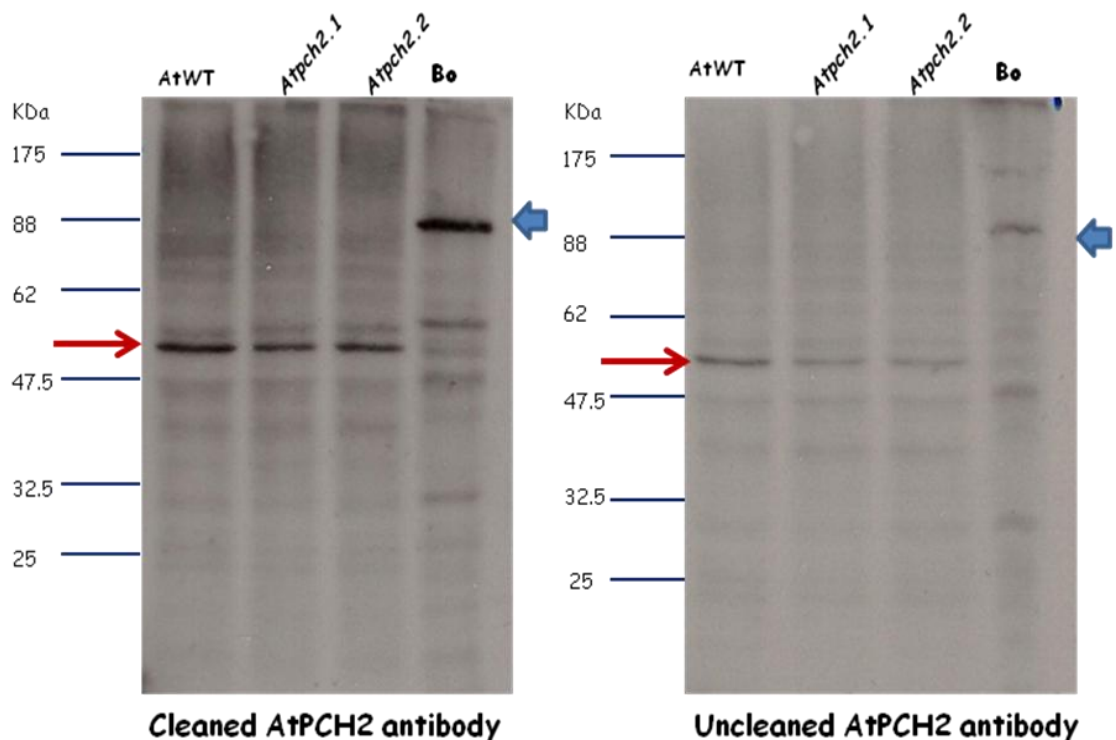
Figure 4. 7: Western blot analysis of plant proteins probed with cleaned and uncleaned AtPCH2 antibody.
The red arrow indicates the expected size of AtPCH2 protein at around 52 KDa that was probed by the AtPCH2 antibody. The blue arrow shows bands at around 90 KDa in Brassica that was probed by ATPCH2 antibody; Bo = extracted protein from Brassica anthers; AtWT, *Atpch2-1* and *Atpch2-2* = extracted protein from wild-type and mutant *Arabidopsis* buds respectively.

4.6 Immunolocalisation of AtPCH2 on chromosome spread preparations of PMCs

In order to investigate the localisation of AtPCH2 in meiotic prophase I, the purified AtPCH2 antibody was used to perform immunolocalisation on spread chromosomes of *Arabidopsis* wild-type and *Atpch2* mutant PMCs. AtASY1 antibody was also used to track the chromosome axis and mark meiotic progression. As the purified AtPCH2 antibody had been produced the first time, it was used at a range of concentrations of 1:100, 1:500, 1:1,000 and 1:5,000 in 1% BSA. The best concentration for immunolocalisation was estimated at a dilution of 1:1,000 (data not shown). Dual-immunolocalisation of AtASY1 and AtPCH2 antibodies on chromosome spread preparation of wild-type and *Atpch2.1* meiocytes were performed. In wild-type, AtPCH2 starts to localise on chromosomes at early leptotene stage and is visualised as numerous foci. The number of AtPCH2 foci seemed to reach a peak at late leptotene/early zygotene and then is reduced at late pachytene to form 7-10 foci (**Figure 4.8**). This result corresponds to AtPCH2 and AtZYP1 dual-immunolocalisation in wild-type (**Figure 4.9**). However, these appearances also occur in *Atpch2* mutants. AtPCH2 protein foci of similar number and dynamics to wild-type were observed in *Atpch2* mutants.
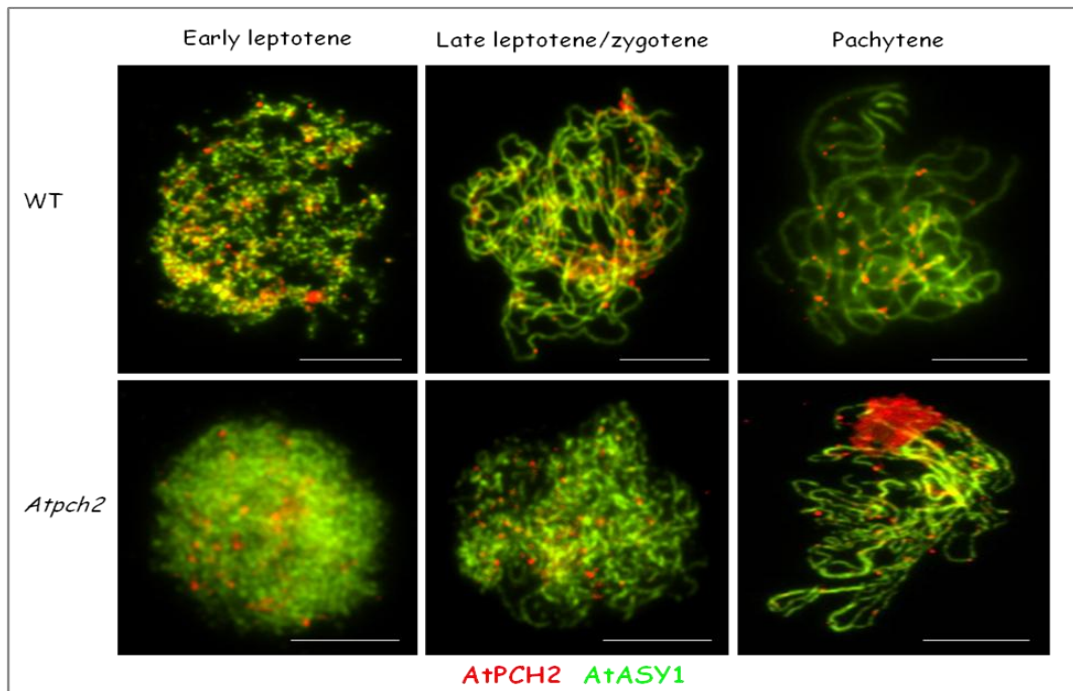
Figure 4. 8: Dual-immunolocalisation of AtASY1 and AtPCH2 antibodies on chromosome spread preparation of AtWT and *Atpch2.1* meiocytes. Scale bar = 5 µm.
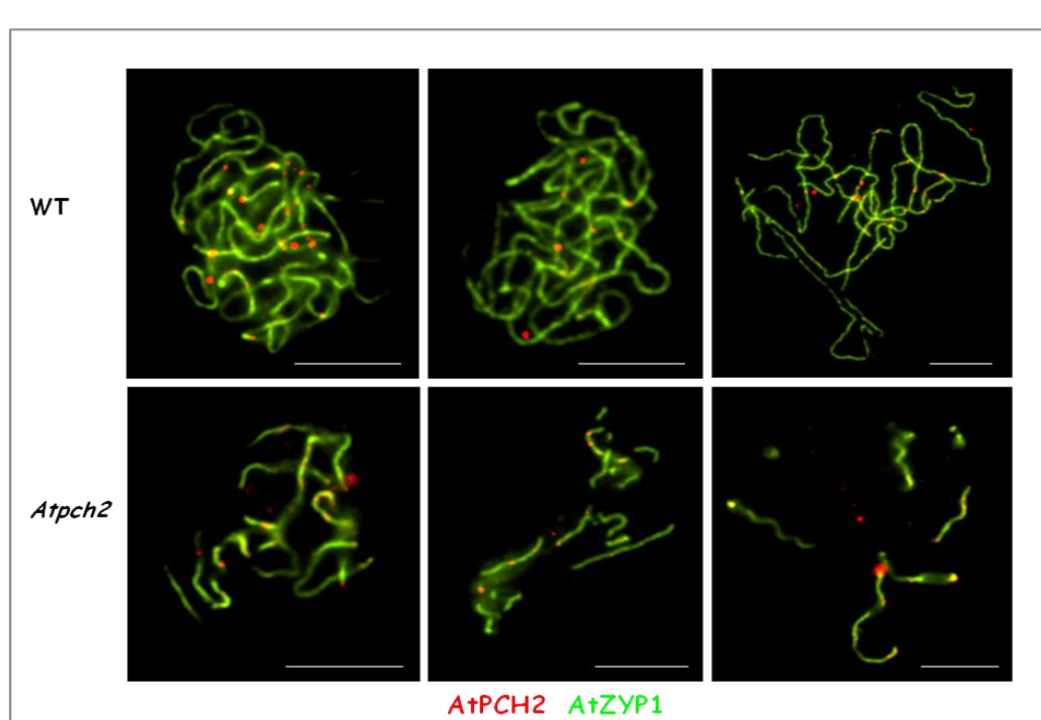
Figure 4. 9: AtPCH2 and AtZYP1 dual-immunolocalisation in wild-type and *Atpch2.1* meiocytes. Scale bar = 5 µm.

4.7 Discussion

The AtPCH2 antibody presented in this chapter was successful in terms of production and purification and could detect a AtPCH2-sized band in plant wild-type extracts. However, it was unclear in terms of specificity in that a AtPCH2-sized band could also be detected using cleaned AtPCH2 antibody in extracted protein from both *Atpch2.1* and *Atpch2.2*, although this was at a lower intensity than in wild-type. It is possible some AtPCH2 protein remains in the mutants. This may also explain the presence of AtPCH2 foci along chromosomes in *Atpch2.1* meiotic prophase I using immunolocalisation. Considering this proposal, it is worth mentioning the RT-PCR results in Chapter III showing that two transcripts were expressed downstream of the T-DNA insertion site of *Atpch2* mutants. Alternatively, the AtPCH2 antibody may be recognizing other proteins besides AtPCH2. When selecting and designing a sequence for antibody production, the aim is to use a region of the protein which is specific to that protein so that the produced antibody should specific recognises only the target protein and not any other protein. Unfortunately, the AtPCH2 protein region was designed containing the conserved AAA-ATPase domain (**Figure 4.1**) so the AtPCH2 antibody may be recognizing other proteins with this domain. Furthermore, proteomic experiments (Kim Osman, unpublished) suggest that CDC48, which also has this domain, is expressed in meiocytes. Therefore it is possible that the AtPCH2 antibody is also recognizing CDC48 during immunolocalisation. This is supported by the western blot of Brassica extracted proteins (**Figure 4.7**) which shows an intense band at around 90 KDa that corresponds to the predicted protein size of CDC48 (89.87

KDa in *B. oleracea*, 89.40 KDa in *A. thaliana*). The Brassica proteins in this experiment were extracted from anthers which will be highly enriched for meiotic proteins, whereas *Arabidopsis* proteins were extracted from whole buds which contain a much lower proportion of meiotic protein. This would explain the intense signal of the protein band in Brassica and the low/absent signal in *Arabidopsis* at ~90 KDa. The ~52 KDa band in *Arabidopsis* presented more intensely than any band of this size in Brassica (**Figure 4.7**). If this is AtPCH2 protein it would suggest that the protein is produced in other tissues besides meiotic tissue. This is consistent with the RT-PCR results (AtPCH2 was transcribed in bud, leaf, stem and root). In another proposal, the ~52 KDa band may consist of several different AAA-ATPase proteins which are around 52 KDa. As a result, this band was reduced in intensity but not absent in the *Atpch2* mutants. One or more of these proteins may also have been detected in foci using immunolocalisation of AtPCH2 antibody in *Atpch2* meiocytes.

Chapter 5

Analysis of *Atchr24*, a SWI2/SNF2 chromatin remodeling family member

5.1 Introduction

SWI/SNF family is one of four ATP remodeling families; the others are ISWI, CHD and INO80/SWR1 (Gangaraju and Bartholomew, 2007). In *S. cerevisiae*, *Drosophila* and Humans, The SWI/SNF complex is present in two versions: SWI/SNF and RSC. RSC is available in larger quantities in the cell than SWI/SNF. In addition, RSC is crucial for cell growth, whereas SWI/SNF is not. In yeast, the SWI/SNF complex functions in an early process of homologous recombination (HR) (Chai *et al*., 2005, Huang *et al*., 2005). SWI/SNF makes nucleosomal DNA accessible to active proteins by forming DNA bulges on the nucleosome surface (Fan *et al*., 2003). SWI/SNF may remove the DNA segment from the surface of the nucleosome and create a large DNA bulge, followed by movement of the bulge along the nucleosome surface. Consequently, the contact between H_2B and DNA can be restored again at a different DNA site (Gangaraju and Bartholomew, 2007). In budding yeast, the protein motifs of Rad54 are similar to switch2/sucrose non-fermenting2 (Swi2/Snf2) super family which are chromatin-related proteins (Eisen *et al*., 1995). RDH54 (TID1), a homolog of RAD54, is also involved in chromatin remodelling activity and acts in homologous chromosome repair. In addition, *RAD26*, *RAD16* and *RAD5* are also yeast SWI2/SNF2 genes and all are required for different aspects in DNA repair (Eisen *et al*., 1995; Shinohara *et al*., 1997). Studying the deficiency of *RAD54* homologs in other organisms have revealed that mutant lines are sensitive to radiation and to alkylating agent and defective in exogenous DNA insertion such as in chicken (Bezzubova *et al*., 1997), fission yeast (Muris *et al*., 1997), mice (Essers *et al*., 1997) and *Drosophila*

(Kooistra *et al.*, 1997). In plants, analysis of SWI2/SNF2 function by gene silencing revealed that SWI2/SNF2 affected various processes. *ddm1* (decreased DNA methylation 1) mutation led to gradual demethylation of the genome and decreased gene silencing. Both *ddm1* and *mom1* (Morpheus molecule 1) mutants are deficient in gene silencing in *Arabidopsis* (Jeddeloh *et al.*, 1999), while RNA-directed DNA methylation required DRD1 (Kanno *et al.*, 2004, 2005) and cell transition from the embryonic to the vegetative state required the gene *PICKLE* (*GYMNOS*) (Ogas *et al.*, 1999). *PICKLE* also controls differentiation of carpel tissue in *Arabidopsis* (Eshed *et al.*, 1999). Another swi/snf family member, *SPLAYED,* has been shown to be required for normal reproductive development (Wagner and Meyerowitz, 2002) Another study showed that At5g63950/CHR24-like protein mutant is sensitive to radiation such that seedlings had no true leaves 10 days after irradiation, with death occurring a few days later (Shaked *et al.*, 2006). Although CHR24-like protein and other Swi2/Snf2 family members in *Arabidopsis* have been studied, their function during meiosis has not been investigated. As CHR24-like protein is a potential SC-associated protein, as identified by proteomic approach (discussed later), investigation of this protein in *Arabidopsis* may provide insight into the functional interrelationships between chromatin remodelling and meiotic recombination pathways.

5.2 Identifying *Atchr24* T-DNA insertion mutant line

CHR24-like protein (chromatin remodeling 24) is a protein encoded by a gene at locus At5g63950 in *Arabidopsis.* CHR24 is a member of Swi2/Snf2 super family (Shaked *et al.*, 2006; **Figure 5.1**). This protein was found in a pull down assay using an anti-ZYP1 antibody on *Brassica* crude extract (Osman K and Franklin FC, unpublished). *Atchr24*, a T-DNA insertion at locus At5g63950 (SALK_007071) will be referred to *Atchr24* in this project. Homozygous plants for the T-DNA insertion were identified by PCR (data not shown). This mutant line was identified and characterized by analysis of fertility and meiotic cytology compared to wild-type. However, SALK_007071 is only one of eight At5g63950 T-DNA lines which present reduced fertility, while two T-DNA insertion lines presented normal fertility compared to wild-type and five lines in which the T-DNA insertion could not be detected (**Figure 5.2**).
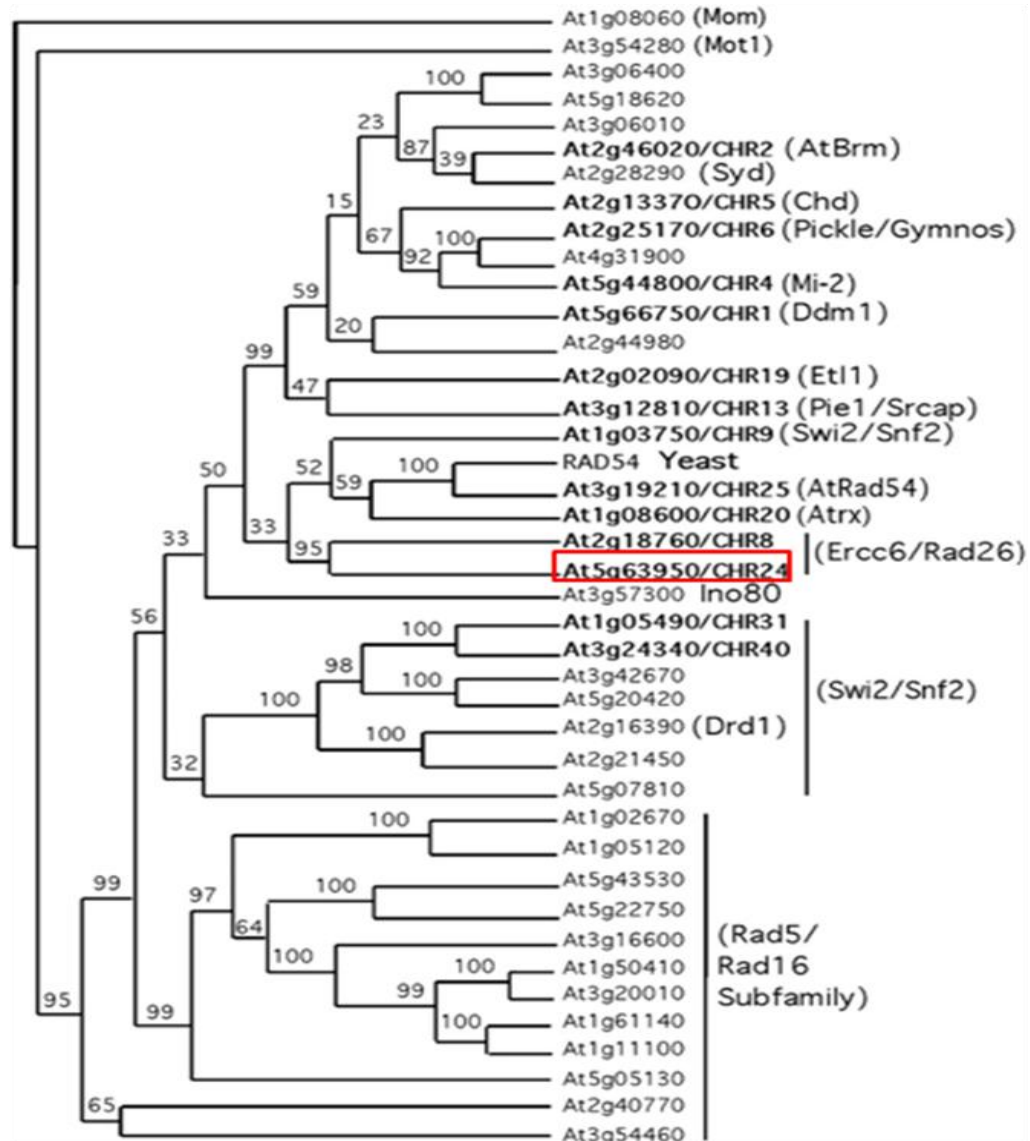
Figure 5. 1: Phylogenetic tree of Swi2/Snnf2-like proteins

The Phylogenetic tree shows At5g63950 /CHR24 (in red block) is a member of *Arabidopsis* Swi2/Snf2-like proteins which are related to the yeast Rad54. Rad54 is implicated in DNA recombination and repair (Eisen *et al*., 1995). Characterised proteins are shown in parentheses (Shaked *et al*., 2006).
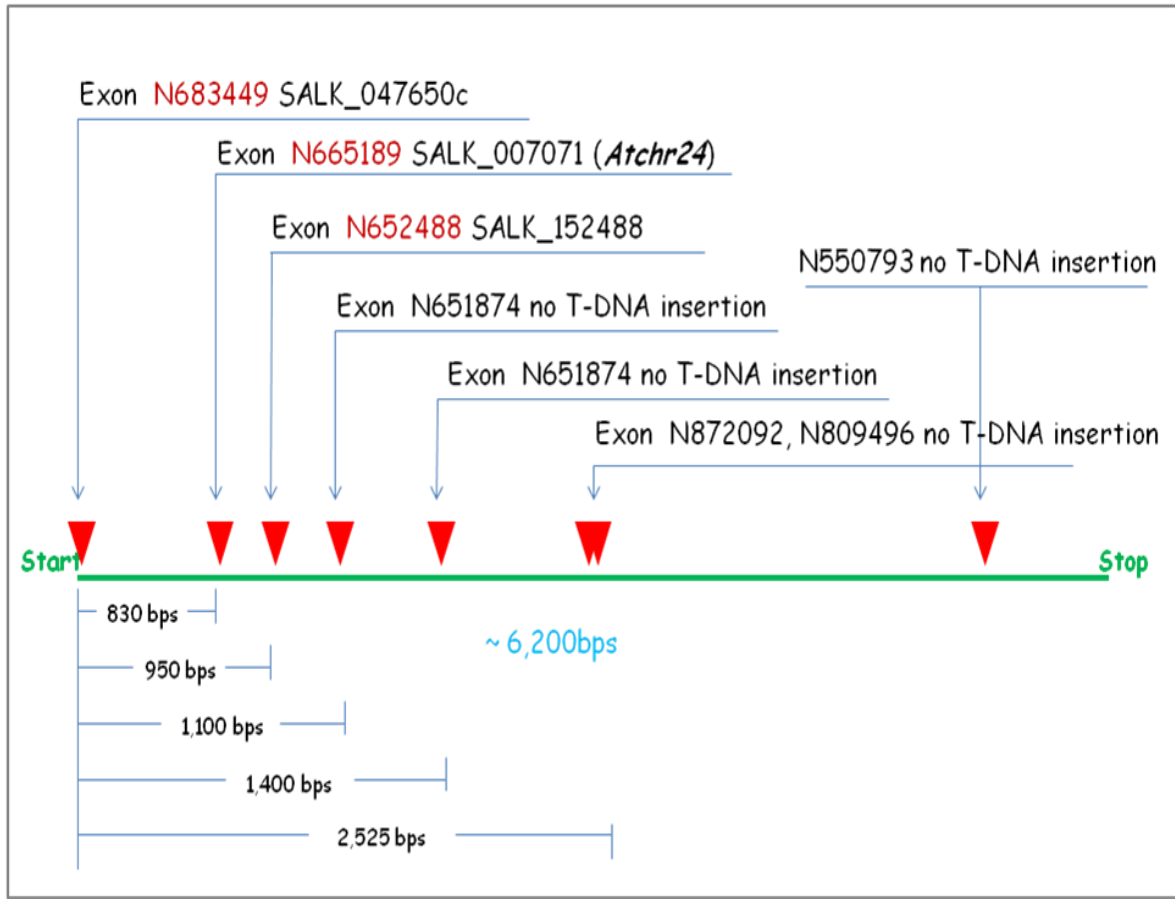
Figure 5. 2: Map of T-DNA insertion lines for At5g63950
The map shows 8 T-DNA insertions (orange triangle) in At5g63950 locus (green bar)
N665189 SALK_007071is referred to *Atchr24* in this experiment, and present a
meiotic defect. N683449 SALK_047650c and N652488 SALK_152488 have normal
fertility and meiotic progression while the other T-DNA lines did not have the T-DNA
inserted in At5g63950 locus.

5.3 Fertility and pollen viability are reduced in *Atchr24* mutant

Atchr24 and wild-type seeds were sown in pots under standard greenhouse conditions

(**see Materials and methods**). Vegetative growth of *Atchr24* was completely normal

compared to wild type plants. However, *Atchr24* plants had short siliques with 1.30 ±

0.03 cm (mean ± sd) in length compared with 1.70 ± 0.04 cm (mean ± sd) in length for

wild type (**Figure 5.3A**). **Figure 5.3B** and **5.3C** shows that the number of seeds in one

silique of *Atchr24* plants is 15.69 ± 4.51(mean ± sd) seeds per silique in average, whereas 68.21 ± 3.2 (mean ± sd) seeds per silique were scored in wild type. Analysis of pollen grains by Alexander staining, showed that a large number of pollen grains were abnormal. Pollen grains can be divided into 6 types based on their appearance (**Figure 5.4**). The appearances of different types with their percentage are presented in **Figure 5.4A** and **5.4B**.
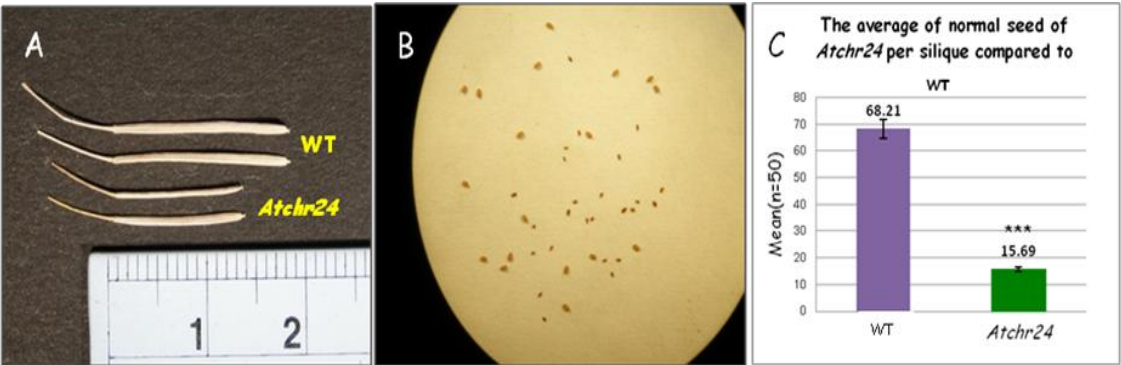
Figure 5. 3: Reduced fertility in *Atchr24*
(A) shows the difference of silique length between *Atchr24* and wild type. (B) shows that a silique consists of both well-developed and withered seeds. The number of seeds per silique in *Atchr24* and wild type shows in C.
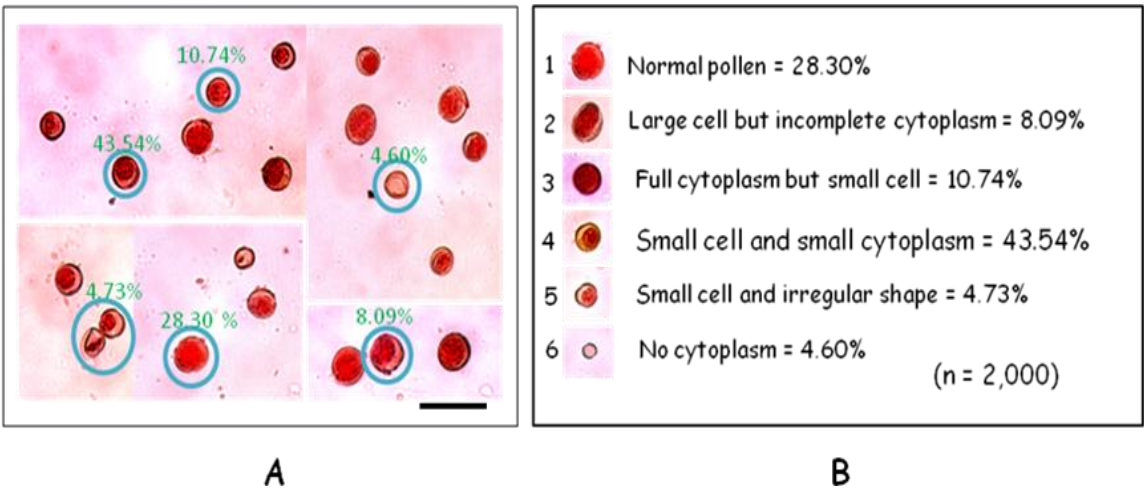
Figure 5. 4: 6 types of *Atchr24* pollen grains and their proportions of the total.
(**A**) and (**B**) show the representative appearance of each type of *Atchr24* pollen grains in percentage. Scale bar = 50 μm.

The first type was the wild-type-like normal pollen (28.30%). Pollen grains were a round shape and had a full cytoplasm that differs from the second type, which showed incomplete cytoplasm, although the sizes of both types were similar. The third type had a full cytoplasm but the pollen were markedly smaller than the second type. The fourth type represents the majority of pollen grains with 43.54%. The pollen and cytoplasms in this type being variable in size relative to each other, but were generally much smaller than the type 1 pollen. The fifth and sixth types were also small but appeared to be irregularly shaped. Moreover, the sixth type had no visible cytoplasm.

5.4 Cytological analysis of *Atchr24* mutants

Although *Atchr24* has only a few well-developed seeds per silique, a large number of meiocytes were visible cytologically. DAPI-staining (**see Materials and methods**) was used with *Atchr24* PMCs. At pre-prophase I and leptotene, their chromosome behaviour appeared normal (data not shown). At pachytene, synapsed chromosomes appeared normal, apart from in some nuclei where chromosomes showed some regions which were not synapsed. **Figure 5.5A** is the pachytene stage of a wild-type PMC. **Figure 5.5B** shows two sites on an *Atchr24* chromosome forming loops (**yellow arrows**), indicating that these sites were unpaired chromosome regions.
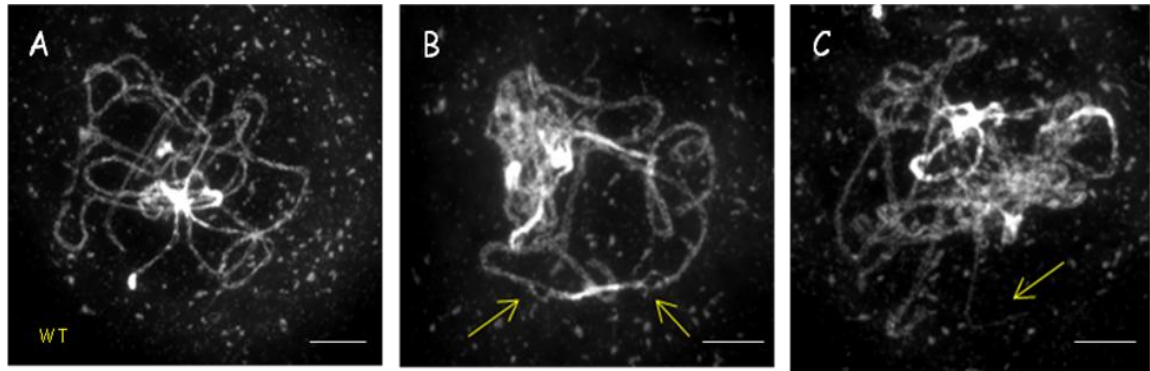
Figure 5. 5: DAPI-stained of *Atchr24* and wild-type at pachytene pollen mother cells. Homologous chromosomes were not fully synapsed, showing chromosomal loops in (B) and chromosomal end opening in (C) (yellow arrows) compared to wild-type in (A). Scale bar = 5 µm.

Also, one end of a *Atchr24* pachytene chromosome (**arrow in Figure 5.5C**) appears to be open, indicating the pairing of homologous chromosomes was not complete at this area. In some cases a small chromosome fragment was observed during the first meiotic cell division (The **yellow arrows in figure 5.6A, 5.6B and 5.6C**). This phenomenon could cause the loss of genes from the genome in these gametes. In addition, the uneven condensation problem still persisted at both the first and second meiotic cell division. This problem was more clearly visualized in highly condensed chromosomes.
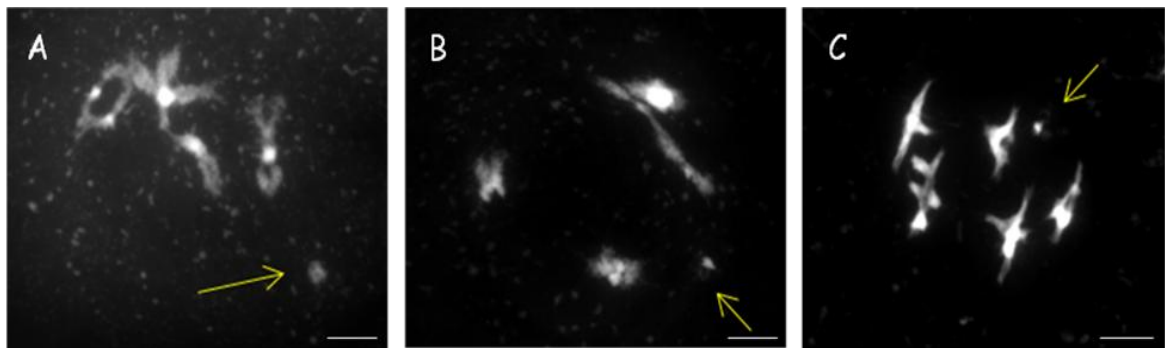
Figure 5. 6: Chromosome fragmentation in *Atchr24* mutant
Yellow arrows show a small chromosome fragment observed in *Atchr24* meiocytes at late diplotene stage (**A** and **B**) and late diakinesis stage (**C**). Scale bar = 5 µm.

Chromosome condensation at diakinesis, MI and tetrads were abnormal. While some nuclei possessed highly compact chromatin, others displayed decondensed chromatin in the same meiocytes. **Figure 5.7A, 5.7B and 5.7C** the yellow arrows show the decondensed bivalents/polar groups which appeared 'fluffy'. The four polar groups of five chromatids of *Atchr24* (**Figure 5.7C**) show the different patterns of condensation with different sizes. Moreover, a few meiocytes showed chromosomes progressing through zygotene and pachytene in several distinct clusters (**Figure 5.8A and 5.8B**). The yellow arrows show a separated cluster.
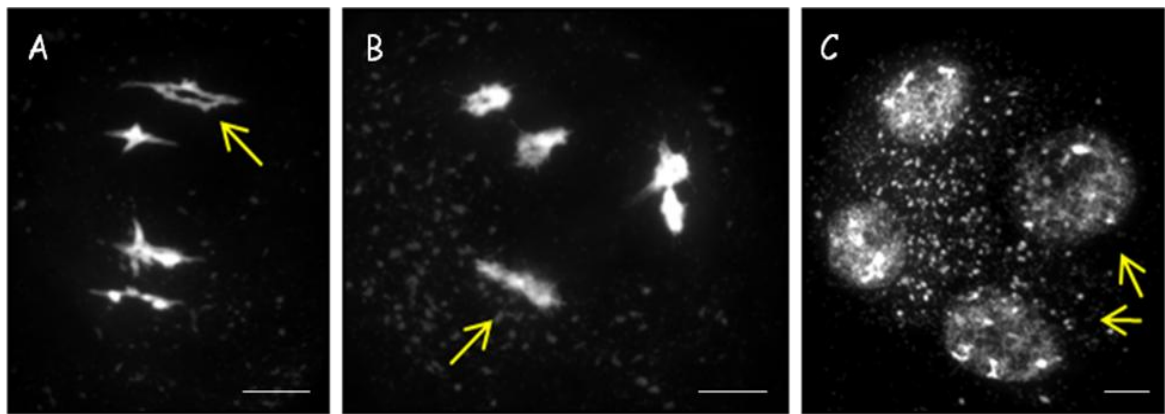
Figure 5. 7: Uneven condensation within meiocytes at several stages of meiosis of *Atchr24*. Yellow arrows show the different patterns of condensation of bivalents (A and B) and polar groups (C) in Atchr24. Scale bar = 5 µm.
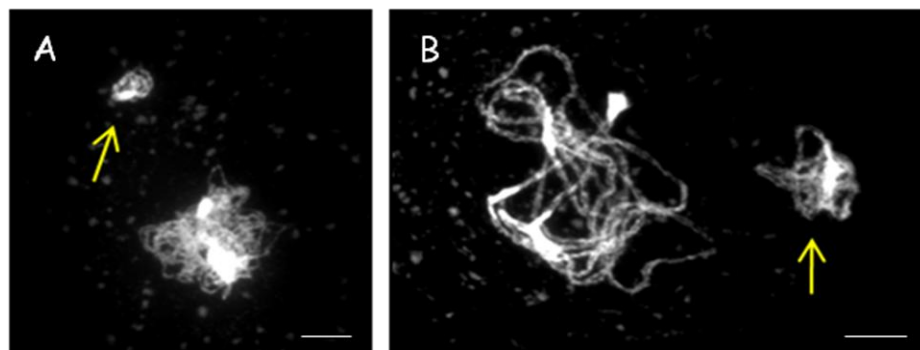
Figure 5. 8: Chromosomes progress in several distinct clusters in *Atchr24*.

Yellow arrows show a separate cluster at zygotene (**A**) and pachytene (**B**) in *Atchr24* mutant. Scale bar = 5 μm.

5.5 Chiasma counting in *Atchr24* mutant

The mean chiasma frequency of *Atchr24* was determined by fluorescence *in situ* hybridisation (FISH) using 45s and 5s rDNA probes (**see Materials and Methods**) on 50 wild-type and *Atchr24* PMCs. The results revealed that the p-values (ANOVA) of the mean chiasma frequency per meiocyte were non-significant at the 5% level, with 9.85 and 9.08 for wild-type and *Atchr24* respectively. However, there were different results for individual chromosomes, in that chromosome I, II, III of *Atchr24* exhibited non-significant differences compared to wild-type, whereas chromosome IV and V had significant difference at 5% level (**Table 5.1**). This may suggest that AtCHR24 might be not required for CO resolution in recombination pathways.
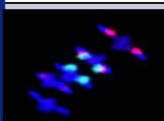
Chiasma scoring using FISH to identify chromosomes						
	Chrm I (mean)	Chrm II (mean)	Chrm III (mean)	Chrm IV (mean)	Chrm V (mean)	Mean total
WT (n=50)	2.36	1.78	1.93	1.71	2.07	9.85
Atchr24 (n=50)	2.22	1.70	1.78	1.50	1.86	9.08
P-value (ANOVA)	N.S. 0.1612	N.S. 0.3197	N.S. 0.2253	* 0.0221	* 0.0339	N.S. 0.3673

Table 5. 1: Chiasma Scoring using FISH to identify *Atchr24* chromosomes

P-value (ANOVA) of all chromosomes between wild-type *(WT) and Atchr24 are non-significant difference at 5% level except chromosome IV and V: (*) is significant difference at 5% level, N.S. is non-significant difference (n=50).*

5.6 Immunolocalisation: functional analysis of the *Atchr24* mutant

Immunolocalisation on spread chromosome preparations of wild-type PMCs, using AtASY1 and AtZYP1 antibodies showed that AtASY1 localised along chromosome axes during leptotene, while AtZYP1 initiated localisation on the central element of homologous chromosomes during zygotene stage and continued to polymerise until extending along the full length of homologous chromosomes at late pachytene. In regions showing AtZYP1 localisation, AtASY1 no longer localises as a clear linear signal, though they could slightly overlap at the edge of their association. This phenomenon also occurred in *Atchr24,* where AtASY1 and AtZYP1 dual-immunolocalisation reveals that localisation of AtASY1 and AtZYP1 in *Atchr24* was indistinguishable from wild-type (**Figure 5.9**).
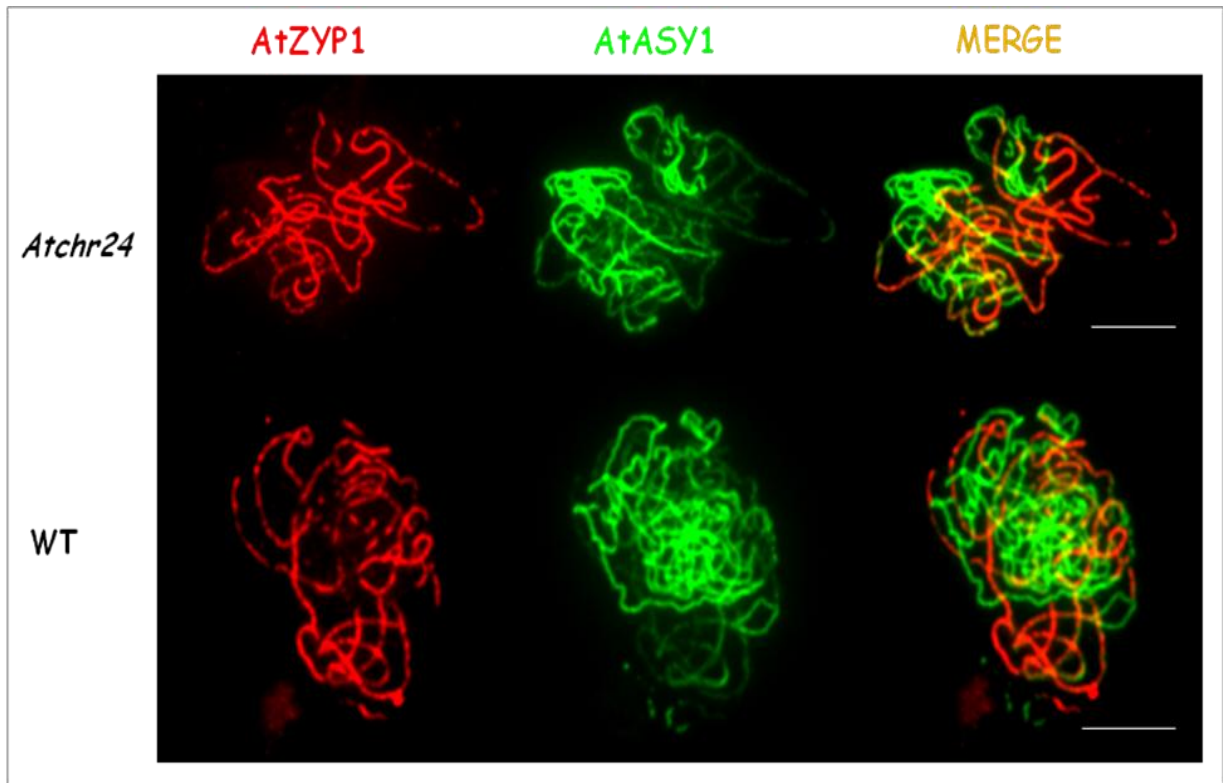
Figure 5. 9: Immunolocalisation in *Atchr24* compared to wild-type
Immunolocalisation of AtASY1 and AtZYP1 in *Atchr24* was normal at zygotene stage compared to wild-type. Scale bar = 5 µm.
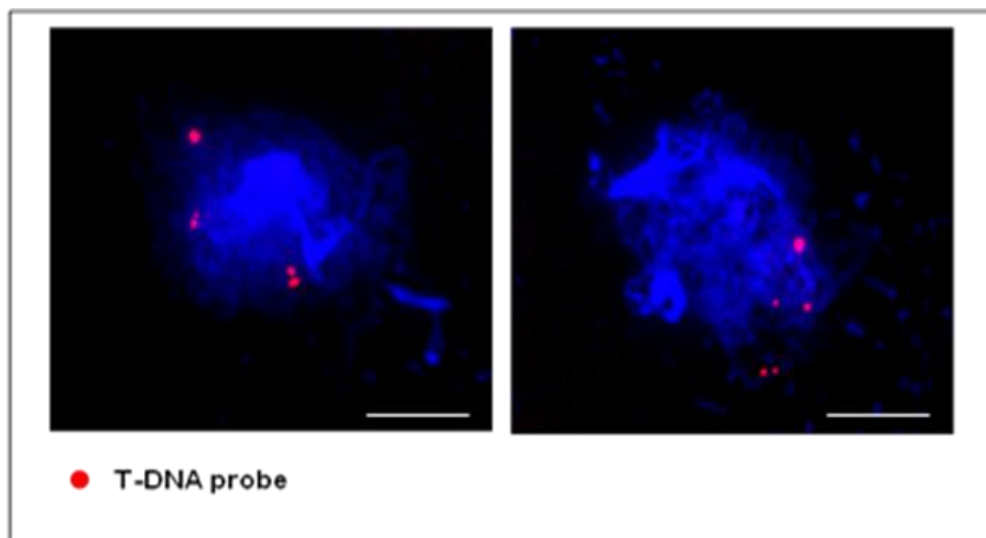
Figure 5. 10: Multiple T-DNA insertions in *Atchr24*
FISH analysis using T-DNA probes (red signals) revealed that *Atchr24* line has more than one site, or at least three sites of T-DNA insertion in the genome. Scale bar = 5 µm.

5.7 Multiple T-DNA insertions were observed in *Atchr24* genome

PCR using gene specific primers and T-DNA insertion primers for At5g63950 was used to identify N683449 (SALK_047650c) and N652488 (SALK_152488) as additional *Atchr24* mutant lines. However, both of them appeared to show completely normal fertility and cytological behaviour (data not shown). The absence of a meiotic phenotype for these two alleles, suggests that the T-DNA insertion may be present in a gene other than *AtCHR24* in SALK_007071. The disruption of that gene would then result in the meiotic phenotype observed in the *Atchr24* mutant. FISH analysis using a T-DNA probe showed multiple insertions in *Atchr24*, at least three loci (**Figure 5.10**), indicating that more than one T-DNA is inserted in the genome.

5.8 Discussion

CHR24-like protein is encoded by a Rad26-like gene at locus At5g63950 in *Arabidopsis,* belonging to the SWI2/SNF2 chromatin remodelling family. The gene has also been reported to be involved in DNA damage response, as a mutant showed radiation sensitivity. Therefore CHR24-like protein was proposed to be involved the modification of nucleosome structure where is amount of proteins implicated in (Shaked *et al*., 2006).

In this experiment, the fertility of *Atchr24* seemed to be affected by showing only 15 seeds per silique, suggesting that AtCHR24 could have a role during meiosis. The low fertility in *Atchr24* was confirmed by Alexander staining, which revealed a large

proportion of abnormal pollen. In DAPI-stained pollen mother cells (PMCs) of *Atchr24*, a few loops (**Figure 5.5B**) were observed on chromosomes in pachytene, indicating that the homologous chromosomes had not properly aligned in this area, and/or both sister chromatids might be not condensed properly, and as a result they were unequal in length. This hypothesis can also explain the occurrence of the pachytene chromosome opening at the one end (**Figure 5.5C**). The condensation defect of chromosomes can be seen in both diakinesis and MI, with the difference in condensation patterns for each bivalent. Some bivalents were highly compact, while some still appeared 'fluffy'. These phenomena were consistent with the appearance of four polar groups of five chromatids occurring with unequal degrees of decondensation.

Due to the similar problems observed at many stages of *Atchr24* meiosis, it is more than plausible that *Atchr24* is defective in chromatin structural maintenance. In some cases, fragments were observed in meiocytes, suggesting that the machinery of DNA repair may be affected. However, the progression of meiotic chromosomes in several distinct clusters remains difficult to explain. Although *Atchr24* chromosomes displayed many problems in several stages of meiosis, only chromosome IV and V had a reduction in the number of chiasmata, with significant differences at 5% level compared with wild-type (**Table 5.1**). This result indicates that either the deficiency of *Atchr24* is not a severe problem in chiasma formation or some of the related homologues contribute to substitutional redundancy. Immunolocalisation of AtASY1

and AtZYP1 in *Atchr24* was indistinguishable from wild type, indicating that the organization of AtASY1 and AtZYP1 is not affected in *Atchr24*. In contrast, a reduced rate of pollen survival was observed. This may suggest that AtCHR24 deficiency may affect the process of PMC development, as only 28.30% can be succeeded. N683449 and N652488 homozygote insertion lines of At5g63950 both display normal fertility and cytology behaviour. There is also evidence which confirms that multiple insertions are present in the *Atchr24* genome. Therefore all defects observed by this T-DNA insertion line in this experiment might be affected from another inserted site in *Atchr24* genome. The observed phenotype suggests that the *Atchr24* mutant is defective in meiosis, and whether this defect is a result of T-DNA insertion into the AtCHR24 gene or another gene, the mutant still warrants further investigation.

Chapter 6

Discussion

6.1 Introduction

Since the mid-1990s *Arabidopsis* has been developed as a model system for the study of plant meiosis. Over the past decade studies in rice and maize have also provided insights into plant meiosis. The identification of meiotic mutants has provided an important approach to studying plant meiosis. However, the availability of the *Arabidopsis* genome sequence together with developments in proteomics and bioinformatics provides an additional route for the identification of meiotic proteins and analysis of their functional interrelationships. This research has used a combination of these approaches to identify candidate meiotic genes and proteins in *Arabidopsis*. This study has analysed homologues of two known meiotic genes, namely *PCH2* and a member of the *SWI2/SNF2* chromatin remodeling gene family.

6.2 Analysis of *Atchr24*

One of the *Arabidopsis SWI2/SNF2* gene family is *AtCHR24* which has been revealed to be an ortholog of *RAD54* and *ERCC6/RAD26*. AtCHR24 is encoded by the locus At5g63950. Based on the analysis of a SALK_0007071 T-DNA insertion mutant AtCHR24 has been proposed to be involved in DNA damage response (Shaked *et al*., 2006). In this project we studied the same T-DNA insertion line as Shaked *et al*., 2006. However, rather than focusing on the somatic DNA repair phenotype, we sought to determine if mutation of the gene resulted in an effect on meiosis. Several defects were observed in our analysis of *Atchr24*. These include a drastic reduction of fertility,

defects in pairing of homologous chromosomes in some regions and uneven condensation of chromosome pairs. However, further analysis of two additional T-DNA insertion lines in the same gene, SALK_047650c and SALK_152488 failed to confirm these observations. In addition the finding that the SALK_007071 T-DNA insertion in At5g63950 contains multiple T-DNA insertions would suggest that the observed meiotic phenotypes may be due to a mutation in another gene, here forth referred to as AtAPD (Abnormal Pollen Development).

The *Atapd* mutant has presented defects involved in meiotic recombination such as homologous chromosomes not pairing properly at pachytene stage. However, the chiasma frequency result using FISH at MI has verified that all defects occurring during prophase I were not vital for *Atapd* fertility as a non-significant difference of chiasma frequency overall was obtained in *Atapd* chiasma scoring. In contrast, a large number of abnormal pollen grains was observed using the Alexander staining method. This might suggest that AtAPD is required for male gametophytic development and/or establishment. It is also possible that loss of AtAPD also affects female gametophyte development and establishment but this was not analysed in this project. Hence, further studies will be required to identify the AtAPD gene.

6.3 AtPCH2 is required for interhomologue CO formation and chromosome axis remodeling

Progression through prophase I of meiosis leading to crossover (CO) formation is accompanied by and dependent on extensive remodelling of the chromosome axis.

This experiment has used a bioinformatics approach to identify a potential orthologue of Pch2/TRIP13 in *Arabidopsis*. PCH2 (Pachytene checkpoint 2) is a member of the AAA+ ATPase family of proteins. This study reveals that AtPCH2 plays an essential role in the controlled formation of meiotic COs. Cytogenetic analysis of two *Atpch2* T-DNA insertion lines, *Atpch2.1/Atpch2.2*, revealed a high frequency of univalents at MI leading to a reduction in the number of chiasmata (COs) to ~ 70% of wild-type. Although the chiasma frequency was reduced, the number of DSBs in *Atpch2* appeared normal confirmed by AtRAD51/AtDMC1 immunolocalisation. This may correspond with promoting interhomolog bias in budding yeast in that Pch2 is involved in promoting Hop1 phosphorylation. Furthermore, Pch2 and Rad17 are required to prevent intersister repair during meiotic recombination in independent pathways (Ho and Burgess, 2011). Therefore meiotic repair using sister chromatids may be upheld in *Atpch2* by using AtRAD17 pathways. Genetic analysis revealed that *Atpch2* has significantly weaker CO interference than wild-type. This is also supported by the distance between AtMLH1 foci in immunolocalisation experiments on *Atpch2* leading to a redistribution of COs along the chromosomes. The recombination defect is accompanied by incomplete chromosome synapsis. Immunolocalisation of the chromosome axis protein AtASY3 and cohesin, AtSYN1 appears normal. However in contrast to wild-type, AtASY1 co-localises with the synaptonemal complex protein, AtZYP1, in *Atpch2* rather than becoming depleted in regions of synapsis and the meiotic progression of *Atpch2* is delayed during pachytene by at least 5h. These

observations suggest a defect in remodeling of the chromosome axis and highlight how this process is essential for normal CO control.

The observation that AtASY1 persists to colocalise with AtZYP1 during pachytene stage in *Atpch2* could be explained by three reasonable proposals. Firstly, invisible AtASY1 along chromosomes during pachytene in wild-type may result from AtASY1 protein degradation. However, a western blot experiment revealed that AtASY1 was detected in meiotic cells during the pachytene stage (Armstrong *et al*., 2002). Secondly, AtASY1 proteins are depleted along the chromosome axis but may be free in the nucleus or nucleolus in wild-type. The third proposal is that AtASY1 still localises on the axes in wild-type but the antibody does not recognize it following synapsis. This may result from protein congestion on the axes/SC during the pachytene stage of wild-type. At the pachytene stage the span of the SC lateral element is shortest (~140 nm) (Figure 3.29), and many proteins are recruited to function on the axes/SC in the meanwhile such as ASY3, SMC3, SYN1 *etc*. The protein congestion may affect the configuration of the AtASY1 epitopes leading to the antibody paratope cannot recognise. Silver-stained chromosomes using EM analysis reveals that the span measurement between axes of homologous chromosome synapsed regions of wild-type and *Atpch2* were presented as equal in size at 140 nm (Figure 3.29). This data might not support the third proposal in that the congestion of proteins on the SC may not affect the configuration of AtASY1 epitope. However, this result could support the second proposal in that AtASY1 is not released from chromosome axis at pachytene in

the *Atpch2* mutant, suggesting that the AtPCH2 protein may be required for releasing AtASY1 in order to allow another protein to be recruited on the SC to function at this stage. A recent study reveals that the Pch2 orthologue in rice, CRC1, may be a conserved SC component (Miao *et al*., 2013). This report may support the results that some regions of homologous chromosomes are unpaired at the pachytene stage in *Atpch2* mutants. This defect may result from the proper SC installation being not facilitated by certain proteins which may be dependent on AtPCH2. As a result, loss of AtPCH2 leads to meiotic progression delay at pachytene and a reduction of CO frequency was observed in this mutant. Complete homologous chromosome paring was not observed at the pachytene stage in *Atpch2* mutants. Therefore AtPCH2 may be involved in ensuring the efficient formation of SC on homologous chromosomes. Although, in budding yeast, the SC has been demonstrated that it is not necessary for CO interference (Borner *et al*., 2004), studying in *C. elegans* using two-chromosome fusion and SYP-1 partial depletion by *syp-1* RNAi, revealed that defect of the efficient SC formation results in attenuation of CO interference (Libuda *et al*., 2013). This might be consistent with *Atpch2* in term of defective SC. *Atpch2* may affect to the efficient formation of the SC as described above, consequently leading to attenuate CO interference as shown in the dual-immunolocalisation of AtMLH1 and AtZYP1 and the fluorescent pollen assay data. Based on RT-PCR experiments, AtPCH2 was also expressed in several other plant tissues, besides buds. However, this project did not analyse the complex roles of AtPCH2 in somatic tissues.

6.4 Future perspectives

Due to the anti-AtPCH2 antibody being raised against a region of the protein containing the conserved AAA-ATPase domain, which is shared in widespread proteins (TAIR), the results of immunolocalisation using the anti-AtPCH2 antibody have been unclear. To solve this obstacle, a new AtPCH2 antibody was raised against a 16 residue peptide from the C-terminal of the protein (**Figure 6.1**). The new AtPCH2 antibody was designed to be specific for the AtPCH2 protein while minimising similarity to any other proteins in *Arabidopsis*, especially AtCDC48.

```
PCH2 full length protein

MEIAEQKPMVEDPIPLPNASMEVSYQNPIEAATIPVQIAVAEPVATPNPPPCLHENKFLVSVEVCLKPSSTARLEDVQRAVE
RMLENRSMSYADGLVLIPADDLFLVDNVQRICICDTEEWVKNNDVLLFWQVKPVVHTFQLIEEGPCEDLCADGQPASFNEWI
LPAKEFDGLWESLIYESGLKQRLLRYAASALLFTQKGVNPNLVSWNRIILLHGPPGTGKTSLCKALAQKLSIRCNSRYPHCQ
LIEVNAHSLFSKWFSESGKLVAKLFQKIQEMVEEDGNLVFVLIDEVESLAAARKAALSGSEPSDSIRVVNALLTQMDKLKSA
PNVIILTTSNITTAIDVAFVDRADIKAYVGPPTLHVRYEILRSCVEELISKGIISSFQGCDGLSIPSFSSLKEKLSESEVHD
TNTVPWFCKQLIEAAKGCEGLSGRSLRKLPFLAHAALADPYSHDPSNFLCTMIETAKREKSEQPE
```

Figuer 6. 1: A AtPCH2 region for producing a new AtPCH2 antibody
Blue highlight, original AtPCH2 antibody; Green highlight, AAA-ATPase domain; Yellow highlight, new AtPCH2 peptide antibody. The new AtPCH2 antibody (C-terminal Peptide antibody) was designed to recognize a 16 residue stretch at the C-terminal of the AtPCH2 protein (Kim Osman, unpublished results).

6.5 Conclusion

The *AtPCH2* gene encodes a protein that is required for the controlled formation of genetic crossovers during meiosis. These studies indicate that loss of the AtPCH2 protein results in a change in crossover distribution. The significance of this is that it may provide the means to alter patterns of recombination in crop species, in particular

the cereals, such as barley where recombination is normally restricted to certain chromosome regions such that 30-50% of the genes do not recombine. Bioinformatic approach provides a powerful route for the identification of meiotic proteins and analysis of their functional interrelationships. However, proteomic approach has a restricted efficiency in identification of candidate meiotic genes and proteins in *Arabidopsis*. This may cause from the variety of the potential SC-associated proteins which were identified from *Brassica oleracea* meiocytes. The results presented in this study represent the first insight into the role of PCH2 and PCH2-related proteins during meiosis in *Arabidopsis* and be could be useful for further studies into the complex functions of these proteins.

Reference list

Abe, K., Osakabe, K., Nakayama, S., Endo, M., Tagiri, A., Todoriki, S., Ichikawa, H. and Toki, S. (2005) *Arabidopsis* RAD51C gene is important for homologous recombination in meiosis and mitosis. *Plant Physiol*, **139**, 896–908.

Agarwal, S., Roeder, G.S. (2000) Zip3 provides a link between recombination enzymes and synaptonemal complex proteins. *Cell* **102**, 245-255.

Agmon, N., Yovel, M., Harari, Y., Liefshitz, B., Kupiec, M. (2011) The role of Holliday junction resolvases in the repair of spontaneous and induced DNA damage. *Nucleic Acids Res*. **39**, 7009–7019.

Akiyama, T., Nagata, M. and Aoki, F. (2006) Inadequate histone deacetylation during oocyte meiosis causes aneuploidy and embryo death in mice. *Proc. Natl Acad. Sci*, **103**, 7339–7344.

Alexandru, G., Uhlmann, F., Mechtler, K., Poupart, M. A. and Nasmyth, K. (2001) Phosphorylation of the cohesin subunit Scc1 by Polo/Cdc5 kinase regulates sister chromatid separation in yeast. *Cell,* **105**, 459–472.

Allers T, Lichten M. (2001) Differential timing and control of noncrossover and crossover recombination during meiosis. *Cell,* **106**, 47–57.

Anderson, L.K., Offenberg, H.H., Verkuijlen, W.M., Heyting, C. (1997) RecA-like proteins are components of early meiotic nodules in lily. *Proc. Natl. Acad. Sci.* **94**, 6868–73.

Anderson, L.K., Stack, S.M. (2005) Recombination nodules in plants. *Cytogenet. Genome Res,* **109**, 198–204.

Argueso, J.L., Wanat, J., Gemici, Z., Alani, E. (2004) Competing crossover pathways act during meiosis in Saccharomyces cerevisiae. *Genetics*, **168**,1805–1816.

Armstrong, S. J. and Jones, G. H. (2001) Female meiosis in wild-type *Arabidopsis thaliana* and in two meiotic mutants. *Sexual Plant Reproduction*, **13**, 177-183.

Armstrong, S.J., Franklin, F.C.H. and Jones, G.H. (2003) A meiotic time course for *Arabidopsis thaliana. Sexual Plant Reproduction*, **16**: (3): 141-149.

Armstrong, S.J. and Jones, G.H. (2003) Meiotic cytology and chromosome behaviour in wild-type *Arabidopsis thaliana*. *J. Exp. Bot*, **54**, 1-10.

Armstrong, S.J. (2013) Spreading and Fluorescence in situ Hybridisation of male and female chromosomes from *Arabidopsis thaliana* for cytogenetical analysis. Plant meiosis: Methods and protocols, methods in molecular biology book, vol. **990**. (Eds. Pawlowski, W.P., Grelon, M., Armstrong, S.J.), Springer Science Business Media New York.

Armstrong, S.J. and Osman, K. (2013) Immunolocalisation of meioticproteins in *Arabidopsis thaliana:* Method 2. Plant meiosis: Methods and protocols, methods in molecular

biology book, vol. **990**. (Eds. Pawlowski, W.P., Grelon, M., Armstrong, S.J.), Springer Science Business Media New York.

Armstrong, S.J., Caryl, A.P., Jones, G.H. and Franklin, F.C. (2002) ASY1, a protein required for meiotic chromosome synapsis, localizes to axis-associated chromatin in *Arabidopsis* and Brassica. *J. Cell Sci*, **115**, 3645-3655.

Arabidopsis **Genome Initiative** (2000) Analysis of the genome sequence of the flowering plant *Arabidopsis thaliana. Nature*, **408**, 796-815.

Ashley, T., Gaeth. A.P., Creemers, L.B., Hack, A.M., de Rooij, D.G. (2004) Correlation of meiotic events in testis sections and microspreads of mouse spermatocytes relative to the mid-pachytene checkpoint. *Chromosoma*, **113**, 126–136.

Aufsatz, W., Mette, M.F., Van Der Winden, J., Matzke, M. and Matzke, A.J. (2002) HDA6, a putative histone deacetylase needed to enhance DNA methylation induced by double-stranded RNA. *EMBO J*, **21**, 6832–6841.

Badie, S., Liao, C., Thanasoula, M., Barber, P., Hill, M.A., *et al.* (2009) RAD51C facilitates checkpoint signaling by promoting CHK2 phosphorylation. *J Cell Biol*, **185**, 587–600.

Bai, X.F., Peirson, B.N., Dong, F.G., Xue, C., Makaroff, C.A. (1999) Isolation and characterization of SYN1, a RAD21-like gene essential for meiosis in *Arabidopsis. Plant Cell,* **11**, 417–430.

Baumann, P., Benson, F.E. and West, S.C. (1996) Human Rad51 protein promotes ATP-dependent homologous pairing and strand transfer reactions in vitro. *Cell*, **87**, 757–766.

Becker, P.B. and Horz, W. (2002) ATP-dependent nucleosome remodeling, *Annu. Rev. Biochem*, **71**, 247–273.

Ben-Shahar, T. R. *et al.* (2008) Eco1-dependent cohesin acetylation during establishment of sister chromatid cohesion. *Science,* **321**, 563–566.

Benson, F.E., Stasiak, A. and West, S.C. (1994) Purification and characterization of the human Rad51 protein, an analogue of E. coli RecA. *EMBO J*. **13**, 5764–5771.

Berchowitz, L.E., Copenhaver, G.P. (2008) Fluorescent *Arabidopsis* tetrads: a visual assay for quickly developing large crossover and crossover interference data sets. *Nature Protocols,* **3**, 41-50.

Berchowitz, L.E. and Copenhaver, G.P. (2010) Genetic Interference: Don't Stand So Close to Me. *Curr Genomics*, **11**, 91–102.

Berchowitz, L.E., Francis, K.E., Bey, A.L., Copenhaver, G.P. (2007) The Role of AtMUS81 in Interference-Insensitive Crossovers in *A. thaliana. PLoS Genet*, **3**, 0001–0010.

Bergerat, A., deMassy, B., Gadelle, D., Varoutas, P.C., Nicolas, A., Forterre, P. (1997) An atypical topoisomerase II from archaea with implications for meiotic recombination. *Nature*, **386**, 414–417.

Bertrand, C., Bergounioux, C., Domenichini, S., Delarue, M. and Zhou, D.X. (2003) *Arabidopsis* histone acetyltransferase AtGCN5 regulates the floral meristem activity through the WUSCHEL/AGAMOUS pathway. *J. Biol. Chem*, **278**, 28246–28251.

Bezzubova, O., Silbergleit, A., Yamaguchi-Iwai, Y., Takedaand, S., Buerstedde, J. M. (1997) Reduced X-ray resistance and homol-ogous recombination frequencies in a RAD54 mutant of the chicken DT40 cell line. *Cell*, **89**,185–193.

Bhalla, N., Dernburg, A.F. (2005) A conserved checkpoint monitors meiotic chromosome synapsis in Caenorhabditis elegans. *Science*, **310**, 1683–1686.

Bhatt, A.T., Canales, C., Dickinson, H.G. (2001) Plant meiosis: the means to 1N. *Trends Plant Sci*, **6**, 114-121.

Bishop, D.K. (1994) RecA homologs Dmc1 and Rad51 interact to form multiple nuclear complexes prior to meiotic chromo-some synapsis. *Cell*, **79**, 1081–1092.

Bishop, D.K., Ear, U., Bhattacharyya, A., Calderone, C., Beckett, M., *et al*. (1998) Xrcc3 is required for assembly of Rad51 complexes in vivo. *J Biol Chem*, **273**, 21482–21488.

Bishop, D.K., Park, D., Xu, L.Z., Kleckner, N. (1992) DMC1 a meiosis-specific yeast homolog of Escherichia coli recA required for recombination, synaptonemal complex-formation, and cell-cycle progression. *Cell*, **69**, 439–456.

Bishop, D.K., Zickler, D. (2004) Early decision; meiotic crossover interference prior to stable strand exchange and synapsis. *Cell,* **117**, 9–15.

Blanco, M.G., Matos, J., Rass, U., Ip, S.C., West, S.C. (2010) Functional overlap between the structure-specific nucleases Yen1 and Mus81-Mms4 for DNA-damage repair in *S. cerevisiae. DNA Repair (Amst)*, **9**, 394–402.

Bleuyard, J.Y. and White, C.I. (2004) The *Arabidopsis* homologue of *Xrcc3* plays an essential role in meiosis. *EMBO J*, **23**, 439-449.

Bleuyard, J.Y., Gallego, M.E. and White, C.I. (2004) Meiotic defects in the *Arabidopsis rad50* mutant point to conservation of the MRX complex function in early stages of meiotic recombination. *Chromosoma*, **113**, 197-203.

Bleuyard, J.Y., Gallego, M.E. and White, C.I. (2006) Recent advances in understanding of the DNA double-strand break repair machinery of plants. *DNA Repair (Amst),* **5**, 1–12.

Bleuyard, J.Y., Gallego, M.E., Savigny, F. and White, C.I. (2005) Differing requirements for the *Arabidopsis* Rad51 paralogs in meiosis and DNA repair. *Plant J*, **41**, 533-545.

Borner, G.V., Barot, A., Kleckner, N. (2008) Yeast Pch2 promotes domainal axis organization, timely recombination progression, and arrest of defective recombinosomes during meiosis. *Proc Natl Acad Sci USA*, **105**, 3327–3332.

Borner, G.V., Kleckner, N., Hunter, N. (2004) Crossover/noncrossover differentiation, synaptonemal complex formation, and regulatory surveillance at the leptotene/zygotene transition of meiosis. *Cell,* **117**, 29–45.

Boxem, M., Maliga, Z., Klitgord, N., Li, N., Lemmens, I., *et al***.** (2008) A protein domain-based interactome network for *C. elegans* early embryogenesis. *Cell*, **134**, 534–545.

Bugreev, D.V., Golub, E.I., Stasiak, A.Z., Stasiak, A. and Mazin, A.V. (2005) Activation of human meiosis-specific recombi-nase Dmc1 by Ca2+. *J. Biol. Chem*, **280**, 26886–26895.

Busygina, V., Saro, D., Williams, G., Leung, W.K., Say, A.F., *et al*. (2011) Novel attributes of Hed1 affect dynamics and activity of the Rad51 presynaptic filament during meiotic recombination. *Journal of Biological Chemistry*, **287**, 1566–1575.

Busygina, V., Sehorn, M.G., Shi, I.Y., Tsubouchi, H., Roeder, G.S., *et al*. (2008) Hed1 regulates Rad51-mediated recombination via a novel mechanism. *Genes & Development*, **22**, 786–795.

Cai, X., Dong, F., Edelmann, R.E. and Makaroff, C.A. (2003) The *Arabidopsis* SYN1 cohesin protein is required for sister chromatid arm cohesion and homologous chromosome pairing. *J. Cell Sci*, **116**, 2999-3007.

Carballo, J.A., Johnson, A.L., Sedgwick, S.G., Cha, R.S. (2008) Phosphorylation of the axial element protein Hop1 by Mec1/Tel1 ensures meiotic interhomolog recombination. *Cell*, **132**, 758–770.

Carballo, J.A., Panizza, S., Serrentino, M.E., Johnson, A.L., Geymonat, M., *et al*. (2013) Budding Yeast ATM/ATR Control Meiotic Double-Strand Break (DSB) Levels by Down-Regulating Rec114, an Essential Component of the DSB-machinery. *PLoS Genet*, **9**: (6): e1003545. doi:10.1371/journal.pgen.1003545.

Caryl, A.P., Jones, G.H. and Franklin, F.C. (2003) Dissecting plant meiosis using *Arabidopsis thaliana* mutants. *J. Exp. Bot*, **54**, 25-38.

Caryl, A.P., Armstrong, S.J., Jones, G.H. and Franklin, F.C.H. (2000) A homologue of the yeast HOP1 gene is inactivated in the *Arabidopsis* meiotic mutant *asy1*. *Chromosoma* **109**, 62-71.

Cavell, A., Lydiate, D., Parkin, I., Dean, C. and Trick, M.A. (1998) A 30 centimorgan segment of *Arabidopsis thaliana* chromosome 4 has six collinear homologs within the *Brassica napus* genome. *Genome*, **41**, 62-69.

Celerin, M., Merino, S.T., Stone, J. E., Menzie, A.M. and Zolan, M. E. (2000) Multiple roles of Spo11 in meiotic chromosome behaviour. *EMBO J*, **19**, 2739–2750.

Cervantes, M.D., Farah, J.A. and Smith, G.R. (2000) Meiotic DNA breaks associated with recombination in *S. pombe*. *Mol. Cell*, **5**, 883-888.

Chai, B., Huang, J., Cairns, B.R., Laurent, B.C. (2005) Distinct roles for the RSC and Swi/Snf ATP-dependent chromatin remodelers in DNA double-strand break repair. *Genes Dev*, **19**, 1656–1661.

Chang, C.R., Wu, C.S., Hom, Y., Gartenberg, M.R. (2005) Targeting of cohesin by transcriptionally silent chromatin, *Genes Dev*, **19**, 3031–3042.

Chelysheva, L., Diallo, S., Vezon, D., Gendrot, G., Vrielynck, N., Belcram, K., Rocques, N., Marquez-Lema, A., Bhatt, A.M., Horlow, C., Mercier, R., Mezard, C. and Grelon, M. (2005) AtREC8 and AtSCC3 are essential to the monopolar orientation of the kinetochores during meiosis. *J. Cell Sci*, **118**, 4621-4632.

Chelysheva, L., Gendrot, G., Vezon, D., Doutriaux, M.P., Mercier, R., *et al*. (2007) Zip4/Spo22 is required for class I CO formation but not for synapsis completion in *Arabidopsis thaliana*. *PLoS Genet*, **3**, e83, doi:10.1371/journal.pgen.0030083.

Chelysheva, L., Vezon, D., Belcram, K., Gendrot, G., Grelon, M. (2008) The *Arabidopsis* blap75 /rmi1 homologue plays crucial roles in meiotic double-strand break repair. *PLoS Genetics*, **4**, e1000309.

Chelysheva, L., Vezon, D., Chambon, A., Gendrot, G., Pereira, L., *et al*. (2012) The *Arabidopsis* HEI10 Is a New ZMM Protein Related to Zip3. *PLoS Genet*, **8**: e1002799. doi:10.1371/journal.pgen.1002799.

Chen, C., Farmer, A.D., Langley, R.J., Mudge, J., Crow, J., May, G.D. *et al.* (2010) Meiosis-specific gene discovery in plants: RNA-Seq applied to isolated *Arabidopsis* male meiocytes. *BMC Plant Biol*, **10**, 280, doi: 10.1186/1471-2229-10-280.

Chen, C.B., Zhang, W., Timofejeva, L., Gerardin, Y., Ma, H. (2005) The *Arabidopsis* ROCK-N-ROLLERS gene encodes a homolog of the yeast ATP-dependent DNA helicase MER3 and is required for normal meiotic crossover formation. *Plant Journal*, **43**, 321–334.

Cheng, C.H., Lo, Y.H., Liang, S.S., Ti, S.C., Lin, F.M., *et al*. (2006) SUMO modifications control assembly of synaptonemal complex and polycomplex in meiosis of *Saccharomyces cerevisiae*. *Genes & Dev*, **20**, 2067–2081.

Chen, Y.K., Leng, C.H., Olivares, H., Lee, M.H., Chang, Y.C., Kung, W.M., Ti, S.C., Lo, Y.H., Wang, A.H., Chang, C.S., *et al*. (2004) Heterodimeric complexes of Hop2 and Mnd1 func-tion with Dmc1 to promote meiotic homolog juxtaposition and strand assimilation. *Proc. Natl. Acad. Sci*, **101**, 10572– 10577.

Chivasa, S., Ndimba, B.K., Simon, W.J., Robertson, D., Yu, X.L., Knox, J.P., Bolwell, P., Slabas, A.R. (2002) Proteomic analysis of the *Arabidopsis thaliana* cell wall. *Electrophoresis*, **23**, 1754-1765.

Clyne, R.K., Katis, V.L., Jessop, L., Benjamin, K.R., Herskowitz, I., Lichten, M., Nasmyth K. (2003) Polo-like kinase Cdc5 promotes chiasmata formation and cosegregation of sister centromeres at meiosis I. *Nat Cell Biol*, **5**, 480–485.

Colaiacovo, M.P., A.J. MacQueen, E. Martinez-Perez, K. McDonald, A. Adamoet *et al*. (2003) Synaptonemal complex assembly in *C. elegans* dispensable for loading strand-exchange proteins but critical for proper completion of recombination. *Dev. Cell*, **5**, 463–474.

Cole, F., Keeney, S., Jasin, M. (2010) Evolutionary conservation of meiotic DSB proteins: more than just Spo11. *Genes & Development*, **24**, 1201–1207.

Collins, I., Newlon, C.S. (1994) Meiosis-specific formation of joint DNA molecules containing sequences from homologous chromosomes. *Cell*, **76**, 65–75.

Copenhaver, G.P., Housworth, E.A., Stahl, F.W. (2002) Crossover interference in *Arabidopsis*. *Genetics*, **160**, 1631–1639.

Costa, Y., Speed, R., Öllinger, R., Alsheimer, M., Semple, C.A. *et al.* (2004) Two novel proteins recruited by synaptonemal complex protein 1 (SYCP1) are at the centre of meiosis. *J Cell Sci*, **118***, 2755-2762.

Couteau, F., Belzile, F., Horlow, C., Grandjean, O., Vezon, D. and Doutriaux, M.P. (1999) Random chromosome segregation without meiotic arrest in both male and female meiocytes of a *dmc1* mutant of *Arabidopsis. Plant Cell*, **11**, 1623-1634.

Cox, M.M. (1999) Recombinational DNA repair in bacteria and the RecA protein. *Prog. Nucleic Acid Res. Mol. Biol*, **63**, 311-366.

Crismani, W. and Mercier, R. (2013) Identifying meiotic mutants in *Arabidopsis thaliana*. Plant meiosis: Methods and protocols, methods in molecular biology book, vol. **990**. (Eds. Pawlowski, W.P., Grelon, M., Armstrong, S.J.), Springer Science Business Media New York.

Cromie, G.A., Hyppa, R.W., Taylor, A.F., Zakharyevich, K., Hunter, N., Smith, G.R. (2006) Single Holliday junctions are intermediates of meiotic recombination. *Cell*, **127**, 1167–1178.

Cubillos, F.A., Yansouni, J., Khalili, H., Balzergue, S., Elftieh, S., Martin-Magniette, M.L., Serrand, Y., Lepiniec, L., Baud, S., Dubreucq, B., Renou, J.P., Camilleri, C., Loudet O. (2012) Expression variation in connected recombinant populations of Arabidopsis thaliana highlights distinct transcriptome architectures. *BMC Genomics.***13**,117. doi:10.1186/1471-2164-13-117.

Da Ines, O., Abe, K., Goubely, C., Gallego, M.E. and White, C.I. (2012) Differ-ing requirements for RAD51 and DMC1 in meiotic pairing of centromeres and chromosome arms in *Arabidopsis thaliana*. *PLoS Genet*. **8**, e1002636.

Da Ines, O., Degroote, F., Amiard, S., Goubely, C., Gallego, M.E. and White, C.L. (2013) Effects of XRCC2 and RAD51B mutations on somatic and meiotic recombination in *Arabidopsis thaliana. The Plant Journal*, **74**, 959–970.

De Boer, E., Heyting, C. (2006) The diverse roles of transverse filaments of synaptonemal complexes in meiosis. *Chromosoma*, **115**, 220-234.

De La Fuente, R., Viveiros, M.M., Burns, K.H., Adashi, E.Y., Matzuk, M.M. and Eppig, J.J. (2004) Major chromatin remodeling in the germinal vesicle (GV) of mammalian oocytes is dispensable for global transcriptional silencing but required for centromeric heterochromatin function. *Dev. Biol*, **275**, 447– 458.

De los Santos, T., Hunter, N., Lee, C., Larkin, B., Loidl, J., Hollingsworth, N.M. (2003) The Mus81/Mms4 endonuclease acts independently of double-Holliday junction resolution to promote a distinct subset of crossovers during meiosis in budding yeast. *Genetics*, **164**, 81-94.

De Muyt, A., Vezon, D., Gendrot, G., Gallois, J.L., Stevens, R., *et al*. (2007) AtPRD1 is required for meiotic double strand break formation in *Arabidopsis thaliana. Embo J*, **26**, 4126–37.

Dernburg, A.F., McDonald, K., Moulder, G., *et al*. (1998) Meiotic recombi-nation in *C. elegans* initiates by a conserved mechanism and is dispensable for homologous chromosome synapsis. *Cell*, **94**, 387-398.

Dernburg, A. F., Sedat, J. W., Cande, W. Z. and Bass, H. W. (1995) Cytology of telomeres. In Telomeres (ed. E. H. Blackburn and C. W. Greider), pp. 295-398. Plainview: Cold Spring Harbor Laboratory.

Diaz, R.L., Alcid, A.D., Berger, J.M., and Keeney, S. (2002) Identifi-cation of residues in yeast Spo11p critical for meiotic DNA double-strand break formation. *Mol. Cell. Biol*, **22**, 1106–1115.

Dobson, M.J., Pearlman R.E., Karaiskakis A., Spyropoulos B., and Moens P.B. (1994) Synaptonemal complex proteins: occurrence, epitope mapping and chromosome disjunction. *J. Cell Sci*, **107**, 2749–2760.

Dong, H. and Roeder, G.S. (2000) Organization of the Yeast Zip1 Protein within the Central Region of the Synaptonemal Complex. *The Journal of Cell Biology*, **148**, 417–426.

Doutriaux, M.P., Couteau, F., Bergounioux, C. and White, C. (1998) Isolation and characterisation of the RAD51 and DMC1 homologs from *Arabidopsis thaliana*. *Mol. Gen. Genet*, **257**, 283-291.

Du, J., Nasir, I., Benton, B.K., Kladde, M.P., Laurent, B.C. (1998) Sth1p, a *Saccharomyces cerevisiae* Snf2p/Swi2p homolog, is an essential ATPase in RSC and differs from Snf/Swi in its interactions with histones and chromatin-associated proteins, *Genetics*, **150**, 987–1005.

Dunin-Horkawicz, S., Feder, M., Bujnicki, J.M. (2006) Phylogenomic analysis of the GIY-YIG nuclease superfamily. *BMC Genomics*, **7**, 98.

Durrant, W.E., Wang, S. and Dong, X. (2007) *Arabidopsis* SNI1 and RAD51D regulate both gene transcription and DNA recombination during the defense response. *Proc. Natl Acad. Sci. USA*, **104**, 4223–4227.

Eisen, J. A., Swederand, K. S. and Hanawalt, **P. C.** (1995) Evolution of the SNF2 family of proteins: subfamilies with distinct sequences and functions. *Nucleic Acids Res*, **23**, 2715-2723.

Eshed, Y., Baum, S.F. and Bowman, J.L. (1999) Distinct mechanisms promote polarity establishment in carpels of *Arabidopsis*. *Cell*, **99**, 199–209.

Essers, J., Hendriks, R.W., Swagemakers, S.M., Troelstra, C., deWit J. et al., (1997) Disruptionofmouse RAD54 reduces ionizing radiation resistance and homologous recombination. *Cell*, **89**, 195–204.

Fan, H.Y., He, X., Kingston, R.E., Narlikar, G.J. (2003) Distinct strategies to make nucleosomal DNA accessible, *Mol. Cell*, **11**, 1311–1322.

Farmer, S., Hong, E-JE., Leung, W-K., Argunhan, B., Terentyev, Y., *et al*. (2012) Budding Yeast Pch2, a Widely Conserved Meiotic Protein, Is Involved in the Initiation of Meiotic Recombination. *PLoS ONE*, **7**: (6): e39724. doi:10.1371/journal.pone.0039724.

Ferdous, M., Higgins, J.D., Osman, K., Lambing, C., Roitinger, E., *et al*. (2012) Inter-Homolog Crossing-Over and Synapsis in *Arabidopsis* Meiosis Are Dependent on the Chromosome Axis Protein AtASY3. *PLoS Genet*, **8**: (2): e1002507. doi: 10.1371/journal. pgen.1002507.

Foss, E.J. and Stahl, F.W. (1995) A test of a counting model for chiasma interference. *Genetics*, **139**, 1201-1209.

Fricke, W.M., Brill, S.J. (2003) Slx1-Slx4 is a second structure-specific endonuclease functionally redundant with Sgs1-Top3. *Genes Dev*, **17**, 1768–1778.

Furukawa, T., Kimura, S., Ishibashi, T., Mori, Y., Hashimoto, J., Sakaguchi, K. (2003) OsSEND-1: a new RAD2 nuclease family member in higher plants. *Plant Mol Biol*, **51**, 59-70.

Gallardo, K., Job, C., Groot, S.P., Puype, M., Demol, H., Vandekerckhove, J., Job, D. (2002) Proteomics *of Arabidopsis* seed germination. A comparative study of wild-type and gibberellins-deficient seeds. *Plant Physiol*, **129**, 823-837.

Gangaraju, V.K. and Bartholomew, B. (2007) Mechanisms of ATP dependent chromatin remodeling. *Mutation Research*, **618**, 3–17.

Gasior, S.L., Olivares, H., Ear, U., Hari, D.M., Weichselbaum, R., and Bishop, D.K. (2001) Assembly of RecA-like recombi-nases: Distinct roles for mediator proteins in mitosis and meiosis. *Proc. Natl. Acad. Sci*, **98**, 8411–8418.

Gerton, J.L., Hawley, R.S. (2005) Homologous chromosome interactions in meiosis: diversity amidst conservation. *Nat Rev Genet*, **6**, 477-487.

Ghabrial, A., Schupbach, T. (1999) Activation of a meiotic checkpoint regulates translation of Gurken during Drosophila oogenesis. *Nat Cell Biol*, **1**, 354–357.

Giroux, C.N., Dresser, M.E., Tiano, H.F. (1989) Genetic control of chromo-some synapsis in yeast meiosis. *Genome*, **31**, 88-94.

Goldfarb,T. and Lichten, M. (2010) Frequent and efficient use of the sister chromatid for DNA double-strand break repair during budding yeast meiosis. *PLoS Biol*, **8**, e1000520.

Goyon, C., Lichten, M. (1993) Timing of molecular events in meiosis in *Saccharomyces cerevisiae*: stable heteroduplex DNA is formed late in meiotic prophase. *Mol Cell Biol*, **13**, 373–382.

Grelon, M., Vezon, D., Gendrot, G. and Pelletier, G. (2001) AtSPO11-1 is necessary for efficient meiotic recombination in plants. *EMBO J*, **20**, 589-600.

Haering, C.H. and Nasmyth, K. (2003) Building and breaking bridges between sister chromatids. *BioEssays,* **25**, 1178–91.

Hamant, O., Ma, H. and Cande, W.Z. (2006) Genetics of Meiotic Prophase I in Plants. *Annu. Rev. Plant Biol*, **57**, 267-302.

Hamer, G., Gell, K., Kouznetsova, A., Novak, I., Benavente, R. and Höög, C. (2006) Characterization of a novel meiosis-specific protein within the central element of the synaptonemal complex. *Journal of Cell Science*, **119**, 4025-4032.

Hartsuiker, E., Mizuno, K., Molnar, M., Kohli, J., *et al*. (2009) Ctp1[CtIP] and Rad32[Mre11] nuclease activity are required for Rec12 Spo11 removal, but Rec12 Spo11 removal is dispensable for other MRN-dependent meiotic functions. *Mol Cell Biol*, **29**, 1671–1681.

Hartung, F. and Puchta, H. (2000) Molecular characterisation of two paralogous Spo11 homologues in *Arabidopsis thaliana*. *Nucleic Acids Research*, **28**, 1548–1554.

Hartung, F. and Puchta, H. (2001) Molecular characterization of homologues of both subunits a (Spo11) and b of the archaebacterial topoisomerase 6 in plants. *Gene*, **271**, 81–86.

Hartung, F., Wurz-Wildersinn, R., Fuchs, J., Schubert, I., Suer, S. and Puchta, H. (2007) The catalytically active tyrosine residues of both SPO11-1 and SPO11-2 are required for meiotic double-strand break induction in *Arabidopsis*. *Plant Cell*, **19**, 3090–3099.

Hayase, A., Takagi, M., Miyazaki, T., Oshiumi, H., Shinohara, M. and Shinohara, A. (2004) A protein complex containing Mei5 and Sae3 promotes the assembly of the meiosis-spe-cific RecA homolog Dmc1. *Cell*, **119**, 927–940.

Henderson, K.A., Kee, K., Maleki, S., Santini, P.A., Keeney, S. (2006) Cyclin-dependent kinase directly regulates initiation of meiotic recombination. *Cell*, **125**, 1321–1332.

Henry, J.M., Camahort, R., Rice, D.A., Florens, L., Swanson, S.K., Washburn, M.P., and Gerton, J.L. (2006) Mnd1/Hop2 facilitates Dmc1-dependent interhomolog crossover formation in meiosis of budding yeast. *Mol. Cell. Biol*, **26**, 2913 – 2923.

Heyting, C. (1996) Synaptonemal complexes: Structure and function.Curr. *Opin. Cell Biol*, **8**, 389–396.

Hickson, I.D. and Mankouri, H.W. (2011) Processing of homologous recombination repair Intermediates by the Sgs1-Top3-Rmi1 and Mus81-Mms4 complexes. *Cell Cycle*, **10**, 3078-85.

Higgins, J.D., Armstrong, S.J., Franklin, F.C., Jones, G.H. (2004) The *Arabidopsis* MutS homolog AtMSH4 functions at an early step in recombination: evidence for two classes of recombination in *Arabidopsis*. *Genes Dev*, **18**, 2557–2570.

Higgins, J.D., Vignard, J., Mercier, R., Pugh, A.G., Franklin, F.C.H., Jones, G.H. (2008a) AtMSH5 partners AtMSH4 in the class I meiotic crossover pathway in *Arabidopsis thaliana*, but is not required for synapsis. *Plant Journal*, **55**, 28–39.

Higgins, J.D., Buckling, E.F., Franklin, F.C., Jones, G.H. (2008b) Expression and functional analysis of AtMUS81 in *Arabidopsis* meiosis reveals a role in the second pathway of crossing-over. *Plant J*, **54**, 152–162.

Higgins, J.D., Sanchez-Moran, E., Armstrong, S.J., Jones, G.H. and Franklin, F.C. (2005) The *Arabidopsis* synaptonemal complex protein ZYP1 is required for chromosome synapsis and normal fidelity of crossing over. *Genes Dev*, **19**, 2488-2500.

Hirota, K., Mizuno, K., Shibata, T. and Ohta, K. (2008) Distinct chromatin modulators regulate the formation of accessible and repressive chromatin at the fission yeast recombination hotspot ade6–M26. *Mol. Biol. Cell*, **19**, 1162–1173.

Hochwagen, A., Tham, W.H., Brar, G.A. and Amon, A. (2005) The FK506 binding protein Fpr3 counteracts protein phosphatase 1 to maintain meiotic recombination checkpoint activity. *Cell*, **122**, 861–873.

Ho, C.K., Mazon, G., Lam, A.F., Symington, L.S. (2010) Mus81 and Yen1 promote reciprocal exchange during mitotic recombination to maintain genome integrity in budding yeast. *Mol Cell*, **40**, 988–1000.

Hodgson, A., Terentyev, Y., Johnson, R.A., Bishop-Bailey, A., *et al*. (2010) Mre11 and Exo1 contribute to the initiation and processivity of resection at meiotic double-strand breaks made independently of Spo11. *DNA Repair (Amst)*, **10**: (2):138-48.

Ho, H.C., Burgess, S.M. (2011) Pch2 acts through Xrs2 and Tel1/ATM to modulate interhomolog bias and checkpoint function during meiosis. *PLoS Genet*, **7**: e1002351. doi:10.1371/journal.pgen.1002351.

Hollingsworth, N.M., Ponte, L., Halsey, C. (1995) MSH5, a novel MutS homolog, facilitates meiotic reciprocal recombination between homologs in *Saccharomyces cerevisiae* but not mis-match repair. *Genes Dev*, **9**, 1728-1739.

Hong, E.L., Shinohara, A. and Bishop, D.K. (2001) *Saccharomyces cerevisiae* Dmc1 protein promotes renaturation of single-strand DNA (ssDNA) and assimilation of ssDNA into homologous super-coiled duplex DNA. *J. Biol. Chem*, **276**, 41906–41912.

Housworth, E.A. and Stahl, F.W. (2003) Crossover interference in humans. *Am. J. Hum. Genet*, **73**, 188-197.

Huang, J. and Laurent, B.C. (2004b) A Role for the RSC chromatin remodeler in regulating cohesion of sister chromatid arms, *Cell Cycle*, **3**, 973–975.

Huang, J., Hsu, J.M. and Laurent, B.C. (2004a) The RSC nucleosome remodeling complex is required for Cohesin's association with chromosome arms. *Mol. Cell*, **13**, 739–750.

Huang, J., Liang, B., Qiu, J., Laurent, B.C. (2005) ATP-dependent chromatin-remodeling complexes in DNA double-strand break repair: remodeling, pairing and (re) pairing. *Cell Cycle*, **4**, 1713–1715.

Hultén, M.A. (2011) On the origin of crossover interference: A chromosome oscillatory movement (COM) model. *Mol Cytogenet*, **4**, 10. doi: 10.1186/1755-8166-4-10.

Hunter, N. (2003). Synaptonemal complexities and commonalities. *Mol. Cell*, **12**, 533–535.

Hunter, N. (2007) in Molecular Genetics of Recombination (Aguilera, A., and Rothstein, R., eds) pp. 381–442.

Hunter, N. and Kleckner, N. (2001) The single-end invasion: anasymmetric intermediate at the double-strand break to double-Holliday junction transition of meiotic recombination. *Cell*, **106**, 59–70.

Inagaki, S., Nakamura, K. and Morikami, A. (2009) A link among DNA repli-cation, recombination, and gene expression revealed by genetic and genomic analysis of TEBICHI gene of *Arabidopsis thaliana*. *PLoS Genet*. **5**, e1000613.

Ip, S.C., Rass, U., Blanco, M.G., Flynn, H.R., Skehel, J,M., West, S.C. (2008) Identification of Holliday junction resolvases from humans and yeast. *Nature*, **456**, 357–361.

Ishikawa, G., Kanai, Y., Takata, K., Takeuchi, R., Shimanouchi, K., Ruike, T., Furukawa T, Kimura S, Sakaguchi K. (2004) DmGEN, a novel RAD2 family endo-exonuclease from *Drosophila melanogaster*. *Nucleic Acids Res*, **32**, 6251– 6259.

Jackson, N., Sanchez-Moran, E., Buckling, E., Armstrong, S.J., Jones, G.H., *et al*. (2006) Reduced meiotic crossovers and delayed prophase I progression in AtMLH3-deficient *Arabidopsis. Embo Journal*, **25**, 1315–1323.

Jantsch, V., Pasierbek, P., Mueller, M.M., Schweizer, D., Jantsch, M., Loidl, J. (2004) Targeted gene knockout reveals a role in meiotic recombination for ZHP-3, a Zip3-related protein inCaenorhab-ditis elegans. *Mol Cell Biol*, 24, 7998-8006.

Jean, M., Pelletier, J., Hilpert, M., Belzile, F. and Kunze, R. (1999) Isolation and characterization of AtMLH1, a MutL homologue from *Arabidopsis thaliana. Mol. Gen. Genet*, **262**, 633–642.

Jeddeloh, J. A., Stokes, T.L and Richards, E.J. (1999) Maintenance of genomic methylation requires a SWI2/SNF2-like protein. *Nat. Genet*, **22**, 94–97.

Jessop, L., Lichten, M. (2008) Mus81/Mms4 endonuclease and Sgs1 helicase collaborate to ensure proper recombination intermediate metabolism during meiosis. *Mol. Cell*, **31**, 313-323.

Jolivet, S., Vezon, D., Froger, N., Mercier, R. (2006) Non conservation of the meiotic function of the Ski8/Rec103 homolog in *Arabidopsis. Genes to Cells*, **11**, 615–622.

Jones, G.H., Franklin, F.C. (2006) Meiotic crossing-over: obligation and interference. *Cell*, **126**, 246–248.

Joshi, N., Barot, A., Jamison, C., Borner, G.V. (2009) Pch2 links chromosome axis remodeling at future crossover sites and crossover distribution during yeast meiosis. *PLoS Genet*, **5**, e1000557. oi:10.1371/journal.pgen.1000557.

Joyce, E.F., McKim, K.S. (2009) *Drosophila* PCH2 Is Required for a Pachytene Checkpoint That Monitors Double-Strand-Break-Independent Events Leading to Meiotic Crossover Formation. *Genetics*, **181**, 39–51.

Joyce, E.F., Pedersen, M., Tiong, S., White-Brown, S.K., Paul, A., *et al*. (2011) *Drosophila* ATM and ATR have distinct activities in the regulation of meiotic DNA damage and repair. *J Cell Biol*, **195**, 359–367.

Kanno, T., Aufsatz, W., Jaligot, E., Mette, M.F., Matzke, M. *et al*., (2005) A SNF2-like protein facilitates dynamic control of DNA methylation. *EMBO Rep*, **6**, 649–655.

Kanno, T., Mette, M.F., Kreil, D.P., Aufsatz, W., Matzke, M. *et al*. (2004) Involvement of putative SNF2 chromatinremodeling protein DRD1 in RNA-directed DNA methylation. *Curr. Biol,* **14**, 801–805.

Kassabov, S.R., Henry, N.M., Zofall, M., Tsukiyama, T., Bartholomew, B. (2002) High-resolution mapping of changes in histone-DNA contacts of nucleosomes remodeled by ISW2. **Mol. Cell. Biol**, **22**, 7524–7534.

Kassabov, S.R., Zhang, B., Persinger, J., Bartholomew, B. (2003) SWI/SNF unwraps, slides, and rewraps the nucleosome. **Mol. Cell**, **11**, 391–403.

Keelagher, R.E., Cotton, V.E., Goldman, A.S., Borts, R.H. (2010) Separable roles for Exonuclease I in meiotic DNA double-strand break repair. *DNA Repair (Amst)*, **10,** 126-37.

Kelly, K.O., Dernburg, A.F., Stanfield, G.M., Villeneuve, A.M. (2000) *Caenorhabditis elegans* msh-5 is required for both normal and radiation-induced meiotic crossing over but not for completion of meiosis. *Genetics*, **156**, 617-630.

Kim, K.P., Weiner, B.M., Zhang, L.R., Jordan, A., Dekker, J., *et al*. (2010) Sister Cohesion and Structural Axis Components Mediate Homolog Bias of Meiotic Recombination. *Cell*, **143**, 924–937.

King, J.S. Mortimer, R.K. (1990) polymerization model of chiasma interference and corresponding computer simulation. *Genetics*, **126**, 1127-1138.

Kirschner, M.W. (2005) The meaning of systems biology. *Cell,* **121**, 503–504.

Kitajima, T. S., Yokobayashi, S., Yamamoto, M., Watanabe, Y. (2003) Rec8 cleavage by separase is required for meiotic nuclear divisions in fission yeast. *Science*, **300**, 1152–1155.

Klapholz, S., Waddell, C.S., Esposito, R.E. (1985) The role of the SPO11 gene in meiotic recombination in yeast. *Genetics*, **110**, 187-216.

Kleckner, N. (2006) Chiasma formation: chromatin axis interplay and the role(s) of the synaptonemal complex. *Chromosoma*, **115**, 175–194.

Kleckner, N., Zickler, D., Jones, G.H., Dekker, J., Padmore, R., *et al.* (2004) A mechanical basis for chromosome function. *Proc. Natl. Acad. Sci. U S A*, **101**, 12592–12597.

Kooistra, R., Vreeken, K., Zonneveld, J.B., deJong, A., Eeken J.C. *et al.* (1997) The *Drosophila melanogaster* RAD54 homolog, DmRAD54, is involved in the repair of radiation damage and re-combination. *Mol. Cell. Biol*, **17**, 6097–6104.

Kouzarides, T. (2007) Chromatin modifications and their function. *Cell*, **128**, 693–705.

Krogh, B.O., Symington, L.S. (2004) Recombination proteins in yeast. *Annu. Rev.Genet*. **38**, 233–71.

Krysan, P.J., Young, J.C., and Sussman, M.R. (1999) T-DNA as an insertional mutagen in *Arabidopsis*. *Plant Cell,* **11**, 2283–2290.

Kumar, R., Bourbon, H.M., de Massy, B. (2010) Functional conservation of Mei4 for meiotic DNA double-strand break formation from yeasts to mice. *Genes & Development*, **24**, 1266–1280.

Lamers, M.H., Perrakis, A., Enzlin, J.H., Winterwerp, H.H.K., de Wind, N., Sixma, T.K. (2000) The crystal structure of DNA mismatch repair protein MutS binding to a G·T mismatch. *Nature*, **407**, 711–717.

Lam, S.Y, Horn, S.R, Radford, S.J, Housworth, E.A, Stahl, F.W, Copenhaver, G.P. (2005) Crossover interference on nucleolus organizing region-bearing chromosomes in *Arabidopsis*. *Genetics*, **170**, 807-812.

Lam, W.S., Yang, X. and Makaroff, C.A. (2005) Characterization of *Arabidopsis thaliana* SMC1 and SMC3: evidence that AtSMC3 may function beyond chromosome cohesion. *J. Cell Sci*, **118**, 3037-3048.

Lange, J., Pan, J., Cole, F., Thelen, M.P., Jasin, M., *et al.* (2011) ATM controls meiotic double-strand-break formation. *Nature*, **479**, 237–240.

Lee, M.H., Chang, Y.C., Hong, E.L., Grubb, J., Chang, C.S., Bishop, D.K., and Wang, T.F. (2005) Calcium ion promotes yeast Dmc1 activity via formation of long and fine helical filaments with single-stranded DNA. *J. Biol. Chem*, **280**, 40980–40984.

Lengronne, A. *et al*. (2006) Establishment of sister chromatid cohesion at the *S. cerevisiae* replication fork. *Mol. Cell,* **23**, 787–799.

Libby, B.J., Reinholdt, L.G., Schimenti, J.C. (2003) Positional cloning and characterization ofMEI1, a vertebrate-specific gene required for normal meiotic chromosome synapsis in mice. *Proceedings of the National Academy of Sciences, USA*, **100**, 15706–15711.

Libeau, P., Durandet, M., Granier, F., Marquis, C., Berthomé, R., Renou, J.P. *et al*. (2011) Gene expression profiling of *Arabidopsis* meiocytes. *Plant Biol*, **13**, 784–793.

Libuda D.E., Uzawa S, Meyer B. J. and Villeneuve A. M. (2013) Meiotic chromosome structures constrain and respond to designation of crossover sites. *Nature*, doi:10.1038/nature12577.

Lichten, M., Goyon, C., Schultes, N.P., Treco, D., Szostak, J.W., *et al.* (1990) Detection of heteroduplex DNA molecules among the products of *Saccharomyces cerevisiaemeiosis*. *Proc Natl Acad Sci U S A*, **87**, 7653–7657.

Liu, J.G., Yuan, L., Brundell, E., Bjorkroth, B., Daneholt, B., Hoog, C. (1996) Localization of the N-terminus of SCP1 to the central element of the synap-tonemal complex and evidence for direct interactions between the N-termini of SCP1 molecules organized head-to-head. *Exp. Cell Res*, **226**, 11–19.

Li, W., Chen, C., Markmann-Mulisch, U., Timofejeva, L., Schmelzer, E., *et al.* (2004) The *Arabidopsis* AtRAD51 gene is dispensable for vegetative development but required for meiosis. *Proc Natl Acad Sci U S A*, **101**, 10596-10601.

Li, W., Yang, X., Lin, Z., Timofejeva, L., Xiao, R., Makaroff, C.A. and Ma, H. (2005) The AtRAD51C gene is required for normal meiotic chromosome synapsis and double-stranded break repair in *Arabidopsis*. *Plant Physiol*, **138**, 965–976.

Li, Z., Golub, E.I., Gupta, R., and Radding, C.M. (1997) Recom-bination activities of HsDmc1 protein, the meiotic human homolog of RecA protein. *Proc. Natl. Acad. Sci*, **94**: 11221– 11226.

Li, W.X., Chen, C.B., Markmann-Mulisch, U., Timofejeva, L., Schmelzer, E., *et al.* (2004) The *Arabidopsis* AtRAD51 gene is dispensable for vegetative development but required for meiosis. *Proceedings of the National Academy of Sciences of the United States of America*, **101**, 10596–10601.

Li, W. and Ma, H. (2006) Double-stranded DNA breaks and gene functions in recombination and meiosis. *Cell Res*, **16**, 402–412.

Li, W., Yang, X., Lin, Z., Timofejeva, L., Xiao, R., Makaroff, C.A. and Ma, H. (2005) The AtRAD51C gene is required for normal meiotic chromosome synapsis and double-stranded break repair in *Arabidopsis. Plant Physiol*, **138**, 965-976.

Li, X.C., Schimenti, J.C. (2007) Mouse pachytene checkpoint 2 (Trip13) is required for completing meiotic recombination but not synapsis. *PLoS Genet*, **3**, e130. doi: 10. 1371/journal.pgen.0030130.

Losada, A., Hirano, M., and Hirano, T. (1998) Identification of Xenopus SMC protein complexes required for sister chromatid cohesion. *Genes Dev*, **12**, 1986-1997.

Lynn, A., Ashley, T., Hassold, T. (2004) Variation in human meiotic recombination. *Annu Rev Genomics Hum Genet*, **5**, 317- 349.

Lynn, A., Soucek, R., Börner, G.V. (2007) ZMM proteins during meiosis: crossover artists at work. *Chromosome Res*, **15**, 591-605.

Macaisne, N., Novatchkova, M., Peirera, L., Vezon, D., Jolivet, S., *et al*. (2008) SHOC1, an XPF endonuclease-related protein, is essential for the formation of class I meiotic crossovers. *Curr Biol*, **18**, 1432–1437.

Macaisne, N., Vignard, J., Mercier, R. (2011) SHOC1 and PTD form an XPF-ERCC1-like complex that is required for formation of class I crossovers. *J Cell Sci*, **124**, 2687–2691.

MacQueen, A.J., Colaiacovo, M.P., McDonald, K., Villeneuve, A.M. (2002) Synapsis-dependent and -independent mechanisms stabilize homolog pairing during meiotic prophase in *C. elegans*. *Genes Dev*, **16**, 2428–2442.

Macqueen, A.J., Roeder, G.S. (2009) Fpr3 and Zip3 ensure that initiation of meiotic recombination precedes chromosome synapsis in budding yeast. *Curr Biol*, **19**, 1519–1526.

Ma, H. (2006) A molecular portrait of *Arabidopsis* meiosis. In The *Arabidopsis* Book. (Eds. Somerville, C.R., Meyerowitz, E.M., Dangl, J., and Stitt, M.), American Society of Plant Biologists, Rockville, MD, doi/10.1199/tab.0009.

Malkova, A., *et al*. (2004) Gene conversion and crossing over along the 405-kb left arm of *Saccharomyces cerevisiae* chromosome VII. *Genetics,* **168**, 49-63.

Manfrini, N., Guerini, I., Citterio, A., Lucchini, G., Longhese, M.P. (2010) Processing of meiotic DNA double-strand breaks requires cyclin-dependent kinase and multiple nucleases. *Journal of Biological Chemistry*, **285**, 11628–11637.

Mao-Draayer, Y., Galbraith, A.M., Pittman, D.L., Cool, M., and Malone, R.E. (1996) Analysis of meiotic recombination path-ways in the yeast *Saccharomyces cerevisiae*. *Genetics*, **144**, 71–86.

Marcon, E., Moens, P. (2003) MLH1p and MLH3p localize to precociously induced chiasmata of okadaic-acid-treated mouse spermatocytes. *Genetics*, **165**, 2283-2287.

Martini, E., Diaz, R.L, Hunter, N., Keeney, S. (2006) Crossover homeostasis in yeast meiosis. *Cell*, **126**, 285-295.

Masson, J.Y., Davies, A.A., Hajibagheri, N., Van Dyck, E., Ben-son, F.E., Stasiak, A.Z., Stasiak, A., and West, S.C. (1999) The meiosis-specific recombinase hDmc1 forms ring structures and interacts with hRad51. *EMBO J*, **18**, 6552–6560.

Masson, J.Y., Tarsounas, M.C., Stasiak, A.Z., Stasiak, A., Shah, R., *et al*. (2001) Identification and purification of two distinct complexes containing the five RAD51 paralogs. *Genes Dev*, **15**, 3296–3307.

Masson, J.Y., West, S.C. (2001) The Rad51 and Dmc1 recombinases: a non-identical twin relationship. *Trends Biochem. Sci*. **26**, 131–36.

Matos, J., Blanco, M.G., Maslen, S., Skehel, J.M., West, S.C. (2011) Regulatory Control of the Resolution of DNA Recombination Intermediates during Meiosis and Mitosis. *Cell*, **147**, 158–172.

Mazina, O.M., Mazin, A.V., Nakagawa, T., Kolodner, R.D., Kowalczykowski, S.C. (2004) *Saccharomyces cerevisiae* Mer3 helicase stimulates 3'–5' heteroduplex extension by Rad51; implications for crossover control in meiotic recombination. *Cell*, **117**, 47–56.

McKim, K. S. *et al*. (1998) Meiotic synapsis in the absence of recombination. *Science*, **279**, 876–878.

McKim, K.S., Hayashi-Hagihara, A. (1998) mei-W68 in *Drosophila melanogaster* encodes a Spo11 homolog: evidence that the mechanism for initiating meiotic recombination is conserved. *Genes Dev*, **12**, 2932-2942.

McMahill, M.S., Sham, C.W., Bishop, D.K. (2007) Synthesis-dependent strand annealing in meiosis. *PLoS Biol*, **5**, e299. doi:10.1371/journal.pbio.0050299.

Meneely, P.M., Farago, A.F., Kauffman, T.M. (2002) Crossover distribution and high interference for both the X chromosome and an autosome during oogenesis and spermatogenesis in *Caenorhabditis elegans*. *Genetics*, **162**, 1169–1177.

Mercier, R., Jolivet, S., Vezon, D., Huppe, E., Chelysheva, L., Giovanni, M., Nogue, F., Doutriaux, M.P., Horlow, C., Grelon, M. *et al*. (2005) Two meiotic crossover classes cohabit in *Arabidopsis*: one is dependent on Mer3, whereas the other one is not. *Current Biology*, **15**, 692–701.

Mercier, R., Vezon, D., Bullier, E., Motamayor, J.C., Sellier, A., Lefevre, F., Pelletier, G., and Horlow, C. (2001) SWITCH1 (SWI1): a novel protein required for the establishment of sister chromatid cohesion and for bivalent formation at meiosis. *Genes Dev*, **15**, 1859-1871.

Merker, J.D., Dominska, M., Greewell, P.W., Rinella, E., Bouck, D.C., Shibata, Y., Strahl, B.D., Mieczkowski, P. and Petes, T.D. (2008) The histone methylase Set2p and the histone deacetylase Rpd3p repress meiotic recombination at the HIS4 meiotic recombination hotspot in *Saccharomyces cerevisiae*. *DNA Repair*, **7**, 1298–1308.

Meuwissen, R.L.J., Offenberg, H.H., Dietrich, A.J.J., Riesewijk, A., Iersel, M.V., Heyting, C. (1992) A coiled-coil related protein specific for synapsed re-gions of meiotic prophase chromosomes. *EMBO (Eur. Mol. Biol. Organ.) J*, **11**, 5091–5100.

Meuwissen, R.L.J., Meerts, I., Hoovers, J.M.N., Leschot, N.J., Heyting, C. (1997) Human synaptonemal complex protein 1 (SCP1): isolation and charac-terization of the cDNA and chromosomal localization of the gene. *Genomics*, **39**, 377–384.

Miao, C., Tang, D., Zhang, H., Wang, M., Li, Y., Tang, S., Yu, H., Gu, M., Cheng, Z. (2013) CENTRAL REGION COMPONENT1, a Novel Synaptonemal Complex Component, Is Essential for Meiotic Recombination Initiation in Rice.http://www. *Plant cell*. org/cgi/ doi/10.1105/tpc.113.113175.

Mieczkowski, P.A., Dominska, M., Buck, M.J., Lieb, J.D. and Petes, T.D. (2007) Loss of a histone deacetylase dramatically alters the genomic distribution of Spo11p-catalyzed DNA breaks in *Saccharomyces cerevisiae*. *Proc. Natl Acad. Sci. USA*, **104**, 3955–3960.

Milman, N., Higuchi, E., Smith, G.R. (2009) Meiotic DNA double-strand break repair requires two nucleases, MRN and Ctp1, to produce a single size class of Rec12 (Spo11)-oligonucleotide complexes. *Mol Cell Biol*, **29**, 5998–6005.

Mimitou, E.P., Symington, L.S. (2009) DNA end resection: many nucleases make light work. *DNA Repair*, **8**, 983–995.

Mitra, N., Roeder, G.S. (2007) A novel nonnull *ZIP1* allele triggers meiotic arrest with synapsed chromosomes in *Saccharomyces cerevisiae*. *Genetics*, **176**, 773–787.

Moens, P.B., Kolas, N.K., Tarsounas, M., Marcon, E., Cohen, P.E., Spyropoulos, B. (2002) The time course and chromosomal localization of recombination-related proteins at meiosis in the mouse are compatible with models that can resolve the early DNA-DNA interactions without reciprocal recombination. *J. Cell Sci,* **15**, 1611–22.

Munoz, I.M., Hain, K., Declais, A.C., Gardiner, M., Toh, G.W., Sanchez-Pulido, L., Heuckmann, J.M., Toth, R., Macartney, T., Eppink, B., et al. (2009) Coordination of structure-specific nucleases by human SLX4/BTBD12 is required for DNA repair. *Mol Cell*, **35**, 116–127.

Muris, D.F., Vreeken, K., Schmidt, H., Ostermann, K., Clever, B. et al., (1997) Homologous recombination in the fission yeast *Schizosaccharomyces pombe*: different requirements for the rhp511, rhp541and rad221genes. *Curr. Genet*, **31**, 248–254.

Nakagawa, T., Flores-Rozas, H., Kolodner, R.D. (2001) The MER3 helicase involved in meiotic crossing over is stimulated by single-stranded DNA-binding proteins and unwinds DNA in the 3'to 5' direction. *J Biol Chem*, **276**, 31487-31493.

Nasmyth, K. (1999) Separating sister chromatids. *Trends Biochem. Sci*, **24**, 98-104.

Nasmyth, K., Haering, C.H. (2005) The structure and function of Smc and kleisin complexes. *Annual Review of Biochemistry*, **74**, 595–648.

Nasmyth, K., Haering C.H. (2009) Cohesin: Its roles and mechanisms. *Annu Rev Genet*, **43**, 525–558.

Nassif, N., Penney, J., Pal, S., Engels, W.R., Gloor, G.B. (1994) Efficient copying of nonhomologous sequences from ectopic sites via P-element-induced gap repair. *Mol Cell Biol*, **14**, 1613–1625.

Nimonkar, A.V., Dombrowski, C.C., Siino, J.S., Stasiak, A.Z., Stasiak, A. and Kowalczykowski, S.C. (2012) *Saccharomyces cerevisiae* Dmc1 and Rad51 Proteins Preferentially Functionwith Tid1 and Rad54 Proteins, Respectively, to Promote DNA Strand Invasion during Genetic Recombination. *The journal of biological chemistry*, **287**, 28727–28737.

Niu, H., Wan, L., Baumgartner, B., Schaefer, D., Loidl, J., et al. (2005) Partner choice during meiosis is regulated by Hop1-promoted dimerization of Mek1. *Molecular Biology of the Cell*, **16**, 5804–5818.

Nonomura, K.I., Nakano, M., Murata, K., Miyoshi, K., Eiguchi, M., Miyao, A., Hirochika, H., Kurata, N. (2004) An insertional mutation in the rice PAIR2 gene, the ortholog of *Arabidopsis* ASY1, results in a defect in homologous chromosome pairing during meiosis. *Molecular Genetics and Genomics*, **271**, 121–129.

Novak, J.E., Ross-Macdonald, P.B., Roeder, G.S. (2001) The budding yeast Msh4 protein functions in chromosome synapsis and the regulation of crossover distribution. *Genetics*, **158**, 1013-1025.

Ogas, J., Kaufmann, S., Henderson, J. and Somerville, C. (1999) PICKLE is a CHD3 chromatin-remodeling factor that regulates the transition from embryonic to vegetative development in *Arabidopsis. Proc. Natl. Acad. Sci. USA*, **96**, 13839 –13844.

Ogawa, T., Yu, X., Shinohara, A., and Egelman, E.H. (1993) Simi-larity of the yeast Rad51 filament to the bacterial RecA fila-ment. *Science*, **259**, 1896 – 1899.

Oh, S.D., Lao, J.P., Taylor, A.F., Smith, G.R., Hunter, N. (2008) RecQ helicase, Sgs1, and XPF family endonuclease, Mus81-Mms4, resolve aberrant joint molecules during meiotic recombination. *Mol. Cell*, **31**, 324–336.

Orr-Weaver, T.L. (1999) The ties that bind: Localization of the sister-chromatid cohesin complex on yeast chromosomes. *Cell*, **99**, 1-4.

Osakabe, K., Abe, K., Yamanouchi, H. *et al.* (2005) *Arabidopsis* Rad51B is important for double-strand DNA breaks repair in somatic cells. *Plant Mol. Biol*, **57**, 819–833.

Osakabe, K., Yoshioka, T., Ichikawa, H., and Toki, S. (2002) Molecular cloning and characterization of RAD51-like genes from *Arabidopsis thaliana*. *Plant Mol. Biol*, **50**, 71- 81.

Osman, K., Higgins, J.D., Sanchez-Moran, E., Armstrong, S.J. and Franklin, F.C.H. (2011) Pathways to miotic recombination in *Arabidopsis thaliana. New philologist*, **190**, 523-44.

Osman, K., Sanchez-Moran, E., Higgins, J.D., Jones, G.H., Franklin, F.C. (2006) Chromosome synapsis in *Arabidopsis*: analysis of the transverse filament protein ZYP1 reveals novel functions for the synaptonemal complex. *Chromosoma*, **115**, 212–219.

Osman, K., Sanchez-Moran, E., Mann, S.C., Jones, G.H. and Franklin, F.C.H. (2009) Replication protein A (AtRPA1a) is required for class I crossover formation but is dispensable for meiotic DNA break repair. *The EMBO Journal*, 28, 394 – 404.

Page, S.L., and Hawley, R.S. (2004) The genetics and molecular biology of the synaptonemal complex. *Annu. Rev. Cell Dev. Biol*, **20**, 525-558.

Page, S.L., Hawley, R.S. (2003) Chromosome choreography: The meiotic ballet. *Science* **301**, 785-789.

Pandey, R., Muller, A., Napoli, C.A., Selinger, D.A., Pikaard, C.S., Richards, E.J., Bender, J., Mount, D.W. and Jorgensen, R.A. (2002) Analysis of histone acetyltransferase and histone deacetylase families of *Arabidopsis thaliana* suggests functional diversification of chromatin modification among multicellular eukaryotes. *Nucleic Acids Res*, **30**, 5036–5055.

Panizza, S., Mendoza, M.A., Berlinger, M., Huang, L., Nicolas, A., Shirahige, K., Klein, F. (2011) Spo11-accessory proteins link double-strand break sites to the chromosome axis in early meiotic recombination. *Cell*, **146**, 372–383.

Paques, F., Haber, J.E. (1999) Multiple pathways of recombination in-duced by double-strand breaks in *Saccharomyces cerevisiae*. *Microbiol Mol Biol Rev*, **63**, 349-404.

Paques, F., Leung, W.Y., Haber, J.E. (1998) Expansions and contractions in a tandem repeat induced by double-strand break repair. *Mol Cell Biol*, **18**, 2045–2054.

Pasierbek, P., Jantsch, M., Melcher, M., Schleiffer, A., Schweizer, D., Loidl, J. (2001) A *Caenorhabditis elegans* cohesion protein with functions in meiotic chromosome pairing and disjunction. *Genes Dev,* **15**, 1349–60.

Pawlowski, W.P., Cande, W.Z. (2005) Coordinating the events of the meiotic prophase. *Trends Cell Bio,* **15**, 674–81.

Pawlowski, W.P., *et al*. (2004) Coordination of meiotic recombination, pairing, and synapsis by PHS1. *Science*, **303**, 89–9.

Pecina, A., Smith, K.N., Mezard, C., Murakami, H., Ohta, K., and Nicolas, A. (2002) Targeted stimulation of meiotic re-combination. *Cell*, **111**, 173–184.

Pradillo, M., Lopez, E., Linacero, R., Romero, C., Cunado, N., *et al.* (2011) Together yes, but not coupled: new insights into the roles of RAD51 and DMC1 in plant meiotic recombination. *Plant Journal Online publication*. doi: 10.1111/j.1365-1313X.2011.04845.x.

Prieto, I., Suja, J.A., Pezzi, N., Kremer, L., Martinez, A.C., *et al*. (2001) Mammalian STAG3 is a cohesin specific to sister chromatid arms in meiosis I. *Nat. Cell Biol,* **3**, 761–66.

Puizina, J., Siroky, J., Mokros, P., Schweizer, D. and Riha, K. (2004) Mre11 deficiency in *Arabidopsis* is associated with chromosomal instability in somatic cells and Spo11- dependent genome fragmentation during meiosis. *Plant Cell*, **16**, 1968-1978.

Resnick, M.A. (1976) Repair of double-strand breaks in DNA–model involving recombination. *J Theor Biol*, **59**, 97–106.

Revenkova, E., Eijpe, M., Heyting, C., Gross, B., Jessberger, R. (2001) Novel meiosis-specific isoform of mammalian SMC1. *Mol. Cell. Biol,* **21**, 6984–98.

Rockmill, B. and Roeder, G.S. (1990) Meiosis in asynaptic yeast. *Genetics*, **126**, 563–574.

Rockmill, B. and Roeder, G.S. (1991) A meiosis-specific protein kinase homolog re-quired for chromosome synapsis and recombination. *Genes &Dev*, **5**, 2392–2404.

Roig, I, Dowdle, J.A., Toth, A., de Rooij, D.G., Jasin, M., Keeney, S. (2010) Mouse TRIP13/PCH2 Is Required for Recombination and Normal Higher-Order Chromosome Structure during Meiosis. *PLOS Genetics*, **8**, 1-19.

Romanienko, P.J. and Camerini-Otero, R.D. (2000) The mouse Spo11 gene is required for meiotic chromosome synapsis. *Mol. Cell*, **6**, 975-987.

Ross, K.J., Fransz, P., Armstrong, S.J., Vizir, I., Mulligan, B., Franklin, F.C.H. and Jones, G.H. (1997) Cytological characterization of four meiotic mutants of *Arabidopsis* isolated from T-DNA-transformed lines. *Chromosome Res*, **5**, 551- 559.

Ross-Macdonald, P., Roeder, G.S. (1994) Mutation of a meiosis-specific MutS homolog decreases crossing over but not mismatch correction. *Cell*, **79**, 1069–1080.

Rothenberg, M., Kohli, J., Ludin, K. (2009) Ctp1 and the MRN-complex are required for endonucleolytic Rec12 removal with release of a single class of oligonucleotides in fission yeast. *PLoS Genet*, **5**: e1000722.

Roth, N., Klimesch, J., Dukowic-Schulze, S., Pacher, M., Mannuss, A. and Puchta, H. (2012) The requirement for recombination factors differs con-siderably between different pathways of homologous double-strand break repair in somatic plant cells. *Plant J*, **72**, 781– 790.

Rowland, B.D. *et al*. (2009) Building sister chromatid cohesion: Smc3 acetylation counteracts an antiestablishment activity. *Mol. Cell,* **33**, 763–774.

Saito, T.T., Youds, J.L., Boulton, S.J., Colaiacovo, M.P. (2009) *Caenorhabditis elegans* HIM-18/SLX-4 interacts with SLX-1 and XPF-1 and maintains genomic integrity in the germline by processing recombination intermediates. *PLoS Genet*, **5**: e1000735.

Sanchez-Moran, E., Armstrong, S.J., Santos, J.L., Franklin, F.C.H., and Jones, G.H. (2001) Chiasma formation in *Arabidopsis thaliana* accession Wassileskija and in two meiotic mutants. *Chromosome Res*, **9**, 121–128.

Sánchez-Morán, E., Mercier, Mercier, R., Higgins, J.D., Armstrong, S.J., Jones, G.H. and Franklin, F.C.H. (2005) A strategy to investigate the plant meiotic proteome. *Cytogenetic and Genome Research*, **109**, 181-189.

Sánchez-Morán, E., Mercier, R., Santos, J.L., Jones, G.H. and Franklin, F.C.H. (2007) ASY1 mediates AtDMC1-dependent interhomolog recombination during meiosis in *Arabidopsis*. *Genes & Development*, **21**, 2220-2233.

San-Segundo, P.A., Roeder, G.S. (1999) Pch2 links chromatin silencing to meiotic checkpoint control. *Cell*, **97**, 313–324.

Scherthan, H. (2001) A bouquet makes ends meet. *Nat. Rev. Mol. Cell. Biol*. **2**, 621– 627.

Scherthan, H., Weich, S., Schwegler, H., Heyting, C., Härle, M. and Cremer, T. (1996) Centromere and telomere movements during early meiotic prophase of mouse and man are associated with the onset of chromosome pairing. *J. Cell Biol*, **134**, 1109-1125.

Schild-Prüfert, K., Saito, T.T., Smolikov, S., Gu, Y., Hincapie, M., *et al.* (2011) Organization of the synaptonemal complex during meiosis in *Caenorhabditis elegans*. *Genetics*, **189**, 411–421.

Schwacha, A. and Kleckner, N. (1994) Identification of joint molecules that form frequently between homologs but rarely between sister chromatids during yeast meiosis. *Cell*, **76**, 51–63.

Schwacha, A. and Kleckner, N. (1995) Identification of double Holliday junctions as intermediates in meiotic recombination. *Cell*, **83**, 783–791.

Schwacha, A. and Kleckner, N. (1997) Interhomolog bias during meiotic recombination: Meiotic functions promote a highly differentiated interho-molog-only pathway. *Cell*, **90**: 1123–1135.

Schwartz, E.K., and Heyer, W.D. (2011) Processing of joint molecule intermediates by structure-selective endonucleases during homologous recombination in eukaryotes. *Chromosoma*, **120**, 109–127.

Shaked, H., Avivi-Ragolsky, N. and Levy, A.A. (2006) Involvement of the *Arabidopsis* SWI2/SNF2 Chromatin Remodeling Gene Family in DNA Damage Response and Recombination. *Genetics*, **173**, 985–994.

Shinohara, A., Gasior, S., Ogawa, T., Kleckner, N., and Bishop, D.K. (1997b) *Saccharomyces cerevisiae* RECA homologues RAD51 and DMC1 have both distinct and overlapping roles in meiotic recombination. *Genes Cells*, **2**, 615–629.

Shinohara, A., Ogawa, H. and Ogawa, T. (1992) Rad51 protein involved in repair and recombination in *S. cerevisiae* is a RecA-like protein. *Cell*, **69**, 457–470.

Shinohara, M., Shita-Yamaguchi, E., Buerstedde, J.M., Shinagawa, H., Ogawa, H., *et al*. (1997a) Characterization of the roles of the *Saccharomyces cerevisiae* RAD54 gene and a homologue of RAD54, RDH54/TID1, in mitosis and meiosis. *Genetics*, **147**, 1545–1556.

Shin, Y.H., Choi, Y., Erdin, S.U., Yatsenko, S.A., Kloc, M., *et al.* (2010) Hormad1 Mutation Disrupts Synaptonemal Complex Formation, Recombination, and Chromosome Segregation in Mammalian Meiosis. *Plos Genetics*, **6**, e1001190. doi: 10.1371/journal.pgen.1001190.

Shogren-Knaak, M., Ishii, H., Sun, J.M., Pazin, M.J., Davie, J.R. and Peterson, C.L. (2006) Histone H4–K16 acetylation controls chromatin structure and protein interactions. *Science*, **311**, 844–847.

Smith, G.R., Boddy, M.N., Shanahan, P., Russell, P. (2003) Fission yeast Mus81.Eme1 Holliday junction resolvase is required for meiotic crossing over but not for gene conversion. *Genetics*, **165**, 2289–2293.

Smith, K.C. and Wang, T.C. (1989) recA-dependent DNA repair processes. *Bioessays*, **10**, 12-16.

Smith, K.C., Wang, T.V. and Sharma, R.C. (1987) recA-dependent DNA repair in UV-irradiated *Escherichia coli*. *J. Photochem. Photobiol. B*, **1**, 1-11.

Snowden, T., Acharya, S., Butz, C., Berardini, M., Fishel, R. (2004) hMSH4-hMSH5 recognizes Holliday junctions and forms a meiosis-specific sliding clamp that embraces homologous chromosomes. *Molecular Cell*, **15**, 437–451.

Sourirajan, A., Lichten, M. (2008) Polo-like kinase Cdc5 drives exit from pachytene during budding yeast meiosis. *Genes Dev*, **22**, 2627–2632.

Stacey, N.J., Kuromori, T., Azumi, Y., Roberts, G., Breuer, C., Wada, T., Maxwell, A., Roberts, K., Sugimoto-Shirasu, K. (2006) *Arabidopsis* SPO11-2 functions with SPO11-1 in meiotic recombination. *Plant Journal*, **48**, 206–216.

Stahl, F.W., Foss, H.M., Young, L.S., Borts, R.H., Abdullah, M.F., Copenhaver, G.P. (2004) Does crossover interference count in *Saccharomyces cerevisiae*. *Genetics*, **168**, 35-48.

Story, R.M., Bishop, D.K., Kleckner, N. and Steitz, T.A. (1993) Structural relationship of bacterial RecA proteins to recom-bination proteins from bacteriophage T4 and yeast. *Science*, **259**, 1892–1896.

Strahl, B.D. and Allis, C.D. (2000) The language of covalent histone modifications, *Nature*, **403**, 41–45.

Strom, L. *et al*. (2007) Postreplicative formation of cohesion is required for repair and induced by a single DNA break. *Science,* 317, 242–245.

Sung, P. (1994) Catalysis of ATP-dependent homologous DNA pairing and strand exchange by yeast RAD51 protein. *Science*, **265**, 1241–3.

Sun, H., Treco, D., Szostak, J.W. (1991) Extensive 3'-overhanging, single-stranded DNA associated with the meiosis-specific double-strand breaks at the ARG4 recombination initiation site. *Cell*, **64**, 1155–1161.

Svendsen, J.M., Smogorzewska, A., Sowa, M.E., O'Connell, B.C., Gygi, S.P., Elledge, S.J., Harper, J.W. (2009) Mammalian BTBD12/SLX4 assembles a Holliday junction resolvase and is required for DNA repair. *Cell*, **138**, 63–77.

Symington, L.S., Heyer, W.D. (2006) Some disassembly required: role of DNA translocases in the disruption of recombination intermediates and dead-end complexes. *Genes Dev*, **20**, 2479–86.

Sym, M. and Roeder, G.S. (1995) Zip1-induced changes in synaptonemal com-plex structure and polycomplex assembly. *J. Cell Biol*, **128**, 455–466.

Sym, M., Engebrecht, J. and Roeder, **G.S.** (1993) ZIP1 is a synaptonemal com-plex protein required for meiotic chromosome synapsis. *Cell*, **72**, 365–378.

Tan, T.L., Kanaar, R. and Wyman, C. (2003) Rad54, a Jack of all trades in homologous recombination. *DNA Repair (Amst.)*, **2**, 787–794.

Tarsounas, M., Davies, A.A., West, S.C. (2004) RAD51 localization and activation following DNA damage. *Philos Trans R Soc Lond B Biol Sci*, **359**, 87–93.

Taylor, S.W., Fahy, E., Ghosh, S.S. (2003) Global organellar proteomics. *Trends Biotechnol*, **21**, 82-88.

Tay, Y.D., Wu, L. (2010) Overlapping roles for Yen1 and Mus81 in cellular Holliday junction processing. *J Biol Chem*, **285**, 11427–11432.

Tease, C. and Hulten, M.A. (2006) Meiosis. *Encyclopedia of life sciences*. Doi: 10.1002/9780470015902.a0005772.

Terasawa, M., Ogawa, H., Tsukamoto, Y., Shinohara, M., Shirahige, K., Kleckner, N., Ogawa, T. (2007) Meiotic recombination-related DNA synthesis and its implications for cross-over and non-cross-over recombinant formation. *Proceedings of the National Academy of Sciences, USA,* **104**, 5965–5970.

Tian, L., Wang, J., Fong, M.P., Chen, M., Cao, H., Gelvin, S.B. and Chen, Z.J. (2003) Genetic control of developmental changes induced by disruption of *Arabidopsis* histone deacetylase 1 (AtHD1) expression. *Genetics*, **165**, 399–409.

Toby, G.G., Gherraby, W., Coleman, T.R., Golemis, E.A. (2003) A novel RING finger protein, human enhancer of invasion 10, alters mitotic progression through regulation of cyclin B levels. *Mol Cell Biol*, **23**, 2109–2122.

Tsubouchi, H. and Roeder, G.S. (2003) The importance of genetic recombination for fidelity of chromosome pairing in meio-sis. *Dev. Cell*, **5**, 915–925.

Tsubouchi, H. and Roeder, G.S. (2004) The budding yeast Mei5 and Sae3 proteins act together with Dmc1 during meiotic recombination. *Genetics*, **168**, 1219–1230.

Tsubouchi, H. and Roeder, G.S. (2006) Budding yeast Hed1 down-regulates the mitotic recombination machinery when meiotic recombination is impaired. *Genes&Dev*, **20**, 1766–1775.

Tsubouchi, H., Zhao, H., Roeder, G.S. (2006) The meiosis-specific Zip4 protein regulates crossover distribution by promoting synaptonemal complex formation together with Zip2. *Dev Cell*, **10**, 809-819.

Tung, K.S. and Roeder, G.S. (1998) Meiotic chromosome morphology and behaviour in *zip1* mutants of *Saccharomyces cerevisiae*. *Genetics*, **149**, 817-832.

Uanschou, C., Siwiec, T., Pedrosa-Harand, A., Kerzendorfer, C., Sanchez-Moran, E., Novatchkova, M., Akimcheva, S., Woglar, A., Klein, F., Schlogelhofer, P. (2007) A novel plant gene essential for meiosis is related to the human CtIP and the yeast COM1/SAE2 gene. *EMBO Journal*, **26**, 5061–5070.

Unal, E. *et al* (2008) A molecular determinant for the establishment of sister chromatid cohesion. *Science,* **321**, 566–569.

Unal, E., Heidinger-Pauli, J.M. and Koshland, D. (2007) DNA double-strand breaks trigger genome-wide sister-chromatid cohesion through Eco1 (Ctf7). *Science,* **317**, 245–248.

van Brabant, A.J., Ye, T., Sanz, M., German, I.J., Ellis, N.A., Holloman, W.K. (2000) Binding and melting of D-loops by the Bloom syndrome helicase. *Biochemistry*, **39**, 14617–14625.

van Veelen, L.R., Cervelli, T., van de Rakt, M.W., Theil, A.F., Essers, J., *et al.* (2005a) Analysis of ionizing radiation-induced foci of DNA damage repair proteins. *Mutat Res*, **574**, 22–33.

van Veelen, L.R., Essers, J., van de Rakt, M.W., Odijk, H., Pastink, A., *et al.* (2005b) Ionizing radiation-induced foci formation of mammalian Rad51 and Rad54 depends on the Rad51 paralogs, but not on Rad52. *Mutat Res*, **574**, 34–49.

Vignard, J., Siwiec, T., Chelysheva, L., Vrielynck, N., Gonord, F., Armstrong, S.J., Schlogelhofer, P. and Mercier, R. (2007) The interplay of RecA-related proteins and the MND1-HOP2 complex during meiosis in *Arabidopsis thaliana*. *PLoS Genet*, **3**, 1894–1906.

Vlachonasios, K.E., Thomashow, M.F. and Triezenberg, S.J. (2003) Disruption mutations of ADA2b and GCN5 transcriptional adaptor genes dramatically affect Arabidopsis growth, development, and gene expression. *Plant Cell*, **15**, 626–638.

Wagner, D., and Meyerowitz, E.M. (2002) SPLAYED, a novel SWI/SNF ATPase homolog, controls reproductive development in *Arabidopsis*. *Curr. Biol*, **12**, 85–94.

Wagstaff, J.E., Klapholz, S., Waddell, C.S., *et al.* (1985) Meiotic exchange within and between chromosomes requires a common Rec function in Saccharomyces cerevisiae. *Mol Cell Biol*, **5**, 3532-3544.

Wang, K., Wang, M., Tang, D., Shen, Y., Miao, C., *et al.* (2012) The Role of Rice HEI10 in the Formation of Meiotic Crossovers. *PLoS Genet*, **8**, e1002809. doi: 10. 1371/journal.pgen. 1002809.

Wang, M., Wang, K., Tang, D., Wei, C., Li, M., Shen, Y., Chi, Z., Gu, M., Cheng, Z. (2010) The central element protein ZEP1 of the synaptonemal complex regulates the number of crossovers during meiosis in rice. *Plant Cell*, **22**, 417–430.

Wang, Q., Yin, S., Ai, J.S., Liang, C.G., Hou, Y., Chen, D.Y., Schatten, H. and Sun, Q.Y. (2006) Histone deacetylation is required for orderly meiosis. *Cell Cycle*, **5**, 766–774.

Wan, L., de los Santos, T., Zhang, C., Shokat, K., and Hollings-worth, N.M. (2004) Mek1 kinase activity functions down-stream of RED1in the regulation of meiotic double strand break repair in budding yeast. *Mol. Biol. Cell*, **15**, 11–23.

West, S.C. (1997). Processing of recombination intermediates by the RuvABC proteins. *Annu Rev Genet*, **31**, 213–244.

Wijeratne, A.J., Chen, C., Zhang, W., Timofejeva, L., Ma, H. (2006) The *Arabidopsis thaliana* PARTING DANCERS gene encoding a novel protein is required for normal meiotic homologous recombination. *Mol Biol Cell*, **17**, 1331–1343.

Wojtasz, L., Daniel, K., Roig, I., Bolcun-Filas, E., Xu H.L., *et al*. (2009) Mouse HORMAD1 and HORMAD2, two conserved meiotic chromosomal proteins, are depleted from synapsed chromosome axes with the help of TRIP13 AAA-ATPase. *Plos Genetics*, **5**: e1000702. doi: 10.1371/journal.pgen.1000702. Epub 2009 Oct 23.

Wood, A.J., Severson, A.F. and Meyer, B.J. (2010) Condensin and cohesin complexity: the expanding repertoire of functions. *Nature reviews genetics*, **11**, 391-404.

Wu, H.Y., Burgess, S.M. (2006) Two distinct surveillance mechanisms monitor meiotic chromosome metabolism in budding yeast. *Curr Biol*, **16**, 2473–2479.

Wu, K., Tian, L., Malik, K., Brown, D. and Miki, B. (2000) Functional analysis of HD2 histone deacetylase homologues in *Arabidopsis thaliana*. *Plant J*, **22**, 19–27.

Wu, L., Hickson, I.D. (2003) The Bloom's syndrome helicase suppresses crossing over during homologous recombination. *Nature*, **426**, 870–874.

Xu, D., Guo, R., Sobeck, A., Bachrati, C.Z., Yang, J., Enomoto, T., Brown, G.W., Hoatlin, M.E., Hickson, I.D., Wang, W. (2008) RMI, a new OB-fold complex essential for Bloom syndrome protein to maintain genome stability. *Genes Dev*, **22**, 2843–2855.

Xu, L., Weiner, B.M., and Kleckner, N. (1997) Meiotic cells monitor the status of the interhomolog recombination com-plex. *Genes&Dev*, **11**, 106–118.

Yamada, T., Mizuno, K.I., Hirota, K., Kon, N., Wahls, W.P., Hartsuiker, E., Murofushi, H., Shibata, T. and Ohta, K. (2004) Roles of histone acetylation and chromatin remodeling factor in a meiotic recombination hotspot. *EMBO J*, **23**, 1792–1803.

Yang, H., Lu, P., Wang, Y., Ma, H. (2011) The transcriptome landscape of *Arabidopsis* male meiocytes from high-throughput sequencing: the complexity and evolution of the meiotic process. *Plant J*, **65**, 503–516.

Yildiz, O., Majumder, S., Kramer, B., Sekelsky, J.J. (2002) Drosophila MUS312 interacts with the nucleotide excision repair endonuclease MEI-9 to generate meiotic crossovers. *Mol Cell*, **10**, 1503–1509.

Yu, H. G. and Koshland, D. (2005) Chromosome morphogenesis: condensin-dependent cohesin removal during meiosis. *Cell,* **123**, 397–407.

Zakharyevich, K., Ma, Y., Tang, S., Hwang, P.Y., *et al.* (2010) Temporally and biochemically distinct activities of Exo1 during meiosis: double-strand break resection and resolution of double Holliday junctions. *Mol Cell*, **40**, 1001–1015.

Zakharyevich, K., Tang, S., Ma, Y., Hunter, N. (2012) Delineation of joint molecule resolution pathways in meiosis identifies a crossover-specific resolvase. *Cell*, **149**, 334–347.

Zanders, S., Alani, E. (2009) The pch2Delta mutation in baker's yeast alters meiotic crossover levels and confers a defect in crossover interference. *PLoS Genet*, **5**: e1000571. doi:10.1371/journal.pgen.1000571.

Zalevsky, J., MacQueen, A.J., Duffy, J.B., Kemphues, K.J., Villeneuve, A.M. (1999) Crossing over during Caenorhabditis elegans meiosis requires a conserved MutS-based pathway that is partially dispensable in budding yeast. *Genetics*, **153**, 1271-1283.

Zenvirth, D., and Simchen, G. (2000) Meiotic double-strand breaks in *Schizosaccharomyces pombe*. *Curr. Genet*, **38**, 33-38.

Zhang, J. *et al.* (2008) Acetylation of Smc3 by Eco1 is required for S phase sister chromatid cohesion in both human and yeast. *Mol. Cell,* **31**, 143–151.

Zhang, L., Kim, K.P., Kleckner, N.E., Storlazzi, A. (2011) Meiotic double-strand breaks occur once per pair of (sister) chromatids and, via Mec1/ATR and Tel1/ ATM, once per quartet of chromatids. *Proc Natl Acad Sci U S A*, **108**, 20036–20041.

Zickler, D. and Kleckner, N. (1998) The leptotene-zygotene transition in meiosis. *Annu. Rev. Genet,* **32**, 619-697.

Zickler, D. and Kleckner, N. (1999) Meiotic chromosomes: integrating structure and function. *Annu. Rev. Genet*, **33**, 603-754.